2008

Numerical Modeling of Continuous Flow Microwave Heating - Coupling of High Frequency Electromagnetism with Fluid Flow and Heat Transfer

Deepti Salvi
Louisiana State University and Agricultural and Mechanical College

NUMERICAL MODELING OF CONTINUOUS FLOW MICROWAVE HEATING - COUPLING OF HIGH FREQUENCY ELECTROMAGNETISM WITH FLUID FLOW AND HEAT TRANSFER

A Dissertation
Submitted to the Graduate Faculty of the
Louisiana State University and
Agricultural and Mechanical College
requirements for the degree of
Doctor of Philosophy
in
The Interdepartmental Program in Engineering Science

by
Deepti Salvi
B. Tech., Dr. B.S. Konkan Agricultural University, 2003
M. E., Asian Institute of Technology, 2005
August 2008

To my father

ACKNOWLEDGEMENTS

First and foremost, I would like to express my sincere gratitude to my major advisor, Dr. Cristina Sabliov for her invaluable guidance, and support throughout my graduate studies at LSU. Her constant encouragement and positive approach has helped me in accomplishing my research goals. Her expert advice and teaching interest made my learning process enjoyable. She has been an excellent mentor and my source of inspiration.

I express my gratefulness to my co-advisor Dr. Dorin Boldor, for his impeccable guidance, constructive criticism, and patience. His thoughtful scientific insights encouraged me to strengthen my knowledge.

I would like to thank Dr. Marybeth Lima, for her encouragement and advice during the course of this work. I am also grateful to Dr. Ram Devireddy for serving on my examination committee and providing excellent suggestions. I thank Dr. Zhimin Xu for accepting to be part of my examination committee and for sharing his experience.

Special thanks are due to Mr. Jeff Ortego and Mr. Chris Arauz who helped me with the experimental work. Cordial thanks are also extended to Dr. Sabliov's and Dr. Boldor's research group. I would also like to thank Dr. Sundar Balasubramanian, Mr. Milton Saidu, and Mr. Nicholas Gerbo for their friendly help. I would like to thank all the staff and faculty of BAE department at LSU for creating a warm and friendly atmosphere to work in. I am also grateful to Mr. Chris Schwehm and Mr. Tyrone Schultz for their help with IT support. I acknowledge the COMSOL and ANSYS support groups for their help. I am grateful to the Louisiana Board of Regents- Research Subprogram and the National Oceanic and Atmospheric Administration for providing financial support for my research. I would also like to thank Industrial Microwave Systems for lending the microwave equipment used in the research.

Thanks to all my friends for their wonderful company and warm affection. I would like to express my deepest regards to my mom, in-laws and family for their eternal love and support. I express my indebtedness towards my husband Abhijit, who has been greatest strength for me. Thank you all. God bless you.

TABLE OF CONTENTS

LIST OF TABLES

LIST OF FIGURES

ABSTRACT

This study focused on numerical and experimental investigation of continuous flow microwave heating. A numerical model was developed to predict the temperature of a liquid product heated in a continuous-flow focused microwave system by coupling electromagnetism, fluid flow, and heat transfer in two different software packages (ANSYS Multiphysics 9.0 and COMSOL Multiphysics 3.4). The temperature and energy distributions simulated in ANSYS were verified against other numerical studies published in the literature. Comparison of the simulated temperature in ANSYS with experimental data for saltwater of two different salinities showed good agreement. To simulate the experimental conditions more accurately, a comprehensive numerical model was developed in COMSOL Multiphysics by incorporating non-Newtonian flow and phase change coupling (which were not considered in the earlier ANSYS model). Comparison of the results from COMSOL model with the results from pre-developed and validated ANSYS model ensured accuracy of the COMSOL model. A comprehensive validation of the model with experimental data suggested that the simulated results were in fairly good agreement with the experimental data for saltwater and CMC solution.

Rigorous experimental data was collected for freshwater, saltwater, and CMC solution flowing at three different flow rates through a 915 MHz continuous flow microwave system at 4 kW of power. A custom made temperature measurement system employing a single fiber optic probe was used to get 110 radial and longitudinal temperatures measurements. The experimental temperature values were used in determining the effect of different dielectric properties and flow rate on heating patterns of freshwater, saltwater and CMC during continuous flow microwave heating.

The presented work greatly aids in understanding of the microwave heating process through accumulation and analysis of a large body of experimental data and through mathematical prediction of temperatures for a variety of operating parameters (i.e. dielectric and physical properties, and flow rates). The methodology developed can be further applied to study temperature distributions for a multitude of materials, and continuous flow microwave cavity geometries. The developed model is a vital tool for researchers and engineers in the academic and industrial settings interested in continuous microwave heating of liquids.

CHAPTER 1

INTRODUCTION

1.1 General Background

Microwave energy has been extensively used by a wide range of industries for food, environmental, and chemical engineering applications since 1940s. Some of the applications in food industries include cooking, thawing, tempering, drying, freeze-drying, pasteurization, sterilization, bleaching, extraction, baking, heating, and re-heating (Metaxas and Meredith, 1983; Oliveira and Franca, 2002).

Thermal processing of materials using microwaves as a source of energy is a well known, viable alternative for high-temperature short-time processing of thermo-sensitive materials. In contrast to conventional heating (where heat is transferred from the surface to the interior of the product), microwaves penetrate in the sample and cause heating throughout the volume of the product. This volumetric heating leads to faster heat transfer rates and shorter processing time than conventional processes. However, the use of batch microwave systems can sometimes result in uneven heating of certain products, depending on their dielectric and thermo-physical properties, as well as on the system design. Emerging technologies such as continuous flow focused microwave systems can alleviate uneven heating by applying an electric field with a more suitable distribution (i.e. maximum at the center of tube where velocity is high and minimum at the edges where velocity is low) to the liquid flowing through the microwave cavity (Falqui-Cao et al., 2001). The advantages of the continuous flow microwave systems include less floor space requirement as compared to conventional furnaces, reproducible and homogeneous treatment within the material if properly controlled, rapid heating to boiling or above boiling (in pressurized systems) temperatures, and no thermal vessel inertia (Clark and Sutton, 1996; Falqui-Cao et al., 2001; Coronel et al., 2003).

The knowledge of the three dimensional temperature profile distribution of heated products is essential to optimize the microwave heating processes (Knoerzer et al., 2005). Temperature inside the heated product can be determined experimentally or it can be predicted numerically. Experimental measurement of temperature in the microwave is limited due to interference of measuring devices with the electromagnetic field and the continuous nature of the process. Numerical methods have been used to understand and optimize the process of microwave heating. Rigorous numerical modeling of continuous microwave heating of pumpable products has challenged the researchers because of the complexity of coupling and simultaneously solving the three sets of equations (Maxwell's equations, Fourier's energy balance equation, and Navier-Stokes equation) which describe the process.

Few studies are reported on numerical modeling of batch microwave heating of liquids (Datta et al., 1992; Ohlsson, 1993; Zhang et al., 2000; Sabliov et al., 2004) as well as continuous flow microwave heating of liquids (Mudgett, 1986; Le Bail et al., 2000; Ratanadecho et al., 2002; Zhu et al., 2007a; Zhu et al., 2006b; Zhu et al., 2006c). Some of these studies assumed simplified approaches including plug flow and homogenous heat dissipation (Mudgett, 1986; Le Bail et al., 2000), or exponential decay of the microwave energy (Datta et al., 1992). Recent models coupling electromagnetism with fluid flow and convective heat transfer (Zhang et al., 2000; Ratanadecho, et al., 2002; Zhu et al., 2007a; Zhu et al., 2006b; Zhu et al., 2006c) used finite difference time domain algorithm to solve Maxwell's equations and finite volume method to solve the energy and momentum equations using independent numerical codes. The numerical models involving coupling of high frequency electromagnetism, heat transfer and fluid flow are very recent developments in the field.

The disadvantages associated with the above mentioned independent codes are complexity in grid generation, equation solving, and result visualization. Furthermore, these methods are computationally extensive, require programming and numerical analysis skills. The lack of experimental temperature data in the processed dielectric material in the focusing cavity has also sabotaged the development and validation of numerical models. In this study we focused on experimental investigation of temperature profile in a continuous flow microwave system and on development of numerical models using different commercial software packages that circumvent above drawbacks and enhance the understanding of the process. The availability of such models is critical for developing a fundamental understanding of microwave heating in a continuous flow focused microwave system.

1.2 Objectives

The present work aims to study numerically and experimentally the process of continuous microwave heating of liquids in a continuous focused microwave system of specified geometry. To numerically model the process, high frequency electromagnetism, heat transfer, and fluid flow were coupled in commercially available multiphysics simulation environment. Finite element software packages ANSYS Multiphysics 9.0 and COMSOL Multiphysics 3.4 were used in the study to allow direct coupling of different physical phenomena (high frequency electromagnetism, heat transfer, and fluid flow involved the process). These software packages also offer many versatile grid options, solvers for different physical phenomena, and multiple choices for the visualization of the results.

The main emphasis of the study was on understanding the heat transfer mechanisms during continuous focused microwave heating of fluids. Specifically, the following objectives were set:

1. To develop a numerical model of the continuous microwave heating of liquids by coupling high frequency electromagnetism, heat transfer, and fluid flow in ANSYS Multiphysics, and to use the developed model to simulate temperature profile in the liquid as it heats up continuously in a focused microwave system;

2. To experimentally measure temperature profile of liquids with different dielectric and physical properties during continuous microwave heating;

3. To develop and improve the numerical model of the continuous flow microwave heating of a liquid in COMSOL Multiphysics by including phase change, and non-Newtonian flow;

4. To validate the continuous flow microwave heating model developed in COMSOL by comparing the experimental data with predicted values.

1.3 Dissertation Organization

The organization of the dissertation includes a total of six chapters. The present chapter provides general background on experimental and numerical aspects of continuous flow microwave heating, the objectives of the research, as well as the structure of the dissertation itself.

The second chapter (published as research article in the Journal of Microwave Power & Electromagnetic Energy, Vol. 41(4)) describes a numerical model coupling three physics phenomena created in ANSYS Multiphysics 9.0. This was the first successful ANSYS model published which coupled high frequency electromagnetism, heat transfer and fluid flow in ANSYS environment to simulate continuous flow microwave heating. Some simplifying assumptions were made to reduce the complexity of the problem and to develop this basic model.

The third chapter (research article in press with the Journal of Marine Environmental Engineering) explains partial validation of the developed model. The numerical model developed in ANSYS was used to understand temperature distribution in ballast water heated in a continuous flow microwave system at different salinities and flow rates. Temperatures were measured using a specially designed system of fiber optic probes placed at three different locations inside the PTFE applicator tube in the cavity.

The fourth chapter describes a new system designed to measure the temperature distribution inside the fluid heated in continuous flow microwave system used to study the effect of different physical and dielectric properties on temperature distribution. This system is used to collect temperatures at 110 different radial and longitudinal positions in three different liquids flowing at three different flow rates in the microwave cavity.

The fifth chapter includes the development of a numerical model coupling electromagnetism, fluid flow and heat transport in COMSOL Multiphysics 3.4. This comprehensive model considered phase change and non-Newtonian flow. The model was validated by comparison of outcomes against previously developed ANSYS model data as well as experimental data. The dissertation closes with the sixth chapter that includes conclusions and future work.

1.4 References

Clark D. E. and W. H. Sutton (1996). "Microwave processing of materials". *Annual Reviews in Material Science*, 26, 299-331.

Coronel, P, Simunovic, J., Sandeep, K.P. (2003). "Temperature profiles within milk after heating in a continuous-flow tubular microwave system operating at 915 MHz". *Journal of food science*, 68(6), 1976-1981.

Datta, A., H. Prosetya and W. Hu (1992). "Mathematical modeling of batch heating of liquids in a microwave cavity". *Journal of Microwave Power and Electromagnetic Energy*, 27(1), 38–48.

Falqui-Cao, C., Wang, Z., Urruty, L., Pommier, J., and M. Montury (2001). "Focused microwave assistance for extracting some pesticide residues from strawberries into water before their determination by SPME/HPLC/DAD". *Journal of Agricultural and Food Chemistry*, 49, 5092-5097.

Knoerzer, K., Regier, M. and H. Schubert (2005). "Measuring temperature distributions during microwave processing". In: *The Microwave Processing of Foods*, H. Schubert and M. Regier (Ed), CRC Press, 243-263.

Metaxas, A.C., Meredith, R.J. (1983). *Industrial Microwave Heating*. London, UK: Peter Peregrinus Ltd.

Mudgett, R. E. (1986). "Microwave properties and heating characteristics of foods". *Food Technology*, 40 (6), 84-93.

Le Bail, A., T. Koutchma and H.S. Ramaswamy (2000). "Modeling of temperature profiles under continuous tube-flow microwave and steam heating conditions". *Journal of Food Process Engineering*, 23, 1-24.

Lin, Y.E., R.C. Anantheswaran and V.M. Puri (1995). "Finite element analysis of microwave heating of solid foods". *Journal of Food Engineering*, 25, 85-112.

Ohlsson, T. (1993). "In-flow microwave heating of pumpable foods". *Developments in Food Engineering: Proceedings of the 6th International Congress on Engineering and Food*, 322-324.

Oliveira, M. E. C. and A. S. Franca (2002). "Microwave heating of foodstuffs". *Journal of Food Engineering*, 53, 347–359.

Ratanadecho, P., K. Auki and M. Akahori (2002). "A numerical and experimental investigation of the modeling of microwave heating for liquid layers using a rectangular wave guide (effects of natural convection and dielectric properties)". *Applied Mathematical Modeling*, 26, 449–472.

Sabliov, C. M., K.P. Sandeep and J. Simunovic (2004). "High frequency electromagnetism coupled with conductive heat transfer – a method to predict temperature profiles in materials heated in a focused microwave system". *The 4th World Congress on Microwave and Radio Frequency Applications*, R.L. Schulz and D.C. Folz (Ed.), 469-476.

Zhang, Q., Jackson, T. H., Ungan, A. (2000). "Numerical modeling of microwave induced natural convection". *International Journal of Heat and Mass Transfer,* 43, 2141-2154.

Zhu J., A.V. Kuznetsov and K.P. Sandeep (2007a). "Numerical simulation of forced convection in a duct subjected to microwave heating". *Heat Mass Transfer*, 43(3), 255-264.

Zhu J., A.V. Kuznetsov and K.P. Sandeep (2007b). "Mathematical modeling of continuous flow microwave heating of liquids (effects of dielectric properties and design parameters)". *International Journal of Thermal Sciences,* 46 (4), 328-341.

Zhu J., A.V. Kuznetsov and K.P. Sandeep (2007c). “Numerical modeling of a moving particle in a continuous flow Subjected to microwave heating”. *Numerical Heat Transfer*, Part A, 52, 417 – 439.

CHAPTER 2

HIGH FREQUENCY ELECTROMAGNETISM, HEAT TRANSFER, AND FLUID FLOW COUPLING IN ANSYS MULTIPHYSICS[1]

2.1 Introduction

Continuous thermal processing of materials using microwaves as a source of energy is known as a viable alternative for high temperature short time processing of thermo-sensitive materials. In contrast to conventional heating, microwaves penetrate into the sample producing dipole rotation and ionic conduction and thus cause heating throughout the volume of the product (Metaxas and Meredith, 1982). This volumetric heating leads to faster heat transfer rates and shorter processing time than the conventional heating process, where heat is transferred from the surface to the interior of the product through convection and heat conduction. Application of microwaves typically results in uneven heating of products, depending on the dielectric and thermo-physical properties of the product and on the design specifications of the microwave system. The use of continuous focused microwave systems can alleviate uneven heating by applying an electric field with a more suitable distribution (Falqui-Cao et al., 2001). The advantages of the focused microwave systems include more homogeneous and reproducible treatment, rapid heating to boiling or above boiling (in pressurized systems) temperatures and no thermal vessel inertia (Falqui-Cao et al., 2001).

There is a large amount of papers related to the modeling of microwave heat transfer and devoted to batch heating of solid food (Lin et al., 1995; Zhou et al., 1995; Oliveira and Franca 2002; Pandit and Prasad, 2003; Campanone and Zaritzky, 2005; Romano et al., 2005; Zhang and Datta, 2006) and liquids (Ohlsson, 1993; Sabliov et al., 2004). Attempts to solve for the temperature profile in a liquid flowing through a microwave cavity were also made. Mudgett

[1] Reprinted with permission from the 'Journal of Microwave Power & Electromagnetic Energy'

(1986) developed a model for the continuous-flow microwave system by using the plug flow approach and assuming a homogenous heat dissipation of the microwave energy. Datta et al. (1992) used a heat generation term that exponentially decayed from the surface into the liquid to solve the energy and flow equations to predict temperature inside a cylindrical container with liquid in a microwave cavity. Le Bail et al. (2000) developed a model to predict the temperature profiles of continuous-flow microwave heating by assuming a uniform volumetric power in the core of the flow.

Ratanadecho et al. (2002) studied modeling of microwave melting of frozen packed beds in a rectangular waveguide; the movement of the liquid induced by microwave heating was taken into account. A finite difference time domain (FDTD) algorithm similar to Ratanadecho et al. (2002) was used by Zhu et al. (2007b) for the mathematical modeling of microwave heating of continuously flowing non-Newtonian liquids in a cylindrical applicator duct. A similar study for a rectangular duct was conducted by the same authors in (Zhu et al., 2007a).

Heating liquid products in a continuous-flow focused microwave system is a complex process involving heat generation due to electromagnetic waves, heat transfer by conduction and convection, and flow of the fluid as the process is continuous. Numerical modeling requires solution of Maxwell's equations to determine the electromagnetic field distribution, the Fourier's energy balance equation to find the heat transfer in the fluid as well as the Navier-Stokes equation to describe the fluid flow. Computer simulation of the microwave heating process in this consideration is really challenging because of interdependency of the involved mechanisms. For instance, the known models coupling electromagnetism with fluid flow and convective heat transfer (Ratanadecho et al., 2002; Zhu et al., 2007a; Zhu et al., 2006b) are complex alliances of FDTD algorithms solving Maxwell's equations and finite volume method solvers handling the

energy and momentum equations. Engineers not trained/experienced in numerical analysis and associated programming of grid generation, solving equations and visualization of the results may avoid these challenges by using commercially available software capable of modeling multiphysics processes.

Several electromagnetic simulators suitable for modeling problems of microwave power engineering are commercially available; they include ANSYS Multiphysics, COMSOL Multiphysics (former FEMLAB), QuickWave-3D, MEFiSTo-3D, Microwave Studio and others (Yakovlev, 2000; Komarov and Yakovlev, 2001; Yakovlev, 2006). The finite element software packages ANSYS Multiphysics and COMSOL Multiphsycis are directly capable of coupling high frequency electromagnetism, heat transfer and fluid flow involved in the process. The ANSYS package (ANSYS, 1995-2007) offers many versatile grid options, solvers for different physical phenomena, and a multiple choice for visualization of the results. A coupling of ANSYS solvers for high frequency electromagnetism, fluid flow, and heat transfer is the basis of the present study. Description of the implemented algorithm is supplemented with numerical results of temperature distribution in water continuously flowing through a focused microwave system.

The major objectives of this study were:

(1) To develop a finite element model in ANSYS Multiphysics coupling high frequency electromagnetism, heat transfer and fluid flow.

(2) To assess the influence of flow rates on the temperature profiles of water heated in a continuous-flow focused microwave system.

2.2 Materials and Methods

2.2.1 Governing Equations and Boundary Conditions

2.2.1.1 Heat Transfer

The temperature profile in a material heated by electromagnetic waves is given by Fourier's energy balance reproduced, e.g., by Datta et al. (1992):

$$\frac{\partial T}{\partial t} + \vec{u}\nabla T = \frac{k}{\rho_m C_P}\nabla^2 T + \frac{q_{gen}}{\rho_m C_P} \tag{2.1}$$

where ρ_m is material density in kg/m^3, C_p is specific heat in J/kgK, T is temperature in Kelvin, $\vec{u}$ is velocity in m/s, k is thermal conductivity in W/mK, and q_{gen} is heat generation in W/m^3. In equation (2.1), the first term on the left-hand side is the rate of change of the thermal energy and the second represents the convection heat transfer. On the right-hand side heat diffusion by conduction is taken into account and the heat generation term for electromagnetic heating is calculated using the expression (Metaxas and Meredith, 1983; Tang, 2005):

$$q_{gen} = 2\pi\varepsilon_o\varepsilon''f\,|\,\vec{E}\,|^2 \tag{2.2}$$

where ε_o = 8.854 x 10^{-12} F/m is free space permittivity, ε'' is relative dielectric loss, f is frequency in Hz, and $\vec{E}$ is electric field intensity in V/m.

2.2.1.2 Electromagnetism

To calculate the heat generation (q_{gen}) in (2.2), the electric field intensity $\vec{E}$ can be obtained either by using Lambert's law (Oliveira and Franca, 2002) or, more accurately, by solving Maxwell's equations. The latter approach used in this study deals with the equations which can be given, e.g., in the form (Regier and Schubert, 2005):

$$\nabla \cdot \vec{D} = \rho \tag{2.3}$$

$$\nabla \times \vec{E} = -\frac{\partial \vec{B}}{\partial t} \tag{2.4}$$

$$\nabla \cdot \vec{B} = 0 \tag{2.5}$$

$$\nabla \times \vec{H} = \vec{j} + \frac{\partial \vec{D}}{\partial t} \tag{2.6}$$

where $\vec{D}$ is electric flux density in C/m^2, $\vec{B}$ is magnetic flux intensity in Wb/m^2, $\vec{H}$ is magnetic field intensity in A/m, ρ is electric charge density in C/m^3, and $\vec{j}$ is electric current density in A/m^2, and t is time in sec.

2.2.1.3 Momentum Balance

The Navier-Stokes equation describing the momentum balance in a fluid of constant ρ and dynamic viscosity μ is formulated by Bird et al., (1960) as,

$$\rho_m \frac{\partial \vec{v}}{\partial t} = -\nabla P + \mu \nabla^2 \vec{v} + \rho_m g \tag{2.7}$$

where v is velocity in m/s, ∇P is pressure force on element per unit volume in N/m^2 and g is acceleration due to gravity in m/s^2. Continuity equation is given by (Bird et al., 1960)

$$\nabla \cdot \vec{v} = 0 \tag{2.8}$$

2.2.1.4 Assumptions

Two numerical techniques have been historically and most commonly employed to solve the above equations: finite differences and finite elements. In this study we use the finite element

method, the underlying technique of all models in ANSYS Multiphysics. An algorithm was developed to couple high frequency electromagnetism with heat transfer and fluid flow. A corresponding code was used to solve the above Maxwell's, Fourier's and Navier-Stokes equations to find temperature and velocity profile of water heated in a continuous-flow focused microwave system. When solving these equations some important assumptions were made to reduce the complexity of the problem, such as follows:

1. Water was considered Newtonian, flowing under laminar conditions. Flow was assumed incompressible.

2. The process was assumed at steady state – in accordance with Gerbo et al. (2007).

3. Physical and dielectric properties of the fluid were considered constant with temperature.

4. The PTFE tube carrying fluid was assumed completely transparent to microwaves.

5. Adiabatic conditions were applied at the applicator wall (i.e., no heat was assumed exchanged between the dielectric and the air in the cavity).

6. No phase change was considered.

Since the goal of this study was to demonstrate that ANSYS Multiphysics can be configured to solve the coupled microwave heating problem, these assumptions were made to keep the model relatively simple. Changes such as modeling non-Newtonian liquids, or including temperature-dependent material properties and a heat loss term can be easily incorporated in the developed model; the related upgrades are planned as future developments of the technique described in this paper.

2.2.2 Model Development

ANSYS Multiphysics provides a comprehensive mechanism to combine numerical analyses of two or more different inter-related physical fields within a single model. Problems in different fields like structural, thermal, electromagnetic physics, acoustics, fluid dynamics can be solved directly or iteratively. ANSYS Multi-field solver is built on the premise that each physical field is analyzed with an independent solid model and mesh, and that a specific type of solver is used for each field. The Multi-field solver automatically transfers surface or volume "loads" across dissimilar meshes based on a set of multi-field solver commands (ANSYS, 2005).

In our ANSYS Multiphysics model, High Frequency Electromagnetic Module (used for high frequency electromagnetic analysis) and FLOTRAN CFD Module (used to solve fluid flow and heat transfer problems) are iteratively coupled via volumetric heat generation term and solved for a steady-state situation. ANSYS Multi-Field solver iterates between the fields' analyses until the "loads" transfer across each interface converges. Maxwell's equations (2.3)-(2.6) are solved using a sparse direct solver to calculate the electric field and the heat loss in the dielectric. This heat loss is used as a heat generation term in solving energy equation (2.1). Energy, momentum and continuity equations (2.6)-(2.8) are solved using a tridiagonal matrix algorithm in FLOTRAN CFD Module. The FLOTRAN temperature output is then used as input in the High Frequency Electromagnetic Module to recalculate the dielectric properties at the new temperatures, and the loop continues. For the present model, however, dielectric properties are assumed temperature independent, and full coupling is replaced by one-way coupling.

The ANSYS model consists of three steps – preprocessing, processing (solving) and postprocessing. Preprocessing involves geometry and mesh generation, specification of the initial and boundary conditions, and material parameters. Processing includes solving equations (2.1)-

(2.8) under the assumptions aforementioned. Postprocessing is the step at which the results are visualized and further processed. These steps are described in more detail below.

2.2.3 Preprocessing

2.2.3.1 Geometry and Grid Generation

The geometry was created based on a continuous-flow microwave system manufactured by Industrial Microwave Systems (IMS), Inc., Morrisville, NC. The system consisted of the waveguide, the elliptical focusing cavity, and the cylindrical tube containing water (**Figure 2.1**). The IMS system was designed to focus the electric field onto the center of the applicator tube for a more uniform cross-sectional heating of the product. In the system of this specific configuration and under fully developed laminar flow of a Newtonian fluid, the volumes near the tube's center (where the flow rate is high and hence the residence time low) travels through a region of maximum energy, whereas the volumes near the tube's wall (where the flow rate is low and the residence time higher) are exposed to less energy due to the electric field distribution. Under these circumstances every volume of the flowing fluid is expected to receive a nearly identical thermal treatment during its respective residence time due to the energy field distribution closely matching the parabolic velocity profile of the fluid.

For the electromagnetic analysis, the geometry was discretized with a mesh of tetrahedral elements (HF119), coarser in the waveguide and elliptical cavity (element size 30 mm), and finer in the applicator tube (element size 2 mm). Mesh quality was checked with the ANSYS mesh tool: the mesh was refined until the results did not change further. At the interface of the elliptical cavity and the applicator tube gradual transition from large elements to small elements was adapted by ANYSY mesh tool to accommodate the difference in mesh sizes. For the FLOTRAN CFD analysis, tetrahedral elements (FLUID142) were applied to the applicator tube

to model the steady-state fluid flow/thermal phenomenon. A denser element grid was applied near the tube's walls since higher heating rates as well as a velocity boundary layer was expected there. A MESH200, a "mesh-only" element (with no degrees of freedom, material properties, real constants, or loadings), was applied to the waveguide during multi-step meshing for the FLOTRAN CFD analysis, where the heat and momentum equations were not solved.

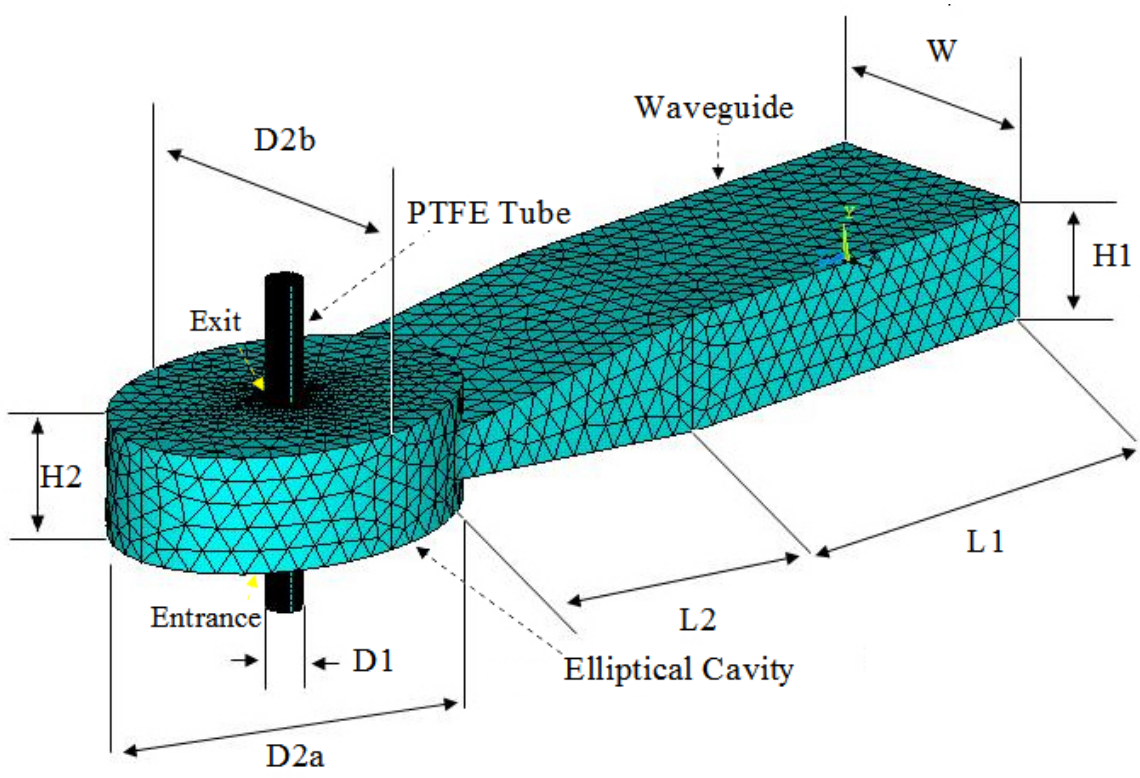

Symbol	Value, mm
D1	38.0
D2a	406.0
D2b	305.0
W	248.0
H1	124.0
H2	124.0
L1	463.5
L2	343.0

Figure 2.1 Continuous flow focused microwave system geometry after meshing

2.2.3.2 Material Properties

Dielectric and thermo-physical properties of water at room temperature were obtained from literature; they were assumed to be constant with temperature (**Table 2.1**).

Table 2.1 Dielectric and thermo-physical properties of water at room temperature

Parameter	Value	Source
Dielectric constant ε' at 915 MHz	71.56	(Komarov and Tang, 2004)
Dielectric loss ε'' at 915 MHz	3.24	(Komarov and Tang, 2004)
Density ρ, kg/m^3	981.7	(Choi and Okos, 1986)
Specific heat C_p, J(/kgK)	4185.8	(Choi and Okos, 1986)
Thermal conductivity k, W/(mK)	0.7	(Choi and Okos, 1986)
Viscosity μ, Pa·s	0.69×10^{-3}	(Geankoplis, 1993)

2.2.3.3 Boundary-Conditions

Maxwell's equations were solved in High Frequency Electromagnetic Module under the following conditions. Microwave energy was supplied to the cavity by means of the dominant TE_{10} mode at a frequency of 915 MHz. A rectangular port was set at the waveguide interfacing the generator; the port was designed such as to appear transparent to the energy reflected back due to a mismatch between the impedance of the waveguide and that of the cavity with a lossy material. The walls of the waveguide were assumed to be perfect conductors. The PTFE tube (ε_r = 2.56-j0.0001, Balbastre et al., 2006) was assumed transparent to microwaves and hence assumed negligible in thickness.

When working with FLOTRAN CFD Module, the flow was assumed laminar with an initial mean velocity of 0.015 m/s and 0.03 m/s corresponding to a flow rate of 1.0 and 2.0 l/min respectively. The Reynolds numbers for water were calculated based on the mean velocity and were 810 at 1.0 l/min and 1620 at 2.0 l/min; zero velocity was applied at the walls. The inlet temperature was set to 25°C and the outlet pressure was set to atmospheric pressure. Adiabatic conditions were applied at the tube's wall (i.e., no heat was assumed exchanged between water and air). The heat generation from the High Frequency Electromagnetic Module was input into

the FLOTRAN CFD Module as a source term in the heat transfer equation. A criterion for convergence was defined as the normalized rate of change of the solution from one global iteration to the next and it was calculated for each degree of freedom (e.g., velocity, temperature, etc.) as follows (ANSYS, 2005);

$$M_{\varphi} = \frac{\sum_{i=1}^{N} \left| \varphi_i^k - \varphi_i^{k-1} \right|}{\sum_{i=1}^{N} \left| \varphi_i^k \right|} \tag{2.9}$$

where M_{φ} is the convergence criterion for degree of freedom, N is the total number of finite element nodes, φ is the degree of freedom, and k is current global iteration number. Convergence was reached when $M_{\varphi} \leq 10^{-9}$ for velocities and pressure, and $M_{\varphi} \leq 10^{-8}$ for temperature.

ANSYS Multiphysics version 9 was used to run the simulation. CPU time required for simulation of the model was 2.5 hrs on a Dell Precision PC with a single 3 GHz Xeon processor with 3GB RAM.

2.2.4 Processing and Postprocessing

First, the electromagnetic analysis was run with the specified material parameters at 915 MHz and the TE_{10} mode in the rectangular waveguide. The dissipated power in each element was calculated from the root-mean-square (rms) electric field values and the properties of the material occupying the element. Next, the dissipated power was uploaded into the FLOTRAN CFD Module where the velocity and temperature were found by solving the momentum and the heat equations.

Electromagnetic power, temperature and velocity profiles were traced as functions of space using the ANSYS postprocessing tools. The distributions were assessed as functions of distance from the entrance into the cavity as well as a function of the tube's radius.

2.3 Results and Discussion

2.3.1 Electromagnetic Power Density

In **Figure 2.2**, electromagnetic energy absorbed by water in the form of heat is expressed as power per unit volume for each element in the model. It can be observed that the radial profile of the energy distribution is consistent with a Mathieu function (with one zero between the center and the side of the tube) which emerges when solving Maxwell's equations in an elliptical cavity (Komarov and Yakovlev, 2007). The higher energy density at the center of the tube corresponded to the higher velocity of the fluid in the same region under the laminar flow conditions. With the 5 kW input power, the values of the electromagnetic power density ranged from 5.84×10^4 to 4.54×10^7 W/m^3. The amount of absorbed microwave energy for water was 24%.

2.3.2 Temperature

The average temperature in the water as a function of distance traveled in the applicator tube was computed for two flow rates, 1.0 and 2.0 l/min (**Figure 2.3**). The results were used to assess the effect of flow rate on the heating profile.

2.3.2.1 Variation in Average Temperature as a Function of Flow Rate

The average exit temperatures were found to be 42°C and 34°C for 1.0 l/min and 2.0 l/min respectively. By doubling the flow rate, the temperature change between the outlet (average exit temperature) and the inlet was roughly halved, from 17°C to 9°C.

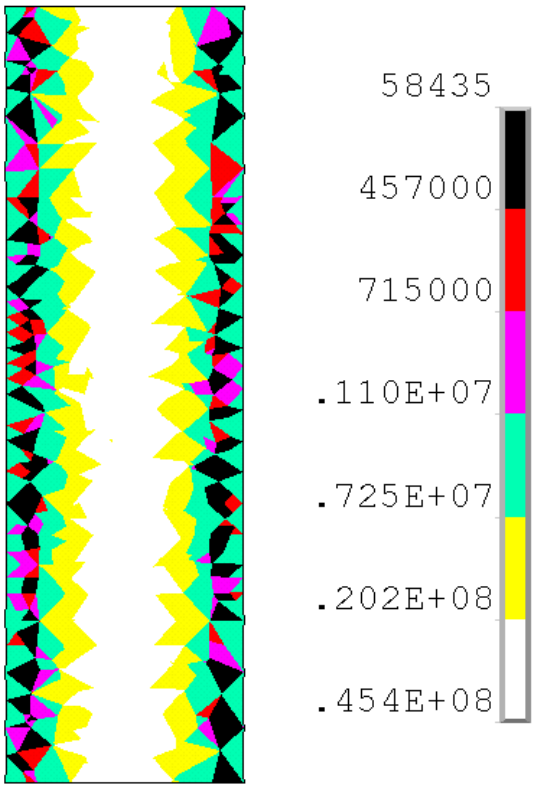

Figure 2.2 Electromagnetic power density (W/m^3) for water

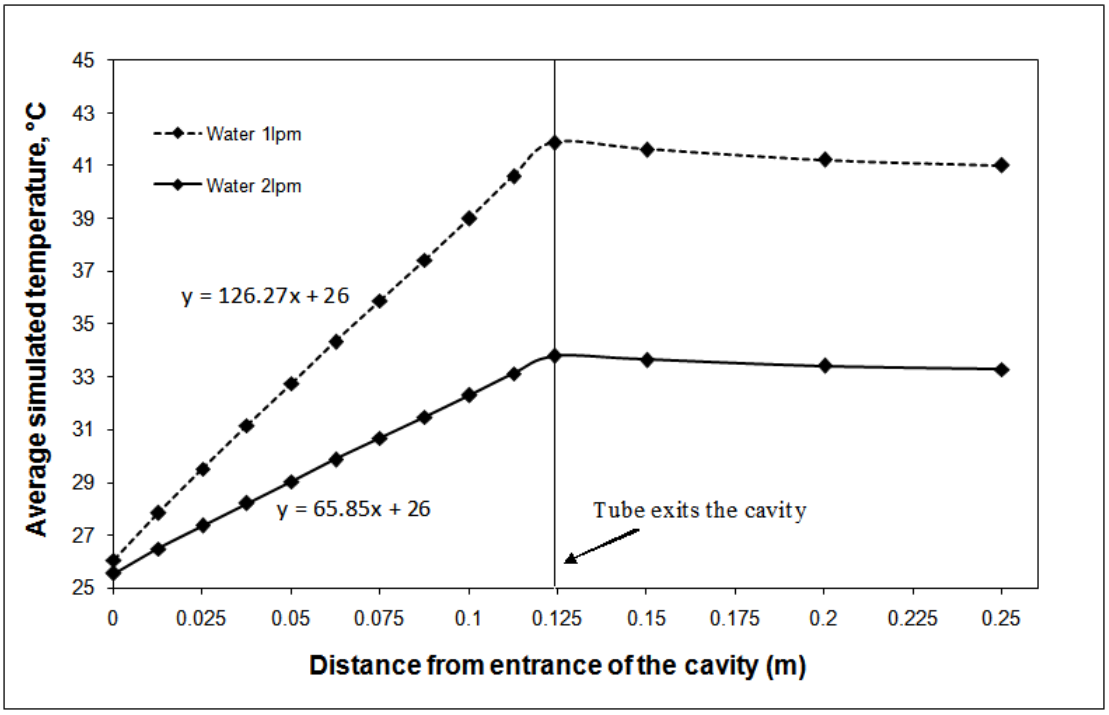

Figure 2.3 Average simulated temperature (^{o}C) in the fluid with distance from entrance in the tube

This result was expected: in the present numerical model the dielectric properties were considered constant with temperature, and therefore the electric field distribution and subsequently the power density did not change when the volumetric flow rate and the corresponding velocity profile did change. It immediately follows that, for water at the flow rates studied, the temperature change between the entrance and the exit approximately doubled when the flow rate was halved (**Figure 2.3**), as a direct consequence of the reduced (halved) residence time of fluid volumes in the microwave cavity.

2.3.2.2 Variation in Temperature as a Function of Distance from the Entrance

An increase in the fluid temperature from the entrance of the applicator in the cavity to the exit (0 mm to 124 mm, **Figure 2.1**) was clearly observed in the region where the flowing fluid was exposed to microwave energy (**Figure 2.3**). These temperature profiles were a direct result of the energy density characteristics consistent with the parabolic velocity profile specific to a fully developed Newtonian flow. A linear increase in temperature was observed with distance towards the point where the fluid exits the cavity, suggesting that the temperatures were linearly dependent on the residence time of the fluid volumes in the cavity. After the exit, the fluid was no longer exposed to microwaves; a slight temperature decrease was observed because of the heat lost through the exit opening.

The temperature distributions in the tube in the vertical *xy*–plane where the water was exposed to microwaves are shown in **Figure 2.4** for the two flow rates studied. Cold spots of less intensity were observed at the lower velocity as the fluid was allowed a longer residence time in the microwave cavity and thus absorbed more electromagnetic energy. Although the power density and the velocity had similar profiles, their magnitudes were different with a distinct advantage on the side of the power density.

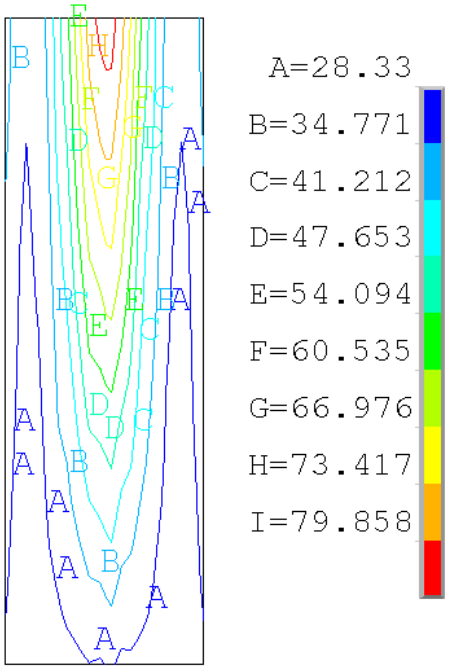

(a)

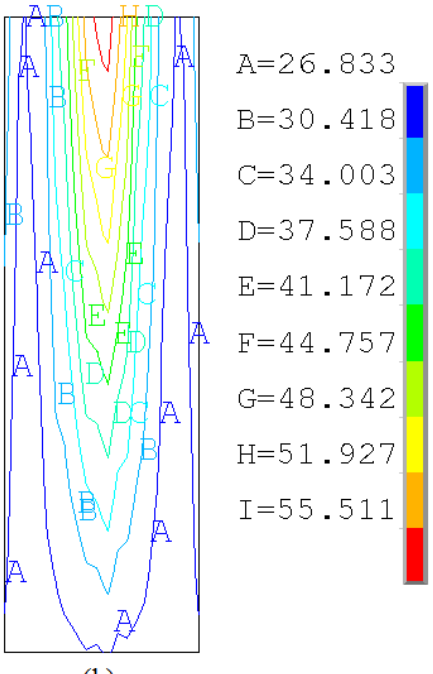

(b)

Figure 2.4 Temperature distribution (^{o}C) in the *xy*-plane for water flowing at the rates of 1.0 l/min (a) and 2.0 l/min (b)

Therefore, higher temperatures were observed in the center of the tube, with the difference being more pronounced as the fluid traveled in the *y*-direction. In other words, the uniformity of the temperature field in the radial direction decreased with the increase of the distance from the entrance to the exit of the cavity (**Figure 2.1**). The hot region near the tube's walls was observed as a result of the energy distribution (Mathieu function with one zero inside the tube wall) overlapping the parabolic velocity profile in the laminar flow (with zero value at the wall).

2.3.2.3 Radial Distribution of the Temperature

Figures 2.5, **2.6**, and **2.7** represent the spatial temperature distribution in the water in the *xz*-plane at different levels with respect to the entrance of the microwave cavity (**Figure 2.1**) for the two flow rates. The scales shown on the right of the contour plots are different for different plots for a better distinction between different contours; to improve readability of the plots, the contours are also marked by letters corresponding to each level on the scale.

The cold region observed in the fluids at the entrance ($y = 0$) of the microwave cavity (**Figure 2.5**) appeared to be ring-shaped (though not well-developed). As the fluid traveled further in the cavity, it absorbed microwaves and the area of the cold region was reduced to a horseshoe-shaped cold spot (**Figures 2.6** and **2.7**). Cold spots of less intensity were observed at the lower velocity due to the less residence time of the fluid in the microwave cavity at the higher flow rates.

The highest temperature regions were achieved near the center of the tube, followed by progressively lower temperature regions as the radial distance from the center increased, and finally followed by a slightly higher temperature region near the wall (**Figures 2.5**, **2.6**, and **2.7**).

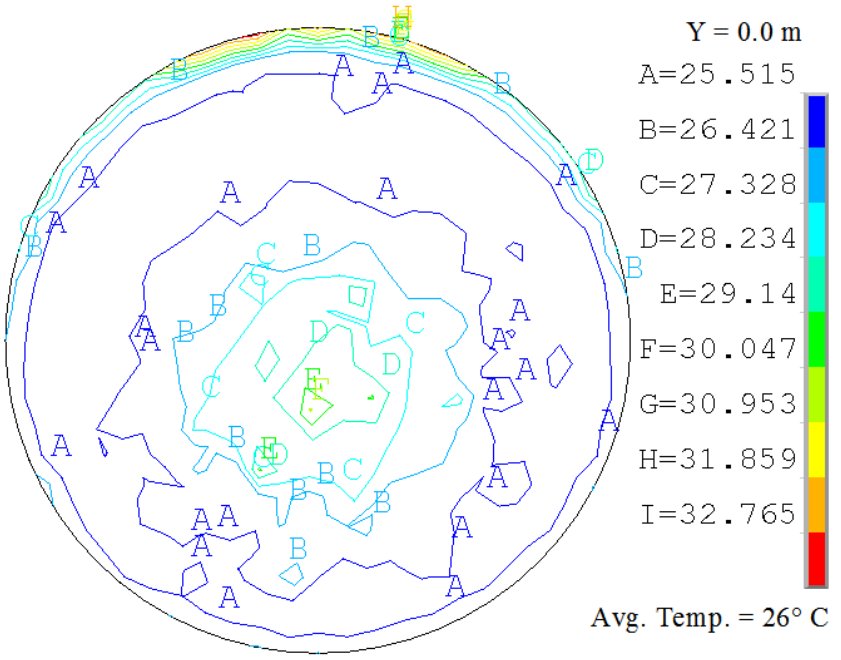

(a)

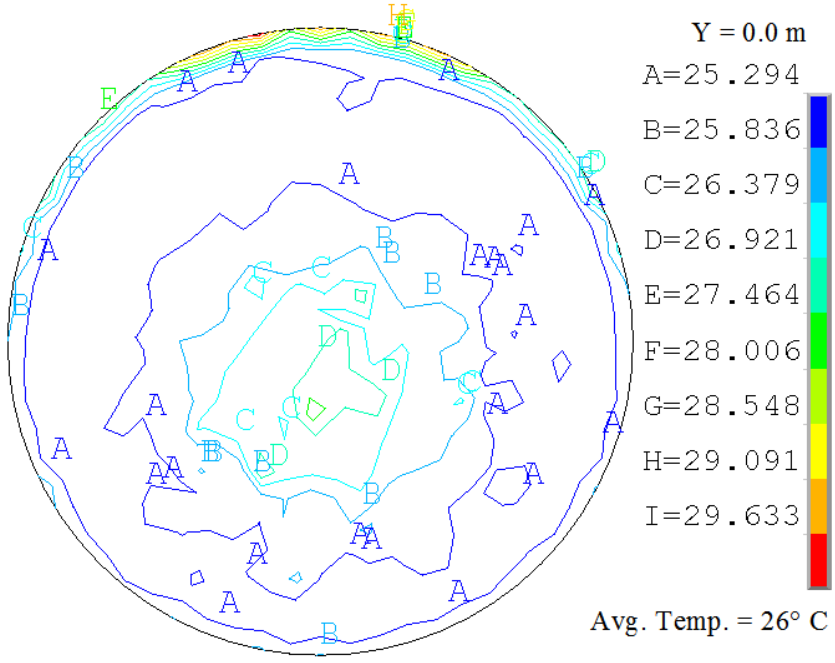

(b)

Figure 2.5 Spatial temperature distribution (^{o}C) in the *xz*-plane for water flowing at the rate of 1.0 l/min (a) and 2.0 l/min (b) at the level $y = 0$ (entrance of the cavity)

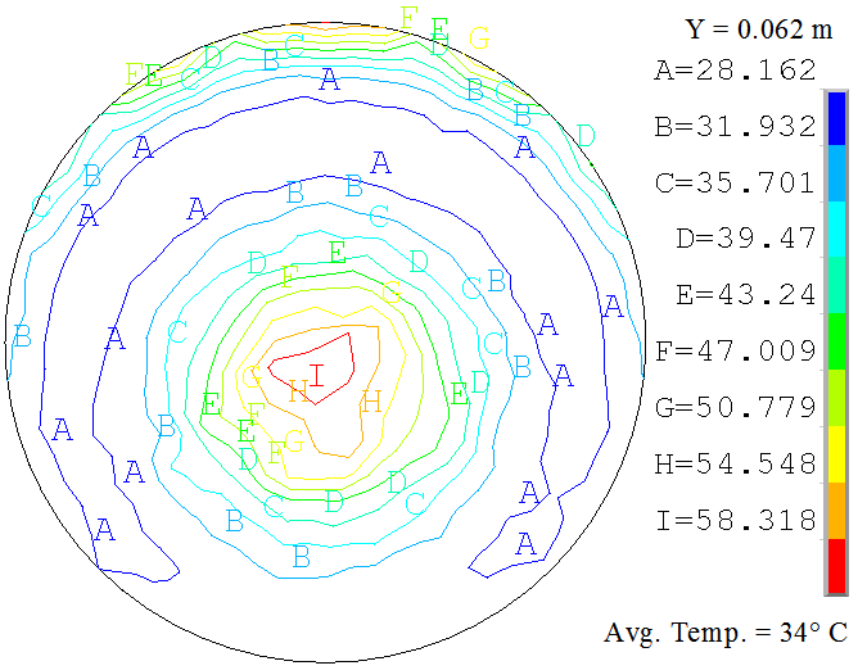

(a)

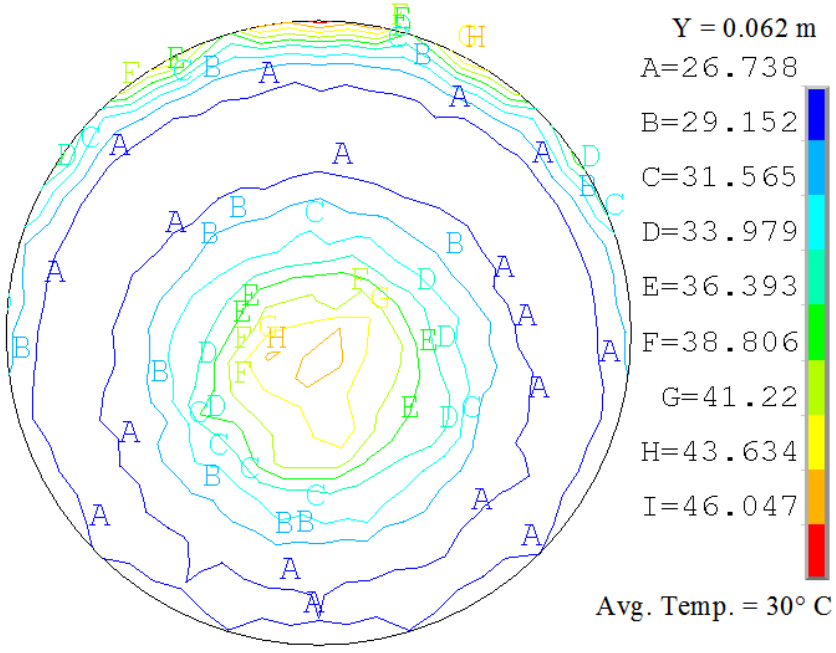

(b)

Figure 2.6 Spatial temperature distribution (^{o}C) in the *xz*-plane for water flowing at the rate of 1.0 l/min (a) and 2.0 l/min (b) at the level of y = 62 mm from the entrance of the cavity

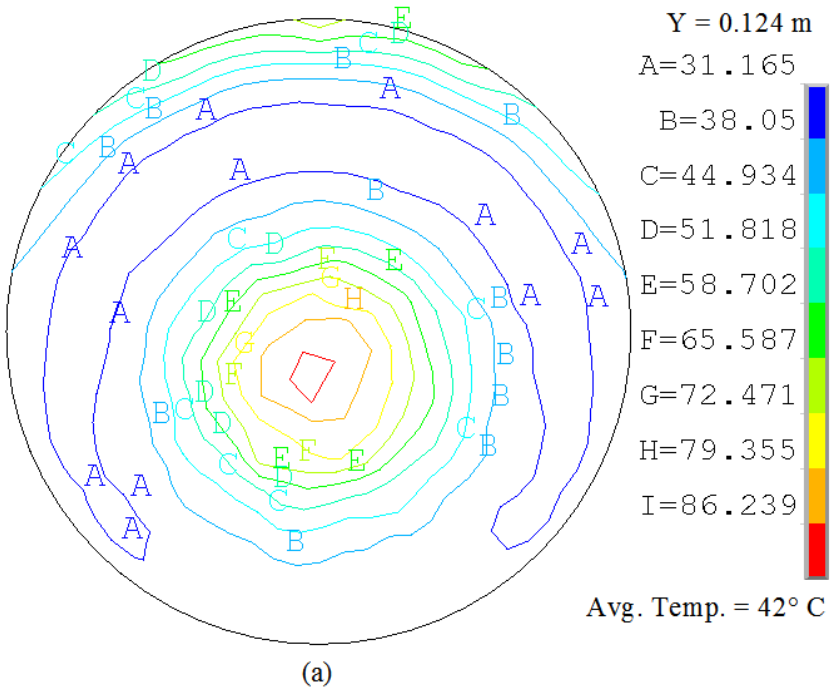

(a)

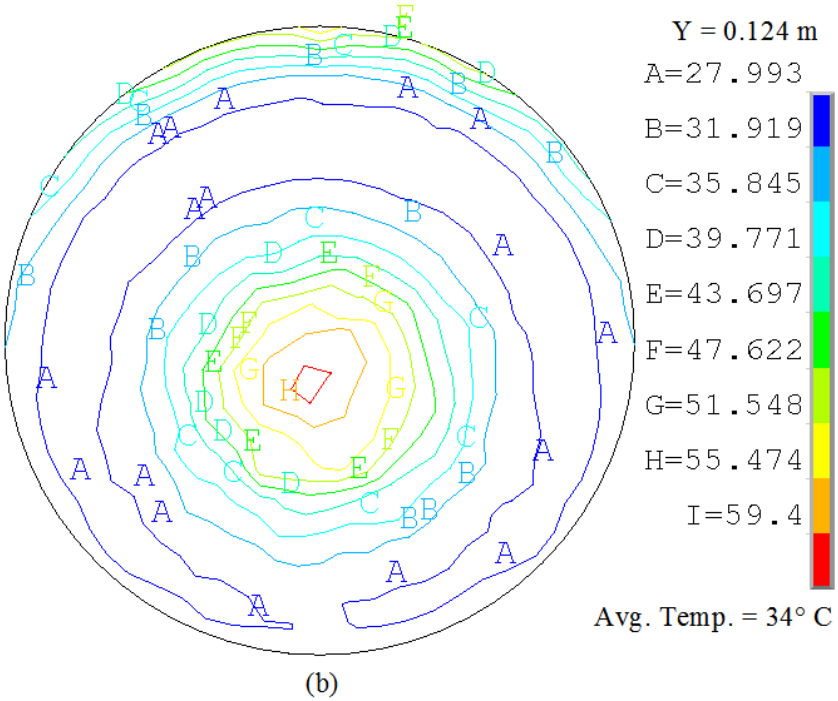

(b)

Figure 2.7 Spatial temperature distribution (^{o}C) in the *xz*-plane for water flowing at the rate of 1.0 l/min (a) and 2.0 l/min (b) at the level y = 124 mm (exit of the cavity)

Similar temperature distribution patterns in the *xy*- and *xz*-planes showing a hot temperature region slightly off center and at the tube wall were predicted by the numerical model for continuous-flow microwave heating by Zhu et al., (2007b). The similarity in the temperature patterns between the two studies was expected because same geometry microwave system was used in both studies; the temperature values could not be compared however because of different materials processed.

Figure 2.8 illustrates more clearly the radial temperature distribution in the heated fluid; the radial distribution was plotted along the *x*-axis through the center of the tube at the cavity's exit (y = 124 mm). The highest temperatures at the center corresponded to the highest energy density created through the design of the microwave system which focuses the electric field in the center of the tube. The region of lowest temperatures corresponded to the area where the intensity of the electric field (described by the Mathieu function) and the energy density profile was near zero (**Figure 2.2**). The secondary higher temperature region near the wall corresponded to the increased power density which in this case was not sufficiently compensated by the almost zero velocity of the fluid near the wall.

2.3.3 Validation

Experimental validation of the results produced by the model presented in this paper is described in detail in Salvi et al., (2008) for a continuous flow and a similar focused microwave system with different dimensions of the cavity. Numerical and experimental axial temperature profiles in the center of the tube for salt water of two different salinities show that the experimental and numerical values of temperature are in a good agreement with the average absolute error of 3.9 ^{o}C for fresh water and 3 ^{o}C for salt water (**Figure 2.9**).

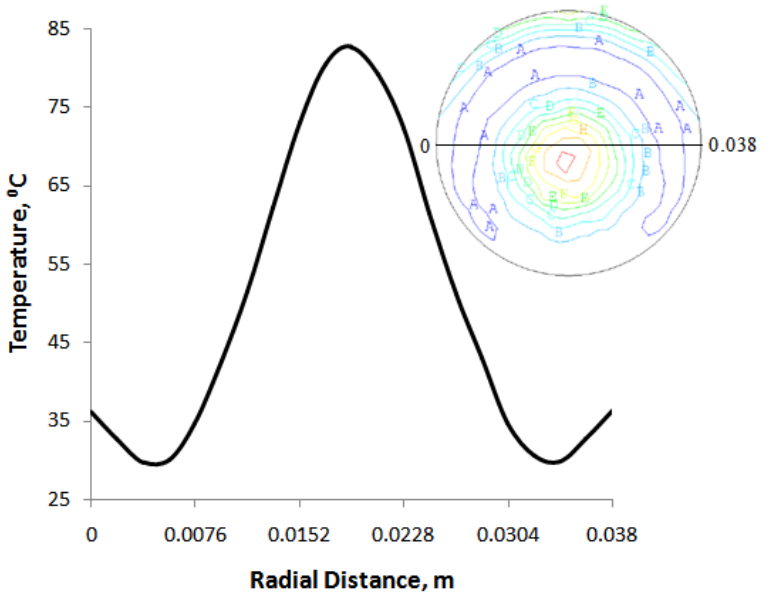

(a)

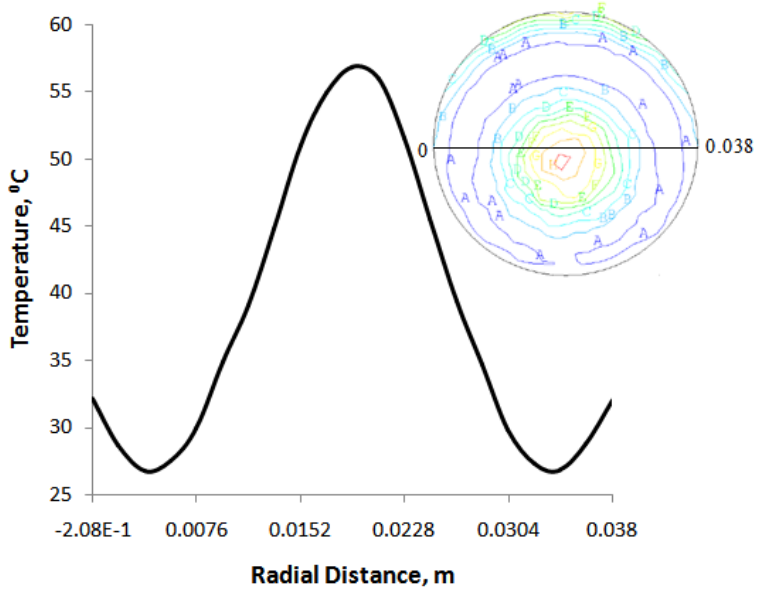

(b)

Figure 2.8 Temperature variation (^{o}C) along the radial distance for water flowing at the rate of 1.0 l/min (a) and 2.0 l/min at the level y = 124 mm (exit of the cavity)

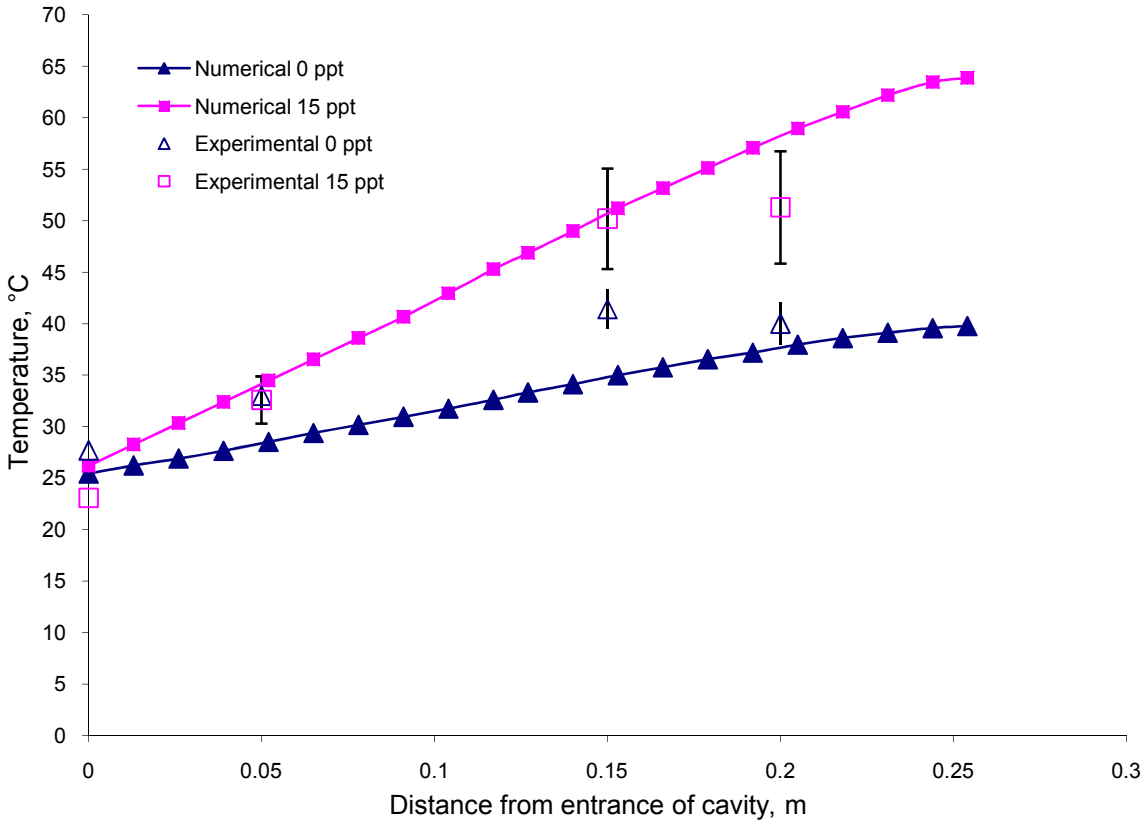

Figure 2.9 Experimental and numerical temperature in the center of the tube for water of two salt concentrations heated continuously in a 4.5 kW microwave system at the flowing rate 1.6 l/min (adapted from Salvi, et. al, 2008)

2.4 Conclusion and Future Studies

The model presented in this paper represents an original attempt to couple electromagnetism, heat transfer, and fluid flow in the ANSYS Multiphysics environment in order to simulate a process of microwave heating. This comprehensive model developed under a number of assumptions can be easily upgraded to incorporate more complex boundary conditions, temperature dependent electromagnetic and physical properties, and other physical phenomena (i.e., mass transfer). The model also does not take phase change into account; this limitation is conditioned by the related capability of the FLOTRAN CFD Module used for fluid flow and heat transfer modeling. These issues will be addressed in future developments of the model.

To illustrate operational features of ANSYS Multiphysics, a model was developed to compute temperature, velocity, electric field distribution and power intensity in water flowing along a PTFE tube in a focused microwave system operating at 915 MHz. A notable influence of fluid flow rates on the residence time and thus the temperature distribution in the heated liquid has been detected. It has been observed that the fluid volumes at the center of the tube received more heat and concluded that a slightly higher temperature of water near the tube's wall was caused by the mismatch between the parabolic velocity profile and the Mathieu-type electric field distribution.

While this work has demonstrated general possibilities of creating multi-physics models with ANSYS Multiphysics, further research is needed for more detailed characterization of functionality of the software in solving this sort of coupled problems, comprehensive experimental validation of the developed model and comparison of its results with the output of other modeling packages.

2.5 References

ANSYS Multiphysics (2005). "Documentation for ANSYS Release 9". ANSYS, Inc., Canonsburg, PA, USA, http://www.ansys.com.

Balbastre, J. V., E. Reyes, M.C. Nuno, C. Plaza (2006). "Design guidelines for applicators used in the microwave heating of high losses material". In: *Advances in Microwave and Radio Frequency Processing,* M. Willert-Porada (Ed.), Springer Publications, 31-38,

Bird, R. B., W.E. Stewart and E.N. Lightfoot (1960). *Transport Phenomenon*, Wiley Publications.

Campanone, L.A. and N.E. Zaritzky (2005). "Mathematical analysis of microwave heating process". *Journal of Food Engineering*, 69, 359–368.

Choi, Y. and M.R. Okos (1986). "Effects of temperature and composition on the thermal properties of foods". In: *Food Engineering and Process Applications, Vol. 1, Transport Phenomenon*. M. Le Maguer and P. Jelen (Ed), Elsevier Publications, 93-101.

Datta, A., H. Prosetya and W. Hu (1992). "Mathematical modeling of batch heating of liquids in a microwave cavity". *Journal of Microwave Power and Electromagnetic Energy*, 27(1), 38–48.

Falqui-Cao, C., Z. Wang, L. Urruty, J. Pommier and M. Montury (2001). "Focused microwave assistance for extracting some pesticide residues from strawberries into water before their determination by SPME/HPLC/DAD". *Journal of Agricultural and Food Chemistry,* 49, 5092-5097.

Geankoplis, C. J. (1993). *Transport Processes and Unit Operations,* McGraw-Hill Publications.

Gerbo, N. M., D. Boldor and C.M. Sabliov (2007). "Microwave heating of pumpable fluids using IR imaging and fiber optic technology". *Journal of Microwave Power and Electromagnetic Energy.* (Submitted).

Komarov, V.V. and J.M. Tang. (2004). "Dielectric permittivity and loss factor of tap water at 915 MHz". *Microwave and Optical Technology Letters,* 42 (5), 419-420.

Komarov, V.V. and V.V. Yakovlev (2001). "Simulations of components of microwave heating applicators by FEMLAB, MicroWaveLab and QuickWave-3D". *Proc. 36th Microwave Power Symposium. San Francisco, CA*, 1-4.

Komarov, V.V. and V.V. Yakovlev (2007). "CAD of efficient TM_{mn0} single-mode elliptical applicators with coaxial excitation". *Journal of Microwave Power and Electromagnetic Energy,* 40(3), 174-185.

Metaxas, A.C. and R.J. Meredith (1983). *Industrial Microwave Heating*, Peter Peregrinus Publications.

Mudgett, R. E. (1986) "Microwave properties and heating characteristics of foods". *Food Technology*, 40 (6), 84-93.

Le Bail, A., T. Koutchma and H.S. Ramaswamy (2000). "Modeling of temperature profiles under continuous tube-flow microwave and steam heating conditions". *Journal of Food Process Engineering*, 23, 1-24.

Lin, Y.E., R.C. Anantheswaran and V.M. Puri (1995). "Finite element analysis of microwave heating of solid foods". *Journal of Food Engineering*, 25, 85-112.

Ohlsson, T. (1993). "In-flow microwave heating of pumpable foods". In: *Developments in Food Engineering: Proceedings of the 6th International Congress on Engineering and Food*, 322-324.

Oliveira, M.E.C. and A.S. Franca (2002). "Microwave heating of foodstuffs". *Journal of Food Engineering*, 53, 347–359.

Pandit, R.B., and S. Prasad (2003). "Finite element analysis of microwave heating of potato—transient temperature profiles". *Journal of Food Engineering*, 60, 193–202.

Ratanadecho, P., K. Auki and M. Akahori (2002). "A numerical and experimental investigation of the modeling of microwave heating for liquid layers using a rectangular wave guide (effects of natural convection and dielectric properties)". *Applied Mathematical Modeling*, 26, 449–472.

Regier, M. and H. Schubert (2005). "Introducing microwave processing of food: principles and technologies". In: *The Microwave Processing of Foods*, H. Schubert and M. Regier (Ed), CRC Press, 3-21.

Romano, V.R., F. Marra and U. Tammaro (2005). "Modeling of microwave heating of foodstuff: study on the influence of sample dimensions with a FEM approach". *Journal of Food Engineering,* 71, 233–241.

Sabliov, C. M., K.P. Sandeep and J. Simunovic (2004). "High frequency electromagnetism coupled with conductive heat transfer – a method to predict temperature profiles in materials heated in a focused microwave system". In: *The 4th World Congress on Microwave and Radio Frequency Applications,* R.L. Schulz and D.C. Folz (Ed.), 469-476.

Salvi, D.A., D. Boldor, C.M. Sabliov and K.A. Rusch (2008). "Numerical and experimental analysis of continuous microwave heating of ballast water as preventive treatment for introduction of invasive species". *Journal of Marine Environmental Engineering* In press.

Tang J. (2005). "Dielectric properties of foods". In: *The Microwave Processing of Foods*, H. Schubert, and M. Regier (Ed), CRC Press, 21-40.

Yakovlev, V.V. (2000), "Commercial EM codes suitable for modeling of microwave heating - a comparative review". In: *Scientific Computing in Electrical Engineering, Lecture Notes in Computational Sciences and Engineering*, Vol. 18, U. van Reinen, M. Gunther and D. Hecht (Eds.), Springer Publications, 87-96.

Zhang, J. and A.K. Datta (2006). "Mathematical modeling of bread baking process". *Journal of Food Engineering,* 75, 78–89.

Zhou, L., V.M. Puri, R.C. Anantheswaran and G. Yeh (1995). "Finite element modeling of heat and mass transfer in food materials during microwave heating – model development and validation". *Journal of Food Engineering*, 25, 509-529.

Zhu J., A.V. Kuznetsov and K.P. Sandeep (2007a). "Numerical simulation of forced convection in a duct subjected to microwave heating". *Heat Mass Transfer*, 43(3), 255-264.

Zhu J., A.V. Kuznetsov and K.P. Sandeep (2007b). "Mathematical modeling of continuous flow microwave heating of liquids (effects of dielectric properties and design parameters)". *International Journal of Thermal Sciences,* 46 (4), 328-341.

CHAPTER 3

NUMERICAL AND EXPERIMENTAL ANALYSIS OF CONTINUOUS MICROWAVE HEATING OF BALLAST WATER AS PREVENTIVE TREATMENT FOR INTRODUCTION OF INVASIVE SPECIES[2]

3.1 Introduction

Ballast water discharges from oceangoing vessels present a worldwide ecological problem in coastal and inland waters throughout the world because of introduction of nonindigenous invasive species. To address this issue, various methods and technologies have been investigated in the past decade (e.g. Mountfort et al., 2003; Kriesel et al., 2004). Unfortunately, no single ballast water management technique has been proven both effective and environmental friendly in the removal of organisms from ballast tanks due to the complexity and diversity of the micro-organisms and macro-organisms present in the ballast water. Thus, investigations have evolved toward the development of combined systems in which a primary treatment removes the larger material and a secondary treatment kills the microbes. Primary methods include the open sea ballast water exchange (Chase et al., 2004), separation (Parsons and Harkins, 2002; Parsons, 2004) and hydrocyclone methods (Parsons, 2003). Several secondary treatments include heating (Hallegraeff et al., 1997; Oemcke, 1998; Rigby et al., 1999), ultraviolet radiation (Oemcke et al., 2003), ozonation (Dragsund et al., 2001; Oemcke and van Leeuwen, 2004), acoustic methods (ultrasonics) (Sullivan et al., 2002), as well as treatments with various chemical biocides (Bolch and Hallegraeff, 1993; Silva and Fernandes, 2001).

Unlike other chemical, biological, and physical treatments, heat treatment denatures cellular proteins and increases metabolism beyond sustainable levels to kill aquatic organism effectively. An added advantage of this method is the lack of chemical byproducts commonly encountered in biocide/chemical treatment. Ballast water is heated most commonly by using the

[2] Reprinted with permission from the 'Journal of Marine Environmental Engineering'

engine cooling system of the ship (Buchholz et al. 1998), but the treatment is limited by the amount of heat provided by the engines and the corrosion problems associated with heated saline water (Dragsund et al., 2004; Mesbahi, 2004). Continuous-flow, focused microwave heating is more efficient and less time consuming, and can overcome some of the problems associated with traditional heating systems for treatment of ballast water by heating it at the discharge point rather than during the voyage, eliminating potential tank corrosion problems.

Microwaves have been commonly used for heating, reheating (Datta et al., 1992), pasteurization (Ozilgen and Ozilgen, 1991), and sterilization (Coronel et al., 2003; Guan et al., 2003) of liquids. Microwaves cause simultaneous ionic conduction and dipole rotation through their direct coupling to a dielectric material, producing volumetric heating throughout the product. As opposed to conventional convection/conduction heating in heat exchangers, microwave heating avoids overheating at the surface and underheating at the center (Coronel et al., 2003). Microwaves have great potential in microbial destruction by thermal as well as non thermal effect (Woo et al., 2000).

A major drawback of the house-hold batch microwave systems includes lack of temperature uniformity in the heated product, and thus a lack of microbiological safety of the heated product. The use of continuous focused microwave systems can alleviate uneven heating by applying an electric field with a more suitable distribution (i.e. maximum at the center of tube where flow rate is high and minimum at the edges where flow rate is low) to the liquid flowing through the microwave cavity. The advantages of focused microwave systems over batch microwave systems include homogeneous and reproducible treatment if properly optimized, rapid heating to boiling or above boiling (in pressurized systems) temperatures, and no thermal vessel inertia (Falqui-Cao et al., 2001). Monitoring the processing history to ensure the

microbiological safety of the processed product is a major challenge in developing a microwave sterilization process (Guan et al., 2003). Especially for ballast water that carries many invasive species including various bacteria, protozoans, unicellular plants (phytoplankton), and small animals (zooplankton), and viruses (Cohen, 1998), it is important to ensure ballast water treatment effectiveness. Accurate temperature measurement or prediction is needed to confirm sterilization, to ensure the microbiological safety of the processed ballast water and to verify effectiveness of the microwave heating treatment. Fiber-optic sensors and infrared imaging systems have been used to measure temperatures in microwave heating (Gerbo et al., 2007; Guan et al., 2003). Numerical methods including finite element - FEM (Lin et al., 1995; Zhou et al., 1995; Komarov and Yakovlev, 2001; Pandit and Prasad, 2003; Sabliov et al., 2007) and finite difference time domain - FDTD (Le Bail et al., 2000; Ratanadecho, et al., 2002; Zhu, et al., 2007a; Zhu, et al., 2007b) methods have been commonly applied to predict spatial temperature of the product being heated by microwaves.

The main goal of the research was to study temperature distribution in water of different salinities heated in a continuous-flow, focused microwave system at different flow rates in an attempt to understand continuous microwave heating of ballast water. A finite element model was developed to numerically predict the temperature of the water using commercially available software. Out of many available finite element software packages, ANSYS Multiphysics^{TM} was selected because of its ability to couple physical phenomena involved in the microwave heating process, including high frequency electromagnetism, heat transfer, and fluid flow. Three sets of equations were solved, Maxwell's equations to determine the electromagnetic field distribution, Fourier's Energy Balance equation to determine the heat transfer in fluid, as well as Navier-Stokes equation describing the fluid flow. The validity of the numerical solution was checked

against experimental results and both sets of data (numerical and experimental) were used to describe the process of continuous focused microwave heating of ballast water under different processing parameters (i.e. salinity and flow rate).

3.2 Materials and Methods

3.2.1 Ballast Water

Model ballast water consisting of tap (fresh) water with no added salts (0 %) and synthetic sea water (1.5 %) prepared by adding sea salt (Crystal Sea Marinemix™ salt, Marine Enterprises International, Baltimore, MD) to tap water were used in this study. The salinity was measured using an optical refractometer/salinity meter (#C7142, Aquatic Eco-Systems, FL).

3.2.2 Microwave System

A 915 MHz continuous-flow, focused microwave system provided by Industrial Microwave Systems, LLC (NC, USA) was used for the experiments. The system consisted of a 5 kW microwave generator, circulator, water load, power coupler, tuning coupler, connecting waveguide, elliptical focusing cavity and an PTFE (polytetraflouroethylene) applicator tube (3.81 cm diameter and 25.4 cm height). **Figure 3.1** illustrates the most relevant components of the microwave system (waveguide, focusing cavity, and applicator tube).

3.2.3 System Operation and Temperature Measurement

For the experimental validation of the model, tap water (0 %) and saltwater (1.5 %) was pumped through the applicator tube in the microwave cavity at 1.6 lpm, using a variable speed electric (DC) pump (model # 4Z528B, Dayton Electric Manufacturing Co., Lake Forest IL, U.S.A.). The power output of the microwave generator was set at 4.5 kW. Flow rates were measured using a graduated cylinder and a stopwatch. The applicator tube was fixed in place using aluminum fittings at the entrance and exit of the focusing cavity.

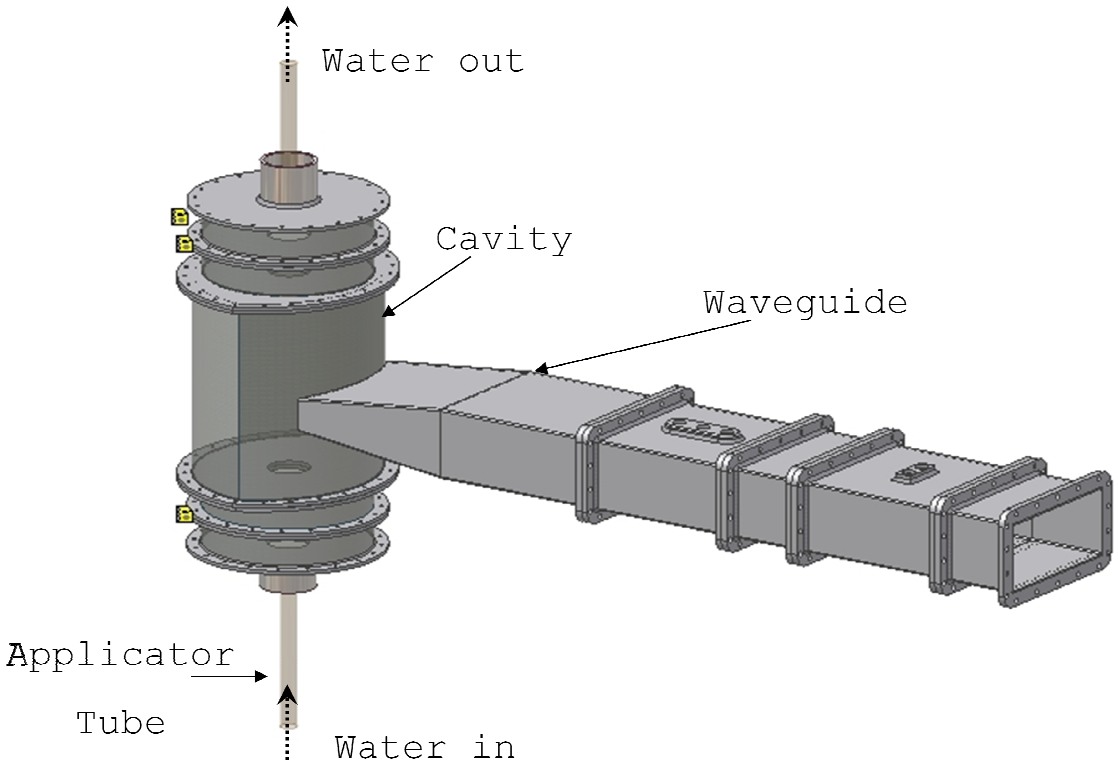

Figure 3.1 Partial rendering of the microwave system (focusing cavity, connecting waveguide, tuning coupler, power coupler). Generator, circulator and water load are not shown

The temperature inside the microwave cavity was measured using a procedure adapted from Gerbo et al. (2007). At both ends of PTFE applicator tube, custom made fittings were inserted to which a string was tensioned. The fittings were designed to hold the string at the center of the tube, and the fiberoptic temperature probes (Neoptix T1, Neoptix Inc., Québec City, Canada) were inserted at different lengths along the axis, with the help of the string (**Figure 3.2**). The temperature probes were inserted at 0, 5, 15 and 20 cm distance form the inlet of the applicator tube in the cavity. All thermocouples were connected to dataloggers (PICO Technologies, Cambrigeshire, UK) to monitor and record the temperature. The experiments were run in triplicate.

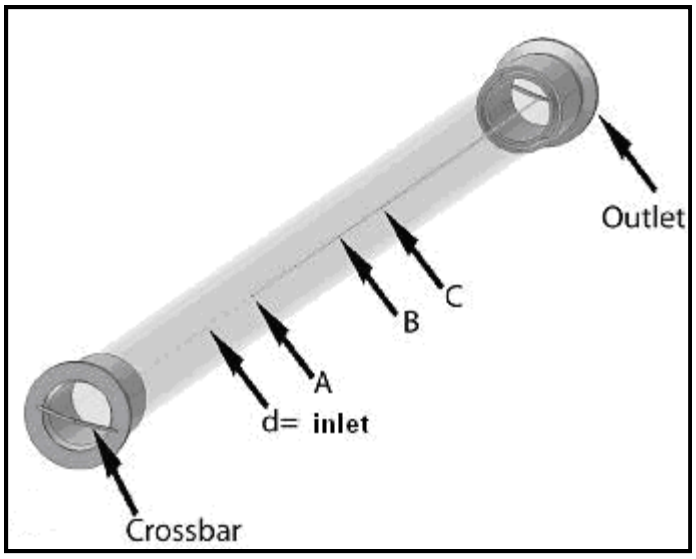

Figure 3.2 Applicator tube with custom made fittings showing the positions of the fiber optic temperature probes along axis (adapted from Gerbo et al., 2007)

3.2.4 Model Development

3.2.4.1 Basic Governing Equations

The heat generation by microwave power in liquid products occurs at molecular level by dipole moment rotation and conduction of ions leading to internal friction. This heat is then distributed by conduction and convection in the liquid. The temperature profile in the material heated by microwaves is given by Fourier's energy balance equation (ANSYS, 2005):

$$\rho_m C_p \left(\frac{\partial T}{\partial t} + \vec{v} \nabla T \right) = Q_{gen} + k \nabla^2 T \qquad (3.1)$$

where, ρ_m is material density (kg/m^3), C_p is specific heat (J/kg.K), k is thermal conductivity, (W/m.K), $\vec{v}$ is velocity (m/s), T is temperature (K) and t is time (sec). The heat generation term Q_{gen} on the right hand side is calculated using (ANSYS, 2005):

$$Q_{gen} = \omega \varepsilon'' \left| \overline{E} \right|^2 \qquad (3.2)$$

where, ω is the angular frequency (rad/s) and ε'' is the relative dielectric loss. The electric field intensity $\overline{E}$ in above equation is calculated by solving Maxwell's equations for electromagnetic heating (ANSYS, 2005).

$$\nabla \cdot \vec{D} = \rho \tag{3.3}$$

$$\nabla \cdot \vec{E} = -\frac{\partial \vec{B}}{\partial t} \tag{3.4}$$

$$\nabla \cdot \vec{B} = 0 \tag{3.5}$$

$$\nabla \cdot \vec{H} = \vec{j} + \frac{\partial \vec{D}}{\partial t} \tag{3.6}$$

where, $\vec{D}$ is electric flux density in C/m^2, $\vec{E}$ is electric field density in V/m, $\vec{B}$ is magnetic flux intensity in Wb/m^2, $\vec{H}$ is magnetic field intensity in A/m, ρ is electric charge density in C/m^3, $\vec{j}$ is electric current density in A/m^2, and t is time in sec.

The Navier – Stokes equation for momentum balance in fluid flow and the continuity equation (below) were solved simultaneously with the heat transfer equation, and coupled iteratively with Maxwell's equations (ANSYS, 2005):

$$\rho_m \frac{D\vec{v}}{Dt} = \rho_m g + \mu \nabla^2 \vec{v} - \nabla P \tag{3.7}$$

$$\nabla \cdot \vec{v} = 0 \tag{3.8}$$

where, ρ_m is density (kg/m^3 – assumed constant), μ is dynamic viscosity of Newtonian fluid (N s/m^2 – assumed constant), ∇P is pressure force on element per unit volume (N/m^2), $\vec{v}$ is velocity (m/s) and g is acceleration due to gravity (m/s^2).

The equations were solved at steady state for Newtonian ballast water under laminar flow conditions (Reynolds numbers N_{Re}≈950 for 1 lpm and N_{Re}≈1500 for 1.6 lpm) in ANSYS Multiphysics™. Some important assumptions were made to reduce the complexity of the problem:

1. Physical and dielectric properties of the fluids were considered constant with temperature;
2. The tube carrying fluid was assumed completely transparent to microwaves;
3. Adiabatic conditions were assumed for the tube such that there was no heat loss through the wall to the surrounding environment; and
4. No phase-change was considered.

3.2.4.2 Code Development in ANSYS Multiphysics™

ANSYS Multiphysics™ is a general purpose finite element software capable of combining analyses from different physics that interact to solve a global engineering problem (ANSYS, 2005). In our case, High Frequency Electromagnetics Module (used to solve high frequency electromagnetism problems) and FLOTRAN CFD Module (used to solve fluid flow and heat transfer problems) were iteratively coupled in ANSYS Multiphysics™ via heat generation term and temperature-dependent properties (**Figure 3.3**).

For electromagnetic analysis, the geometry was created and meshed with a tetrahedral element grid (HF119), coarser in the waveguide and elliptical cavity (element size 0.03m), and finer in the applicator tube (element size 0.005m) in High Frequency Electromagnetic Module (**Figure 3.4**). Material properties were obtained from the literature and were assumed constant with temperature. Dielectric properties for 1.5 % saltwater were calculated by interpolation of data obtained from Ikediala et al. (2002) (**Table 3.1**).

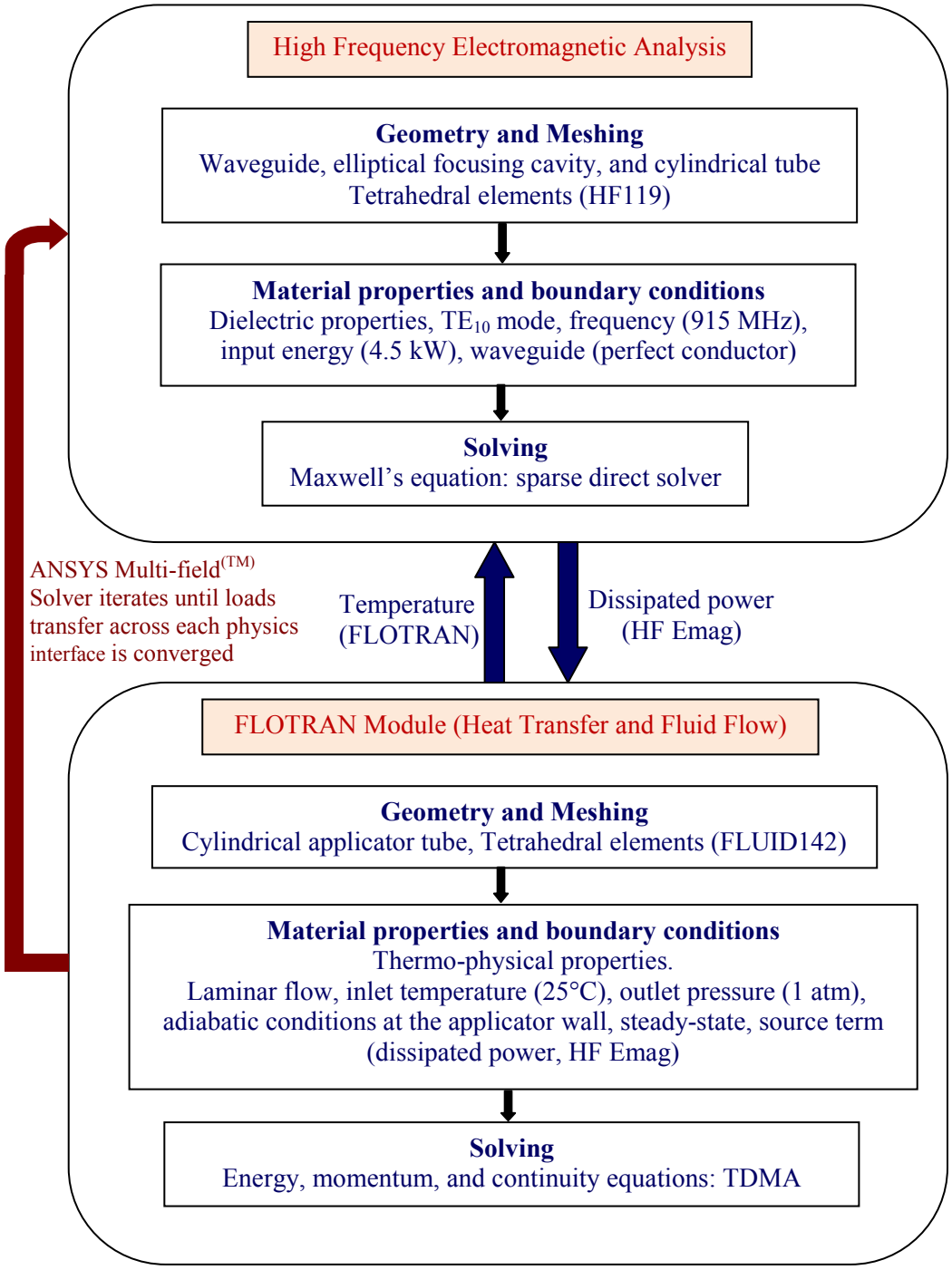

Figure 3.3 Model development in ANSYS Multiphysics™

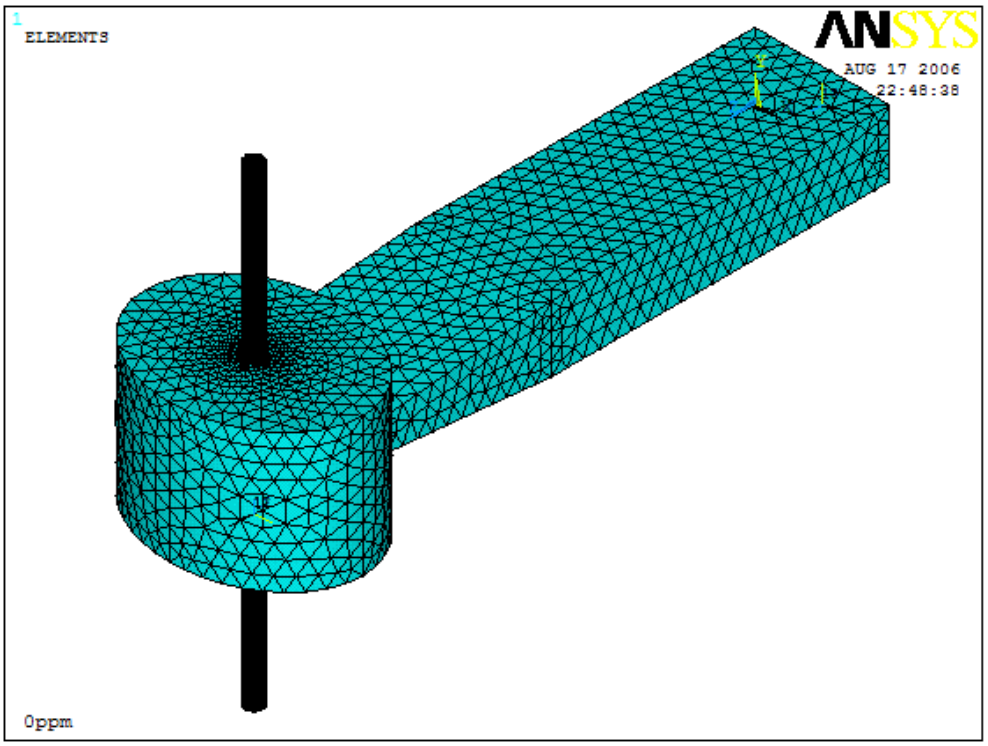

Figure 3.4 Continuous-flow, focused microwave system geometry after meshing

Table 3.1 Dielectric properties of saltwater at 915 MHz at room temperature *

Salt Concentration (%)	ε'	ε''	tan δ
0	78.9*	4.500*	0.0570
0.05	78.1*	21.800*	0.2791
0.10	77.3*	37.200*	0.4812
0.15	76.5	52.086	0.6809
0.20	75.7*	67.100*	0.8864

* Ref: Ikediala *et al.*, 2002

Boundary conditions were applied, including the TE_{10} mode specific to rectangular waveguides, 915 MHz frequency, and 4.5 kW power. The applicator tube was considered transparent to microwaves, and the walls of the waveguide and cavity were set as perfect electric conductors.

Next step involved solving Maxwell's equations using sparse direct solver to calculate the electric field and thus the heat loss in the water. Heat loss or dissipated power was then uploaded in FLOTRAN CFD analysis.

Table 3.2 Physical and thermal properties of water at room temperature.

Property	Value	Reference
Density (ρ), kg/m^3	981.7	Choi and Okos (1986)
Specific heat (*Cp*), J/kg K	4185.8	Choi and Okos (1986)
Thermal conductivity (k), W/mK	0.7	Choi and Okos (1986)
Viscosity (μ) (Pas)	0.69×10^{-3}	Geankoplis (1993)

For the FLOTRAN CFD analysis, applicator tube geometry was meshed with FLUID142 element to model the steady state fluid flow/thermal phenomena; the momentum, continuity, and energy equations were not solved in the waveguide. Physical and thermal properties (**Table 3.2**) were assumed independent of temperature and of equal values for fresh water and saltwater at 1.5 %, knowing that the increase in concentration had a minimum effect on the properties of the water. Boundary conditions included inlet velocities (0.021 m/s at 1 lpm and 0.034 m/s at 1.6 lpm), inlet temperature (25°C), outlet pressure (1 atm), and adiabatic conditions at the applicator wall. Heat generation term (dissipated power) in the energy equation was obtained from the High Frequency Electromagnetic Module. Energy, momentum, and continuity equations were solved using tri-diagonal matrix algorithm (TDMA) in FLOTRAN CFD Module to obtain temperature profiles in the fluid. These temperature profiles were uploaded in High Frequency Electromagnetic Module and solved again repeatedly until the load transfer (heat loss and temperature) between High Frequency Electromagnetic and FLOTRAN CFD Module converged. Iterative solver (ANSYS Multi-field$^{(TM)}$ Solver) was used to achieve the load transfer from one

physics to the other. The electromagnetic power density, temperature, and velocity profiles were plotted as a function of spatial coordinates.

3.3 Results and Discussions

The temperature of water at different salt concentrations (0 and 1.5 %), thus of different dielectric properties, was predicted numerically and the numerical results were validated against experimental data at 1.6 lpm flow rate. The validated model was further used to assess the influence of salinity (0 and 1.5 %) and flow rates (1 and 1.6 lpm) on the temperature profile of synthetic ballast water treated by continuous microwave heating.

3.3.1 Model Validation

Numerical axial temperature profiles in the center of the tube for the saltwater of two different salinities (0 and 1.5 %) flowing at 1.6 lpm were compared with experimental values (**Figure 3.5**). Results showed that the experimental and numerical values of temperature were in good agreement for both salinities, with a minimum difference of 0.5°C between experimental and numerical data for 1.5 % saltwater and a maximum difference of 6.6°C for 0 % saltwater.

The differences between the experimental and numerical data can be explained by the simplifying assumptions made in developing the numerical model, and by the experimental error such as the temperature measurement in the fluid at a certain position (i.e. center of the tube) and measurement of salinity. The numerical temperature predicted in the center of the tube increased linearly with time; in comparison, the experimental temperature increased to a point where a plateau was reached (**Figure 3.5**). This difference was attributed to the change in the dielectric properties as a function of temperature, as follows. For salt water, dielectric loss decreased with temperature (Coronel et al., 2008) which affected the heat generation (eq. 3.2), fact not accounted for by the model, which assumed a temperature independent dielectric loss. Therefore,

the numerical results showed a steady increase in the temperature throughout the cavity, whereas experimental data showed that as the saltwater heated, the temperature leveled after 0.15 m in the cavity, at 50.7°C (**Figure 3.5**). Similarly, a plateau was observed for fresh water at 34.7°C due to the temperature dependence of the dielectric loss (**Figure 3.5**).

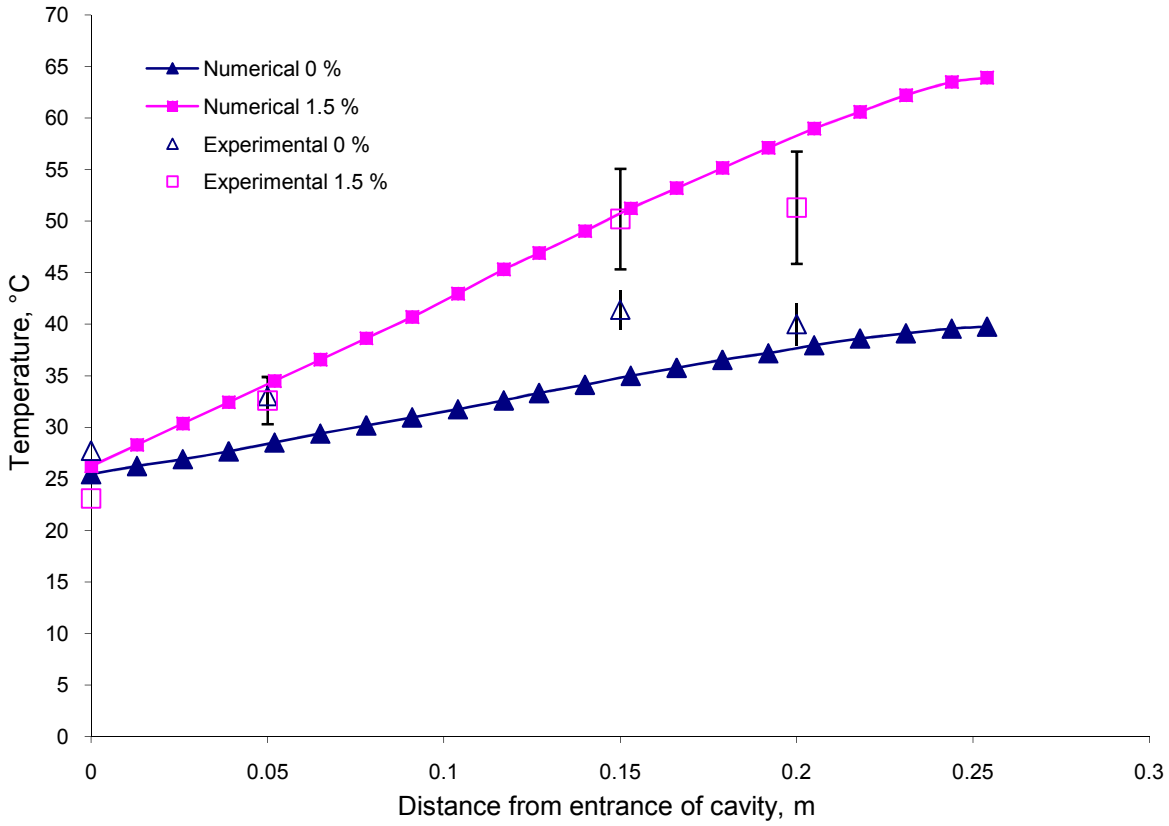

Figure 3.5 Experimental and numerical temperature at the center of the applicator for water at two salt concentrations (0 and 1.5 %) heated continuously at 1.6 lpm in a 4.5 kW microwave system

It was also observed that the temperature of water at 0 % salinity was under-predicted in comparison to experimental results (average absolute error of 3.9°C), whereas the temperature of 1.5 % saltwater was in general over-predicted (average absolute error of 3°C); the average absolute error was defined as the difference between the numerical and the experimental temperature. One of the factors that contributed to the over/under prediction may be the horizontal momentum transfer from hot to cold spots. The flow was considered laminar in the

model (as confirmed by the Reynolds numbers N_{Re}≈950 for 1 lpm and N_{Re}≈1500 for 1.6 lpm); however the flow may have been disturbed by the presence of the experimental temperature measurement setup. Hot spots might have also introduced small vapor bubbles and hence turbulence in the flow. For 0 % water, the hottest spot was off-center, which may have caused horizontal momentum transfer between the hotter regions to the center (**Figure 3.6a and 3.6b**) not accounted for in the model, resulting in an experimental temperature higher than that predicted numerically (**Figure 3.5**). For 1.5 % salt water, the center was located in the highest temperature region (**Figure 3.6c and 3.6d**), surrounded by lower temperature fluid, resulting in horizontal momentum transfer from the center to the surroundings, and hence the experimental temperatures were lower than those predicted by the model (**Figure 3.5**). The heat dissipated to the surrounding environment by convection and radiation from the applicator tube was not captured by the model and may have contributed to the temperature over-prediction for salt water as well. Higher temperature difference between salt water and ambient air (ΔT of 29°C) resulted in heat loss to surrounding and hence experimental temperatures were seen lower than those predicted by the model. Finally, possible experimental errors might have occurred in this study due to small longitudinal deviation of the fiber optic probes from the axis or erroneous measurement of the salinity, and hence the difference observed between experimental and numerical data. As an example, a 5 mm deviation from the center can result in a 4°C difference in the measured temperature (**Figures 3.7 and 3.8**), and a 0.1% error in measuring the salinity may generate a 10% change in dielectric loss (**Table 3.1**). The model was validated solely for below boiling temperatures, since phase change or turbulence induced by boiling were not taken into account by FLOTRAN CFD module.

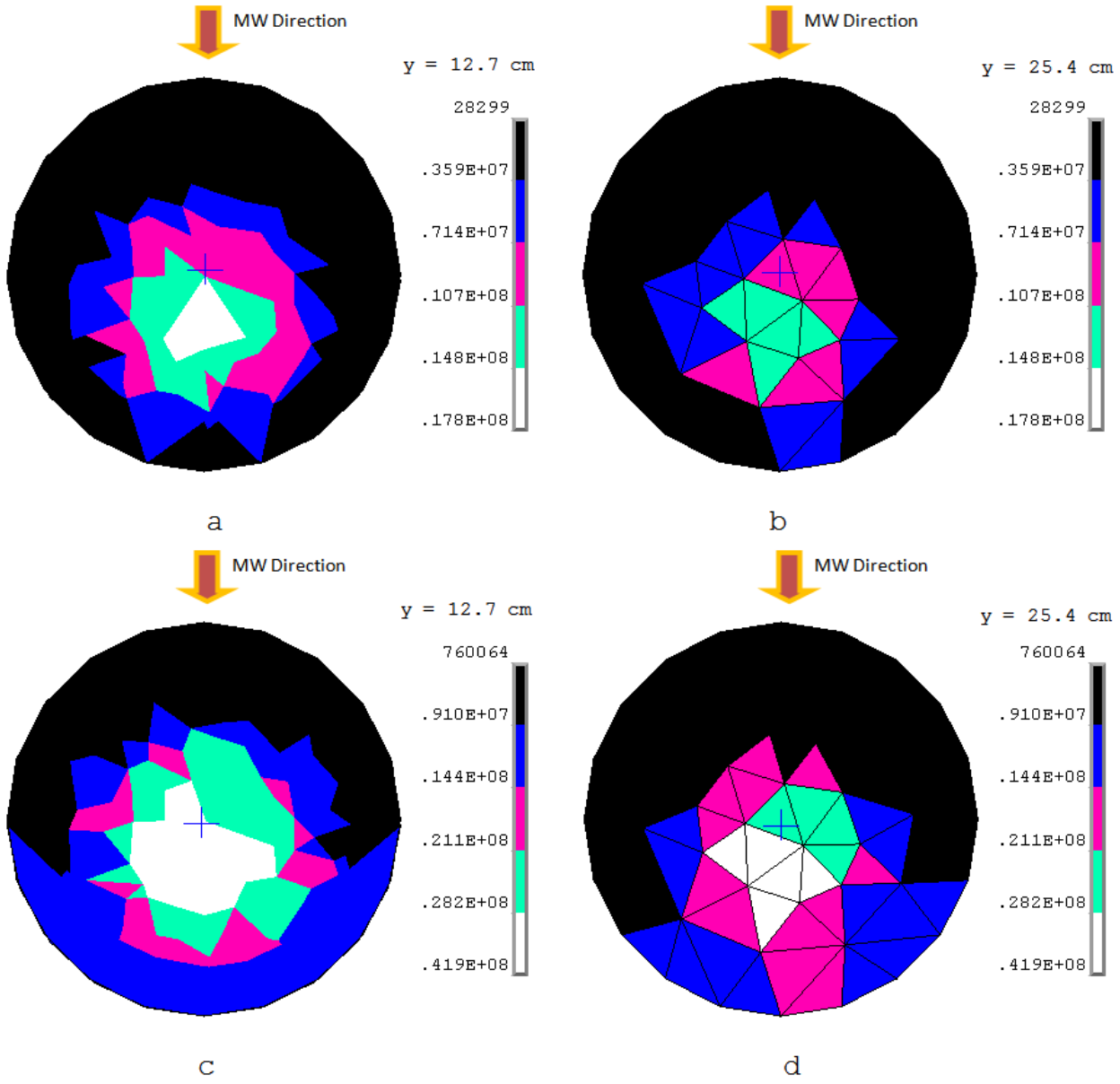

Figure 3.6 Cross-section spatial view electromagnetic power density (W/m^3) for fresh water (0 % salt) at a. *y =12.7 cm (middle)* and b. *y = 25.4 cm (exit)* and for saltwater (1.5 % salt) at c. *y = 12.7 cm (middle)* and d. *y = 25.4 cm (exit)*

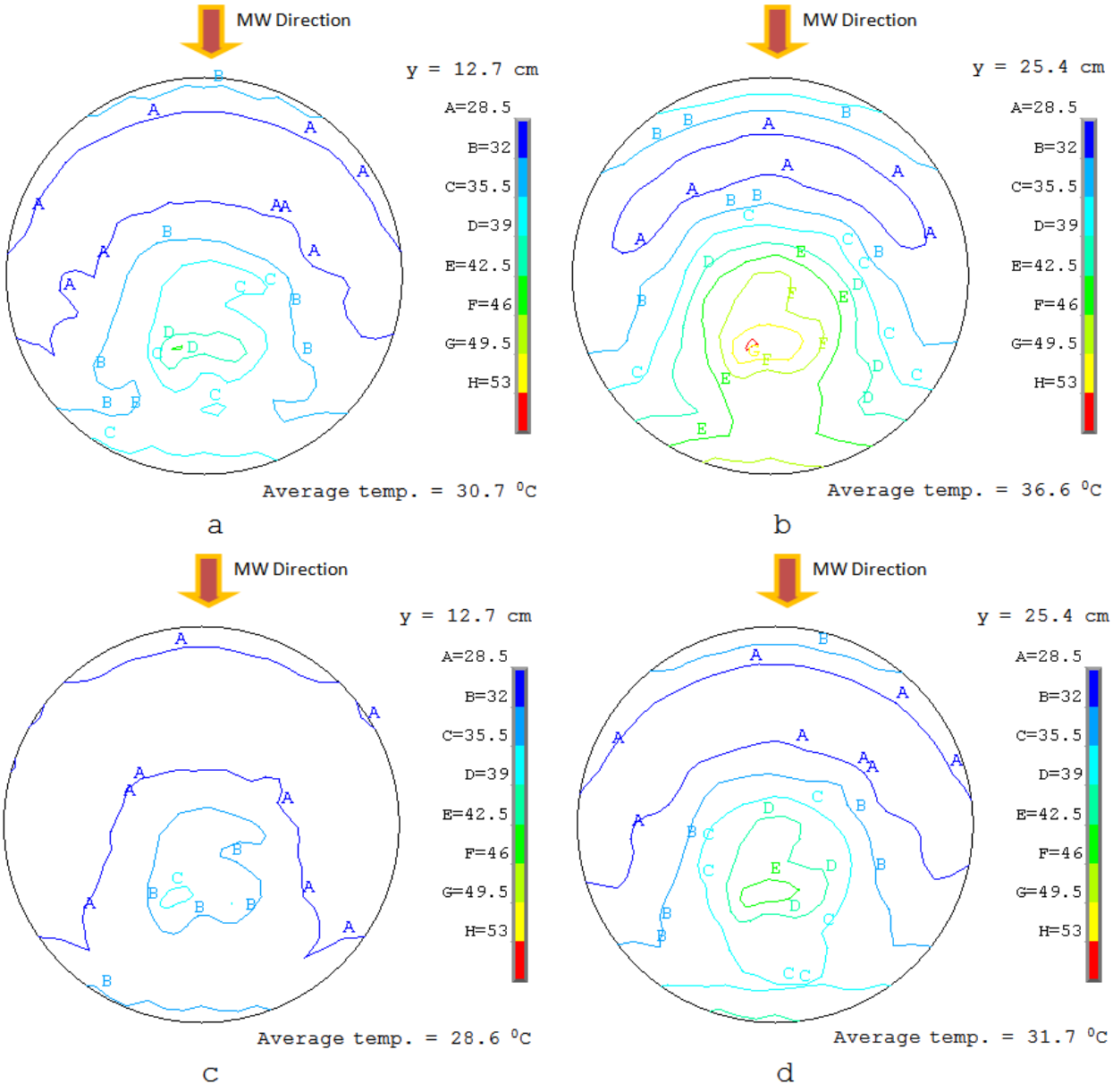

Figure 3.7 Cross-section spatial temperature distribution (x-z plane) for fresh water (0 % salt) heated at 1 lpm at a. *y =12.7 cm (middle)* and b. *y = 25.4 cm (exit)* and at 1.6 lpm at c. *y = 12.7 cm (middle)* and d. *y = 25.4 cm (exit)*

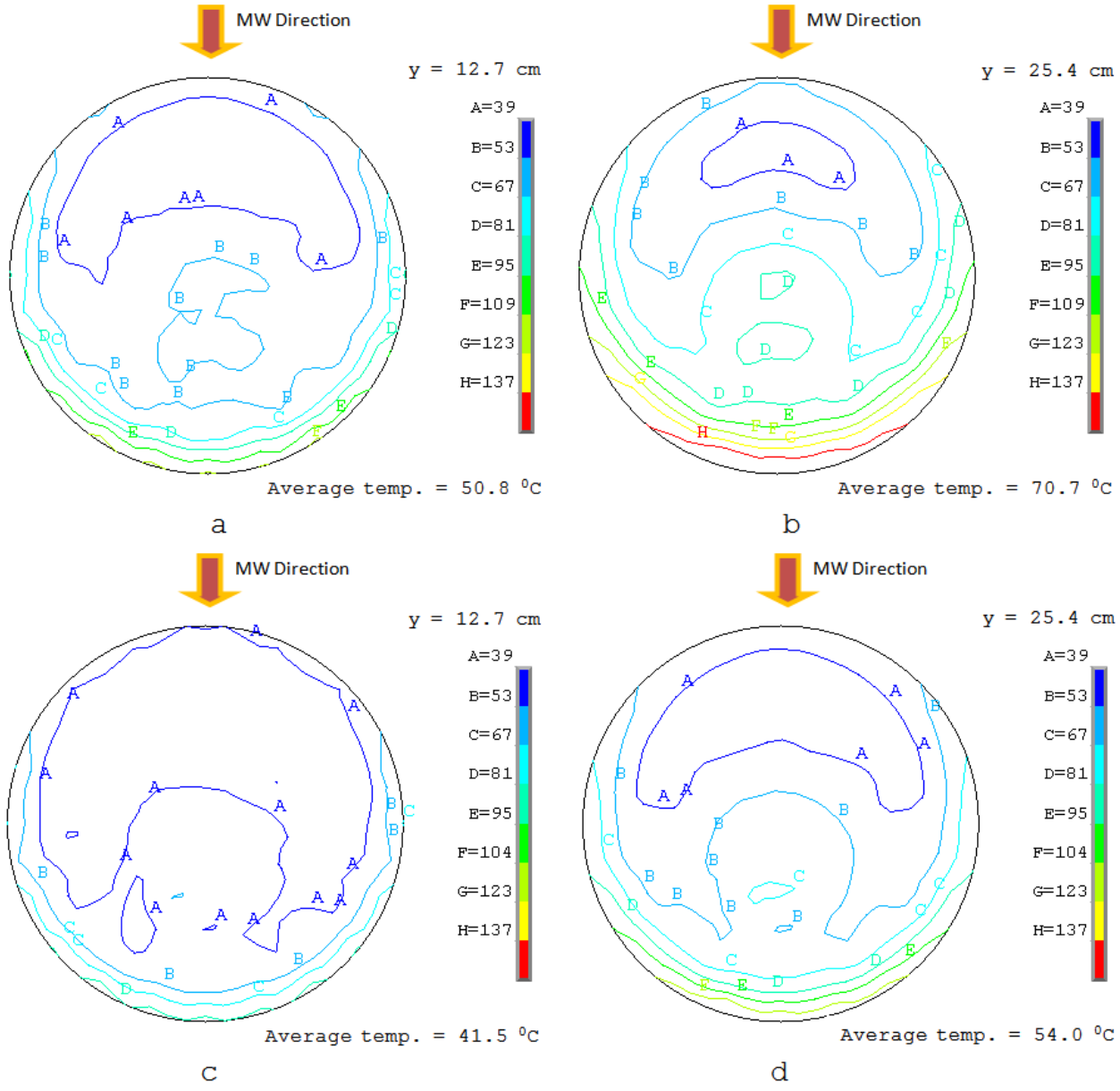

Figure 3.8 Cross-section spatial temperature distribution (x-z plane) for saltwater (1.5 % salt) heated at 1 lpm at a. *y =12.7 cm (middle)* and b. *y = 25.4 cm (exit)* and at 1.6 lpm at c. *y = 12.7 cm (middle)* and d. *y = 25.4 cm (exit)*

Even under these circumstances the model can be used as a tool to understand ballast water treatment and inactivation of ballast water organisms by continuous microwave processing. Some organisms such as microalgae (Nannochloropsis oculata- inactivation temperature 53°C), zooplankton at two different growth stages (newly hatched brine shrimp-Artemia nauplii and adult Artemia- inactivation temperatures 47°C and 43°C), and oyster larvae (Crassosstrea virginica- inactivation temperature 51°C) shown to be completely inactivated at temperatures of 55°C during continuous microwave processing (Boldor et. al, 2008).

Once validated, the numerical model was used to develop an understanding for the continuous microwave heating of ballast water. To reach this goal, temperature and power spatial distributions were studied in different (x-y and x-z) planes, and average temperatures were compared at two salinities (0 and 1.5%) and two flow rates (1 and 1.6 lpm), as follows.

3.3.2 Temperature Distribution in the Cross-axial (x-y) Plane

The cross-axial power loss for fresh water followed a Mathieu function distribution (obtained by solving Maxwell's equations in an elliptical cavity; Komarov and Yakovlev, 2007), with very little heat generated (10^4 W/m^3 order of magnitude) at the tube wall as compared to the center of the tube (10^7 W/m^3 order of magnitude) **(Figure 3.9a)**. The power loss ranged from a minimum of 2.8 x 10^4 W/m^3 to a maximum of 1.7 x 10^7 W/m^3 with a total heat loss of 0.7 kW in the tube. Even though the velocity of the fluid at the center of tube was highest, higher temperatures were observed at the center due to highest electromagnetic heat generation for fresh water. It was interesting to observe that the temperature distribution patterns were similar for water at both flow rates studied (1 lpm and 1.6 lpm) (**Figures 3.9b** and **3.9c** or **Figures 3.10b** and **3.10c**), with higher contour temperature values at the lower flow rate, as expected.

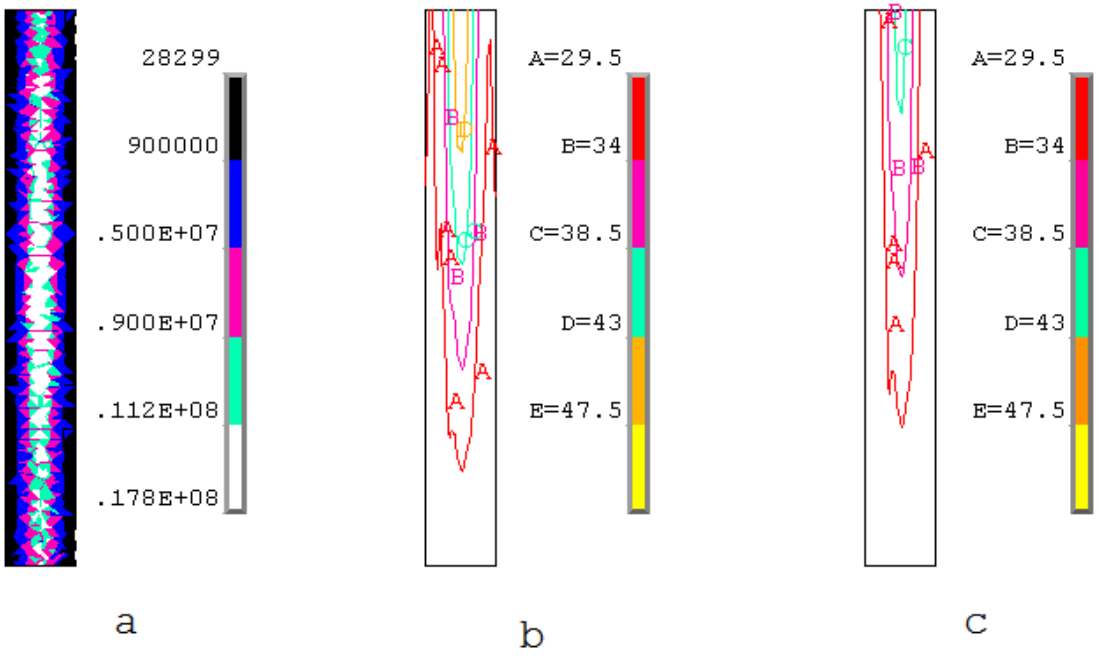

Figure 3.9 Cross-axial (x-y) plane view of a. e*lectromagnetic power density (W/m^3)*; b. *temperature distribution at 1 lpm*; and c. *temperature distribution at 1.6 lpm* for fresh water (0% salt)

For the 1.5 % saltwater a Mathieu-type distribution (with one zero between the center and the side of the tube) of power was observed as well (**Figure 3.10a**). The power density ranged from 7.6 x 10^4 W/m^3 to 4 x 10^7 W/m^3, with a total power loss of 2.5 kW in the tube, more than three times higher than in fresh water; these results were expected considering that saltwater had a higher dielectric loss as compared to fresh water.

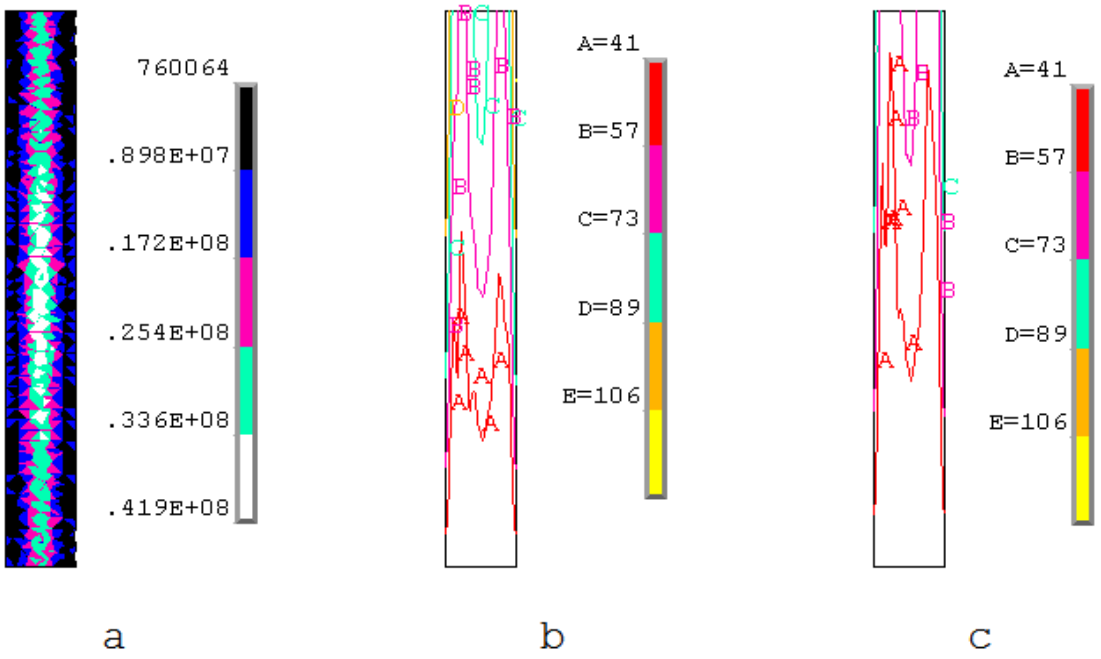

Figure 3.10 Cross-axial (x-y plane) view of a. *electromagnetic power density (W/m^3)*; b. *temperature distribution at 1 lpm*; and c. *temperature distribution at 1.6 lpm* for saltwater (1.5 % salt)

3.3.3 Cross-sectional Spatial Temperature and Electromagnetic Power Density Distribution (x-z plane)

The cross-sectional spatial temperature distribution is most indicative of temperature uniformity in the heated ballast water. Thus, the cross-sectional temperature distribution was studied for ballast water at two locations, 12.7 cm (middle) and 25.4 cm (exit) inside the applicator for both salinities (**Figures 3.7** and **3.8**).

For water with 0 % salt at 1 lpm, the average temperatures in the middle (y = 12.7 cm) and exit (y = 25.4 cm) were 30.7°C and 36.6°C, respectively (**Figure 3.7a** and **3.7b**). This increase was obviously expected as the water traveling through the cavity converted electromagnetic energy into heat. For the same sample at a higher flow rate (1.6 lpm), the average temperature increased from 28.6°C at 12.7 cm into the cavity to 31.7°C at 25.4 cm (**Figure 3.7c** and **3.7d)**. At the

higher flow rate (1.6 lpm) the residence time of the liquid in the microwave cavity decreased thus resulting in less absorption of power and lower temperatures than those achieved at the lower flow rate (1 lpm).

The temperature distribution patterns were similar for water at the same distance into the cavity, regardless of the flow rate for same salt concentration (compare **Figure 3.7a** with **3.7c** or **Figure 3.7b** with **3.7d)**. The diameter of the tube and its position in the cavity were fixed and the dielectric properties of the material were assumed constant, hence the similar temperature distribution patterns. Yet, the temperature range changed when the flow rate was varied: at 1 lpm the temperature was higher than the temperature achieved by the water flowing at 1.6 lpm, because of the higher retention time in the microwave cavity. At 12.7 cm height into the tube, the highest temperature was observed slightly off the center, with a maximum value of 42.5°C at a flow rate of 1 lpm (**Figure 3.7a**) and of 35.5°C at a flow rate of 1.6 lpm (**Figure 3.7c**). At 25.4 cm height, hot spots increased in size and reached 53°C at 1 lpm (**Figure 3.7b**) and 42.5°C at 1.6 lpm (**Figure 3.7d**).

For water with 1.5 % salinity at 1 lpm, in the middle (i.e. y = 12.7 cm) the average temperature was 1.65 times higher than that of fresh water (**Figure 3.7a** and **3.8a)**, while at the exit (i.e. y = 25.4 cm) the average temperature was double that of fresh water (**Figure 3.7b** and **3.8b**). Similarly for 1.6 lpm, average temperature was 1.45 times that of fresh water in the middle of the applicator tube (i.e. y = 12.7 cm) (**Figure 3.7c** and **3.8c)** and 1.7 times that of fresh water at exit (**Figure 3.7d** and **3.8d**).

It was observed that as the loss tangent of the liquid increased from 0.05 to 0.68 with salinity, the temperature distribution pattern changed in a specific manner (**Figure 3.7 and 3.8**).

As the dielectric properties of the liquid in the cavity changed, the relatively hot temperature spot was shifted from off center to the edge of the cylinder (facing away from waveguide).

Spatial distribution of the electromagnetic power density (W/m^3) at different salinities (0 and 1.5 %) at y = 12.7 cm and y = 25.4 cm in the applicator tube can be seen in **Figure 3.6**. Higher power loss density was observed in the middle of the applicator tube (y = 12.7 cm) at both salinities (0 and 1.5 %) as compared to exit (y = 25.4 cm). The waveguide junction with the cavity is located near the middle part of applicator tube, which explains the higher heat generation observed in the middle as compared to the exit of the tube. For 1.5 % saltwater the relative power loss was almost 15 times more than that of fresh water, and thus the total power loss was more than 3.5 times higher (2.5 kW for saltwater vs. 0.7 kW for fresh water).

The power loss distribution determines the temperature distribution; i.e. where greater heat generation was seen in cross-section of the applicator tube, higher temperature contours were observed (compare **Figure 3.6a** with **3.7a** and **3.7c** at y =12.7 cm and **Figure 3.6b** with **3.7b** and **3.7d** at y = 25.4 cm for fresh water), obviously with higher temperature values achieved at lower flow rate. Similarly to fresh water, the cross-sectional temperature profiles for 1.5 % saltwater followed the power distribution profiles (compare **Figure 3.6c** with **3.8a** and **3.8c** at y =12.7 cm and **Figure 3.6d** with **3.8b** and **3.8d** at y = 25.4 cm for saltwater).

3.3.4 Numerical Average Cross-axial (x-z) Temperature Profiles as a Function of Distance Traveled in the Cavity (y)

The numerically modeled average cross-axial (x-z) temperature increased linearly with distance traveled inside the applicator tube (**Figure 3.11**); the temperature increase was affected by the salt concentrations and flow rates. The temperature increased from room temperature to

32°C at 0 % salinity, and to 54°C at 1.5 % salinity at 1.6 lpm flow rate. At 1 lpm flow rate the temperature of water increased to 36°C at 0 % salinity and to 70°C at 1.5 % salinity.

Dielectric properties and incident microwave power are important variables that affected the microwave power absorption and hence the average temperature of the water. For the experimental conditions studied, incident microwave power was constant and there was not much difference (≈3%) in the dielectric constant (ε') for fresh and saltwater. The dielectric loss (ε''), a measure of efficiency of a material to convert microwave energy into heat (Eskilsson and Bjorklund, 2000), was much higher at 1.5 % salinity and hence saltwater achieved higher temperatures as compared to the 0 % salinity water. The higher temperatures achieved at the lower flow rate can be explained by the increased exposure time to microwave radiation in the cavity.

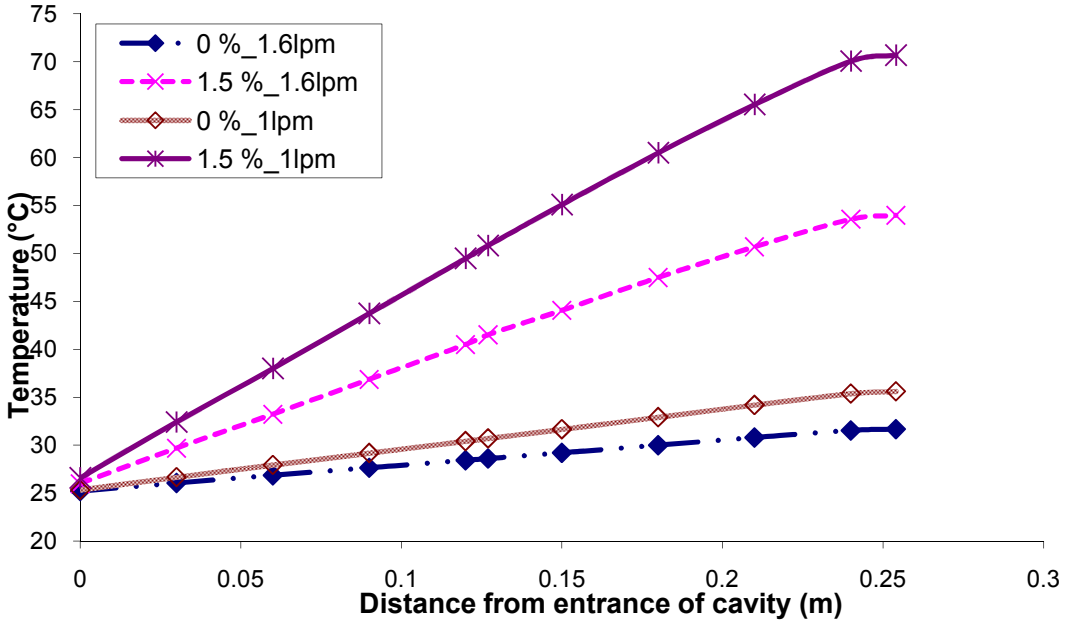

Figure 3.11 Numerical average cross-sectional temperature profile for water at two salt concentrations (0 and 1.5 %) heated continuously in the microwave system at two flow rates (1 lpm and 1.6 lpm)

3.4 Conclusions

A finite element model was developed in ANSYS Multiphysics™ to predict temperature of ballast water undergoing microwave heat treatment. The predicted temperature values were in good agreement with the experimental results for temperatures below boiling. The average absolute errors between the experimental and modeling data were approximately 3°C and 3.9°C for the 0 % and the 1.5 % salinity studies, respectively. The validated model was further used to study temperature distribution at different salinities (0 and 1.5 %) and flow rates (1 and 1.6 lpm). Higher temperatures were observed at lower flow rates and higher salinity. At the higher flow rate, the temperature increased from room temperature to 32°C at 0 % salinity, and to 54°C at 1.5 % salinity. At the lower rate the temperature of water increased to 36°C at 0 % salinity and to 70°C at 1.5 % salinity. Dielectric properties and residence time in the cavity influenced microwave power generation and thus the temperature profile most. For fresh water, the highest temperature region was located slightly off-center, whereas for salt water, the highest temperatures were observed at the edges of the applicator, away from the incident microwaves, following the power loss profiles. The developed model was found useful in understanding the microwave heating process of saline water. The model can be further used to identify optimum parameters (microwave power, dimensions of the applicator tube, flow rates) for complete inactivation of a particular ballast water organism at temperatures below boiling. Improvements of the model planned for the future include addressing temperature-dependent properties, turbulent flow conditions, and phase change.

3.5 References

ANSYS Multiphysics (2005). "Documentation for ANSYS Release 9". ANSYS, Inc., Canonsburg, PA USA, http://www.ansys.com.

Bird, R.B., Stewart, W.E., Lightfoot, E. N. (1960). *Transport Phenomenon.* England: John Wiley & Sons Publications Ltd.

Bolch, C.J., Hallegraeff, G.M. (1993). "Chemical and physical treatment options to kill toxic dinoflagellate cysts in ships' ballast water". *Journal of Marine Environmental Engineering*, 1 (1), 23-29.

Boldor, D., Balasubramanian, S., Purohit, S., Rusch, K.A. (2008). "Design and implementation of a continuous microwave heating system for ballast water treatment". *Environmental Science & Technology* (accepted).

Buchholz, K., Tanis, D., Macomber, S., Farris, E. (1998). "Ballast water secondary treatment technology review. Battelle Duxbury Operations". Retrieved on June 07, from http://www.nemw.org/balsurv_contents.htm.

Chase, C., Christine, R., Pederson, J. (2004). "Marine bioinvasions fact sheet: ballast water treatment options". Retrieved on June 07, from http://massbay.mit.edu/resources/pdf/ballast-treat.pdf.

Choi, Y., Okos, M.R. (1986). "Effects of temperature and composition on the thermal properties of foods". In: Maguer M.L., Jelen, P. (Ed), *Food Engineering and Process Applications, Vol. 1, Transport Phenomenon.* London: Elsevier Applied Science Publishers Ltd, 93-101.

Cohen, A.N. (1998). "Ships' ballast water and the introduction of exotic organisms into the San Francisco estuary: current status of the problem and options for management". San Francisco Estuary Institute, Richmond CA. Retrieved on May 07, from http://www.sfei.org/bioinvasions/Reports/1999-Exotic%20Organisms.pdf.

Coronel, P, Simunovic, J., Sandeep, K.P. (2003). "Temperature profiles within milk after heating in a continuous-flow tubular microwave system operating at 915 MHz". *Journal of food science,* 68(6), 1976-1981.

Coronel, P, Simunovic, J., Sandeep, K.P., Cartwright, G.D., Kunar, P. (2008). "Sterilization solutions for aseptic processing using a continuous flow microwave system". *Journal of Food Engineering*, 85(4), 528-536.

Datta, A., Prosetya, H., Hu, W. (1992). "Mathematical modeling of batch heating of liquids in a microwave cavity". *Journal of Microwave Power and Electromagnetic Energy*, 27(1), 38–48.

Dragsund, E., Adersen, A.B., Johannesen, O. (2001). "Ballast water treatment by ozonation". *1st International Ballast Water Treatment R&D Symposium, IMO London, March 2001: Symposium Proceedings.* GloBallast Monograph Series No. 5. IMO London.

Dragsund, E., Johannessen, B.O., Andersen, A.B., Noklebye, J. O. (2004)."Corrosion effects of ballast water treatment methods". In: *2nd International Ballast Water Treatment R&D Symposium, IMO London, July 2003: Proceedings.* Matheickal, J.T., Raaymakers, S. (Ed), GloBallast Monograph Series No. 15. IMO London.

Eskilsson, C.S., Bjorklund, E. (2000). "Analytical-scale microwave-assisted extraction". *Journal of Chromatography A,* 902, 227–250.

Falqui-Cao, C., Wang, Z., Urruty, L., Pommier, J., Montury. M. (2001). "Focused microwave assistance for extracting some pesticide residues from strawberries into water before their determination by SPME/HPLC/DAD". *Journal of Agricultural and Food Chemistry*, 49, 5092-5097.

Geankoplis, C.J. (1993). *Transport Processes and Unit Operations*, New York: McGraw-Hill Publications.

Gerbo, N.M., Boldor, D., Sabliov, C.M. (2007). "Microwave heating of pumpable fluids using IR imaging and fiber optic technology". *Journal of Microwave Power and Electromagnetic Energy.* 42(1), 62-72.

Griffiths, D.J. (1999). *Introduction to electrodynamics*.3rd Ed., NJ: Prentice-Hall Publications.

Guan, D., Gray, P., Kang, D.H., Tang, J., Shafer, B., Ito, K., Younce, F., Yang, T.C.S. (2003). "Microbiological validation of microwave-circulated water combination heating technology by inoculated pack studies". *Journal of Food Science- Food Microbiology and Safety*, 68(4), 1428-32.

Hallegraeff, G.M., Valentine, J.P., Marshall, J-A., Bolch, C.J. (1997). "Temperature tolerances of toxic dinoflagellate cysts: application to the treatment of ships ballast water". *Aquatic Ecology*, 31, 47-52.

Ikediala, J.N., Hansen, J.D., Tang, J., Drake, S.R., Wang, S. (2002). "Development of a saline water immersion technique with RF energy as a postharvest treatment against codling moth in cherries". *Postharvest Biology and Technology*, 24, 209–221.

Komarov, V.V. and V.V. Yakovlev (2001). "Simulations of components of microwave heating applicators by FEMLAB, MicroWaveLab and QuickWave-3D", *Proceedings on 36th Microwave Power Symposium (San Francisco, CA, April 2001)*, 1-4.

Komarov, V.V. and V.V. Yakovlev (2007). "CAD of efficient TMmn0 single-mode elliptical applicators with coaxial excitation". *Journal of Microwave Power and Electromagnetic Energy*, 40(3), 174-185.

Kriesel, I., Kolodny, Y., Cairns, W.L., Galil, B.S., Sasson, Y., Joshi, A.V., Cangelosi, A., Blatchley E.R., TenEyck, M.C., Blacer M.D., Brodie, P. (2004). "The ternary effect for ballast water treatment". In: *2nd International Ballast Water Treatment R&D Symposium, IMO London, July 2003: Proceedings,* Matheickal, J.T., Raaymakers, S. (Ed), GloBallast Monograph Series No. 15. IMO London.

Le Bail, A., Koutchma, T., Ramaswamy, H.S. (2000). "Modeling of temperature profiles under continuous tube-flow microwave and steam heating conditions". *Journal of Food Process Engineering*, 23, 1-24.

Lin, Y.E., Anantheswaran, R.C., Puri, V.M. (1995). "Finite element analysis of microwave heating of solid foods". *Journal of Food Engineering*, 25, 85-112.

Mesbahi, E. (2004). “Latest results from testing seven different technologies under the EU MARTOB project - Where do we stand now?” In: *2nd International Ballast Water Treatment R&D Symposium,* Matheickal, J.T., Raaymakers, S. (Ed), *IMO London, July 2003: Proceedings*. GloBallast Monograph Series No. 15. IMO London.

Metaxas, A.C., Meredith, R.J. (1983). *Industrial Microwave Heating*. London, UK: Peter Peregrinus Publications Ltd.

Mountfort, D., Dodgshun T., Taylor, M. (2003). “Ballast water treatment by heat”. In: Raaymakers, S. (Ed), *1st International Ballast Water Treatment R&D Symposium, IMO London, March 2001: Symposium Proceedings.* GloBallast Monograph Series No. 5. IMO London.

Oemcke, D., Van Leeuwen, J. (2003). “Chemical and physical characterization of ballast water. Part 1: Effects of Ballast Water Treatment Processes”. *Journal of Marine Environmental Engineering*, 7(1), 47-64.

Oemcke, D., Van Leeuwen, J. (2004). “Seawater ozonation of bacillus subtilis spores: implications for the use of ozone in ballast water treatment”. *Ozone: Science and Engineering,* 26, 389-401.

Oemcke, D.J. (1998). *Treatment of Ships’ Ballast Water*. Doctoral Thesis, James Cook University, Townsville, Australia.

Ozilgen, S., Ozilgen, M. (1991). “A model for pasteurization with microwaves in a tubular flow reactor”. *Enzyme Microbial Technology*, 13, 419-423.

Pandit, R.B. and S. Prasad (2003). ‘Finite element analysis of microwave heating of potato—transient temperature profiles”. Journal of Food Engineering, 60, 193–202.

Parsons, M. G., Harkins, R. W. (2002). “Full scale particle removal performance of three types of mechanical separation devices for the primary treatment of ballast water”. *Marine Technology,* 39, 211-222.

Parsons, M.G. (2003). “Considerations in the Design of the Primary Treatment for Ballast Systems. *Marine Technology”*, 40(1), 49-60.

Parsons, M.G. (2004). *Ballast exchange system for marine vessels*, Patent Number 6766754.

Ratanadecho, P., Auki, K., Akahori, M. (2002). “A numerical and experimental investigation of the modeling of microwave heating for liquid layers using a rectangular wave guide (effects of natural convection and dielectric properties)”. *Applied Mathematical Modeling*, 26, 449–472.

Rigby, G., Hallegraeff, G., Sutton, C. (1999). “Novel ballast water heating technique offers cost-effective treatment to reduce risk of global transport of harmful marine organisms”. *Marine Ecology Progress Series*, 191, 293-298.

Roussy, G., Pearce, J. A. (1995). *Foundations and Industrial Applications of Microwave and Radio Frequency Fields*. West Sussex, England: John Wiley & Sons Publications Ltd.

Sabliov, C.M., Salvi, D. and Boldor, D. (2007). “High frequency electromagnetism, heat transfer, and fluid flow coupling in ANSYS Multiphysics”. *Journal of Microwave Power & Electromagnetic Energy*. 41(4), 4-16.

Silva, J., Fernandes, F. (2001). “Use of chlorine for ballast water treatment”. Paper presented at *2nd International Ballast Water Treatment R&D Symposium IMO*, London.

Sullivan, P.K., Bourke, R.E., Sullivan, C.J. (2002). *Ship ballast water ultrasonic treatment.* US Patent 6402965.

Woo, I., Rhee, I., Park, H. (2000). “Differential damage in bacterial cells by microwave radiation on the basis of cell wall structure”. *Applied and Environmental Microbiology*, 66 (5), 2243–2247.

Zhou, L., Puri, V.M., Anantheswaran, R. C., Yeh, G. (1995). “Finite element modeling of heat and mass transfer in food materials during microwave heating – model development and validation”. *Journal of Food Engineering,* 25, 509-529.

Zhu J., Kuznetsov, A.V., Sandeep, K.P. (2007a). “Numerical simulation of forced convection in a duct subjected to microwave heating”. *Heat Mass Transfer*, 43 (3), 255-264

Zhu J., Kuznetsov, A.V., Sandeep, K.P. (2007b). “Mathematical modeling of continuous flow microwave heating of liquids (effects of dielectric properties and design parameters)”. *International Journal of Thermal Sciences*, 46 (4), 328-341.

CHAPTER 4

EXPERIMENTAL TEMPERATURE MEASUREMENT OF FLUIDS DURING CONTINUOUS FLOW MICROWAVE HEATING TO STUDY EFFECT OF DIFFERENT DIELECTRIC AND PHYSICAL PROPERTIES ON TEMPERATURE DISTRIBUTION

4.1 Introduction

Continuous flow microwave heating is a viable heating method for several industries, as the material can be heated instantaneously and volumetrically. The method requires less floor space as compared to conventional furnaces and it avoids overheating at the surface and under-heating at the core while generating uniform heating within the material if properly controlled (Clark and Sutton, 1996; Coronel et al., 2003). Temperature distribution is a function of the dielectric and thermal properties of the material, frequency, power, and geometry of the microwave heating system (Gerbo et al., 2008; Sabliov et al., 2004; Hu and Mallikarjunan, 2002). Knowledge of three dimensional temperature profile distribution in heated products is critically needed to optimize the microwave heating process (Knoerzer et al., 2005). Several method including thermocouples (Swain et al., 2008; Yang and Gunasekaran, 2004), shielded thermocouples (Ramaswamy et al., 1998), fiber optic probes (Knoerzer et al., 2005; Mullin and Bows, 1993), chemical markers (Lau et al., 2003; Pandit et al., 2007), model substances (Risman et al., 1993), infrared imaging (IR) (Goedeken et al., 1991), magnetic resonance imaging (MRI) (Nott and Hall, 2005; Knoerzer et al., 2005), thermo-paper (Knoerzer et al., 2005), and microwave radiometry (Stephan and Pearce, 2005), are currently being used to experimentally determine temperature distribution inside and at the surface of materials during batch microwave processing. Thermo-paper, IR, and microwave radiometry can only be used to measure surface temperatures, and model substance or chemical markers provide only approximate temperature distribution in the actual product. MRI techniques are best suited to obtain three dimensional

temperature distribution but these methods are very complex and expensive (Knoerzer et al., 2005), and thermocouples cannot be reliably used inside microwave fields due to their metallic nature. Fiber optic temperature probes, on the other hand, have the potential to greatly improve the ability to measure temperatures at select locations within a microwave field without changing electromagnetic field distribution inside the cavity (Knoerzer et al., 2005). Fiber optic probes have been used in the past to measure temperature in microwave fields and to validate temperature measurements by other methods such as MRI and IR imaging (Knoerzer et al., 2005), mainly in batch microwave heating.

In continuous flow microwave heating systems, thermocouples have been used to measure the temperature in fluids at the exit of the cavity (Coronel et al., 2005; Coronel et al., 2003; Coronel et al., 2008). Very few studies are available on use of fiber optic probes for temperature measurement in continuous flow microwave heating. For example, a novel fiber optic temperature measurement system was used to measure the temperatures at the central axis of applicator tube at four locations (Gerbo et al., 2008; Salvi et al., 2008); the system was based on the method employed by Zhong et al. (2003, 2004) to measure temperature inside a continuous flow radio frequency unit. However, the above studies did not provide complete information on temperature distribution in the product due to temperature being measured at only a few points. The attributes of microwave heating can be controlled only if exact temperature distribution is known. Therefore, numerous points of measurement are needed to understand the complete temperature profile of the fluid as it heats during continuous flow microwave heating. In this study we collected temperature data at as many as 110 points in a continuous flow microwave system using custom made temperature measurement system employing a single fiber optic probe. The experimental data was used to understand the effect of different dielectric

and physical properties, as well as the effect of flow rate on heating patterns of three fluids heated in a continuous flow microwave system. Specific objective of the study were:

1. To obtain radial and longitudinal temperature profiles in freshwater, saltwater, and carboxymethylcellulose (CMC) solutions heated in a continuous flow microwave system,
2. To study the effect of dielectric and physical properties, as well as the effect of flow rate on microwave heating of freshwater, saltwater and CMC solution.

4.2 Material and Methods

4.2.1 Preparation of Fluids

The fluids selected for the experiments were freshwater, saltwater and CMC solution. Saltwater was prepared by adding sea salt (Crystal Sea Marinemix^{TM} salt, Marine Enterprises International, Baltimore, MD) to tap water. The salinity was measured using an optical refractometer (#C7142, Aquatic Eco-Systems, FL) and was adjusted to 3 %. Pre-Hydrated CMC 6000 Powder (TIC Gums Inc., Belcamp, MD) was used to prepare 0.5% CMC solution. Both CMC and saltwater solution was prepared by using a mechanical hand mixer 24 hours prior to starting the experiments to allow chemical equilibrium to be reached.

4.2.2 Microwave System

A 915 MHz continuous-flow microwave system (**Figure 4.1**) provided by Industrial Microwave Systems, LLC (Morrisville, NC) was used in the experiments. The system consisted of a 5 kW microwave generator, circulator, water load, power coupler, tuning coupler, connecting waveguide, elliptical focusing cavity and an PTFE (polytetraflouroethylene) applicator tube (3.18 cm diameter and 25.4 cm height). A nominal power of 4 kW was used for all experiments. All three fluids were pumped through the microwave applicator tube (the flow direction is shown in **Figure 4.1**) at three flow rates of 1 lit/m, 1.6 lit/m, and 2 lit/m.

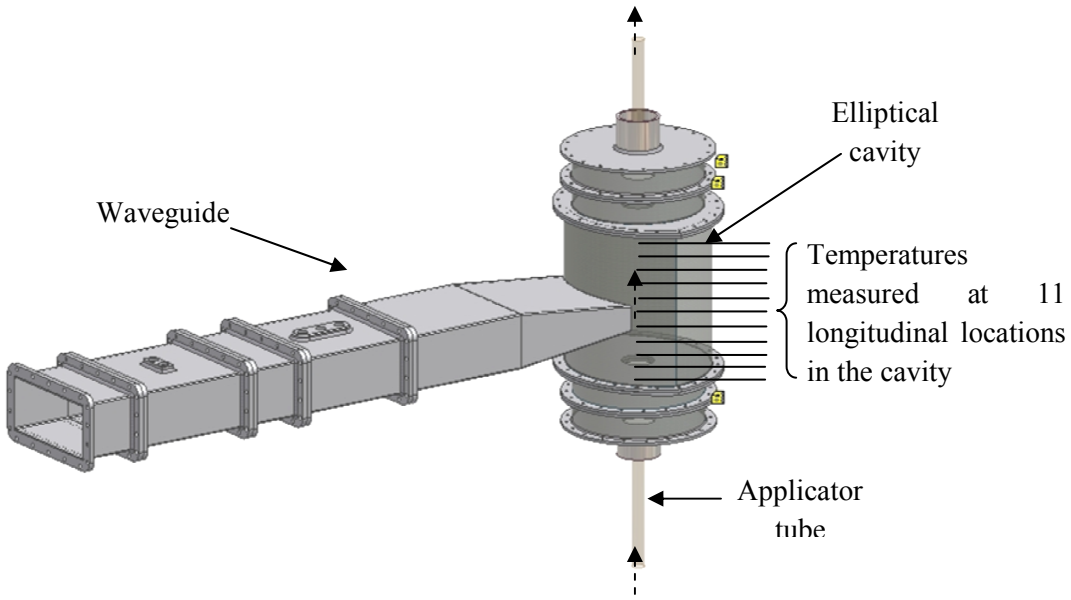

Figure 4.1 Microwave system provided by Industrial Microwave Systems, (Morrisville, NC)

4.2.3 Temperature Measurement System

The temperature measurement system consisted of fiber optic temperature probes (Neoptix T1, Neoptix Inc., Québec City, Canada) tied to a string. The longitudinal movement of the string was possible due to a ratchet wheel mounted after the outlet T section of the applicator tube. The temperature was measured at ten radial points (**Figure 4.2**) in a cross section of the fluid and at eleven different longitudinal locations (separated by 2.54 cm distance) for a total of 110 measurements. In all, 90 runs were conducted for three fluids and three different flow rates. Each run consisted of temperature measurement at one radial location and eleven longitudinal locations in triplicate for a particular fluid and flow rate.

4.3 Dielectric and Physical Properties of Freshwater, Saltwater and CMC Solution

Dielectric properties of the fluids used in the study were calculated based on the equations given by Coronel et al. (2008) and Komarov and Tang (2004) (**Figure 4.3**). Dielectric constant (ε') is a measure of the material's ability to store electric energy and dielectric loss (ε'') is a measure of efficiency of a material to convert electromagnetic energy into heat.

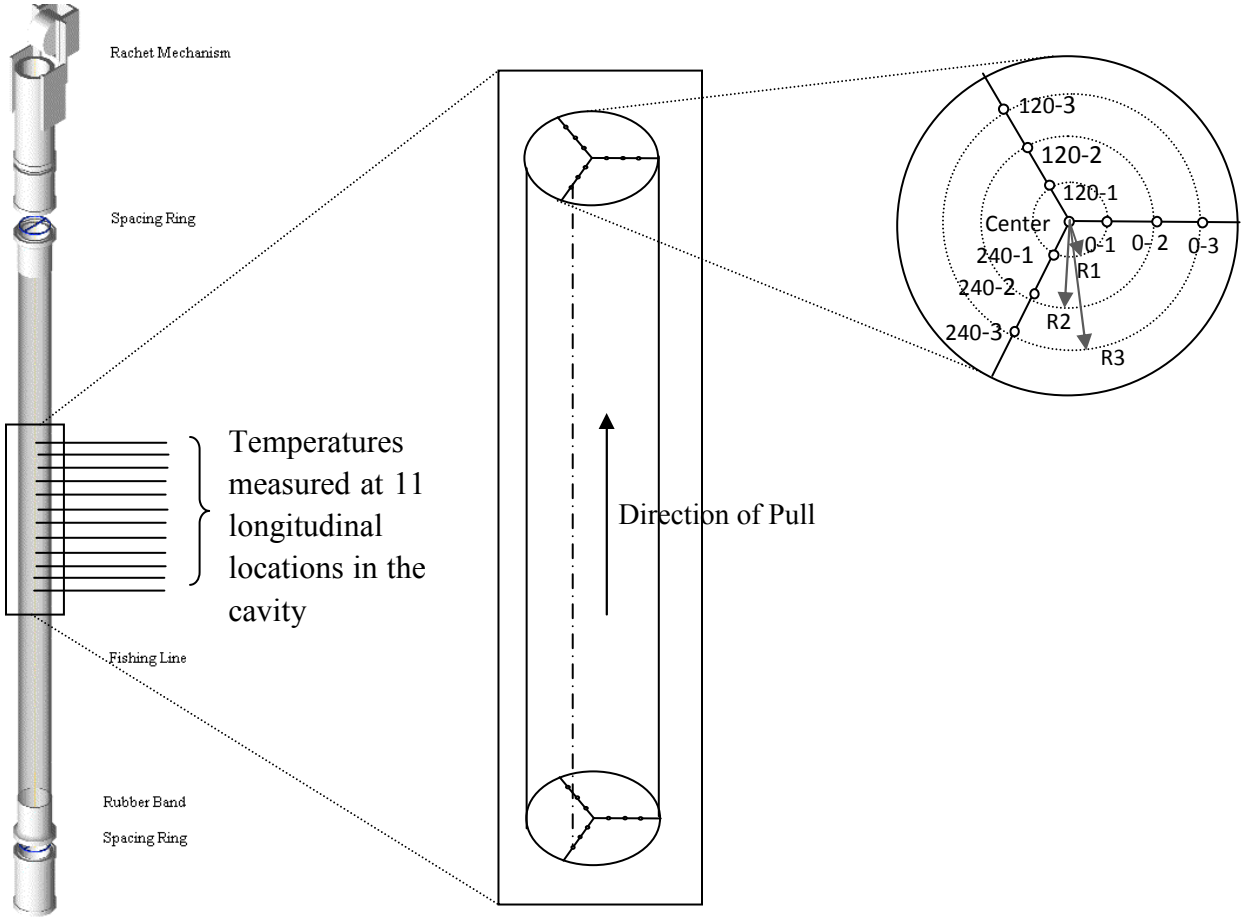

Figure 4.2 Fiber optic temperature measurement system and applicator tube

The dielectric constant for all three fluids showed a decrease with an increase in temperature. The dielectric loss for freshwater (ε''=3.81 at 25 ^{o}C) and CMC solution (ε''=8.94 at 25 ^{o}C) were comparable but lower as compared to saltwater (ε''=101.69 at 25 ^{o}C). The dielectric loss increased with temperature for CMC solution and saltwater (dielectric loss for saltwater was 11 times higher than that of CMC at room temperature), indicating that CMC and saltwater solutions will convert more electromagnetic energy into heat as they travel up through the cavity. For freshwater, the dielectric loss decreased slightly with temperature suggesting that as the fluid heated up in the cavity less electromagnetic energy was converted into heat.

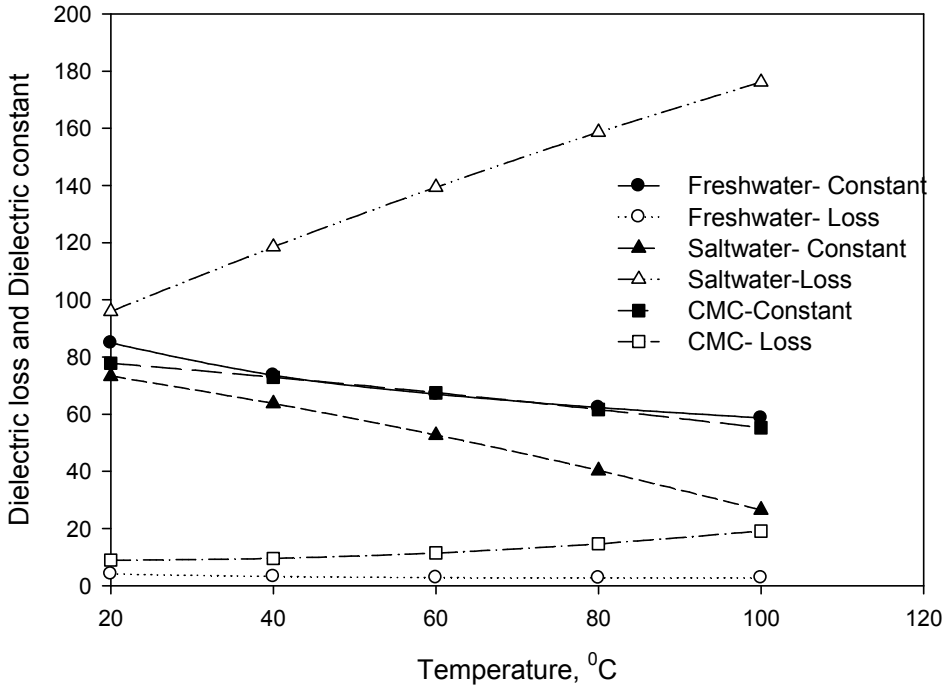

Figure 4.3 Dielectric properties of freshwater, saltwater and CMC solutions (Coronel et al., 2008 and Komarov and Tang, 2004)

Physical properties including thermal conductivity, material density, specific heat and viscosity have a significant effect on the rate of heat transfer in the fluid. Thermal conductivity, material density and specific heat are very similar for all three fluids, but rheological behavior of CMC solution is different than that of freshwater and saltwater (**Table 4.1** and **4.2**). Both these solutions are Newtonian fluids whereas, CMC solution exhibits non-Newtonian behavior as described by power law (Steffe, 1996)

$$\sigma = K\dot{\gamma}^n \tag{4.1}$$

where, σ is shear stress (Pa), $\dot{\gamma}$ is shear rate (s^{-1}), K is consistency coefficient and n is flow behavior index.

Table 4.1 Physical properties of the fluids at room temperature

Fluid	***k*, thermal conductivity [W/m K]**	**ρ, material density [kg/m^3]**	**C_p, specific heat [J/kg K]**
Freshwater	0.6110	994.9	4177.3
Saltwater	0.6035	1037.6	4086.2
CMC	0.6091	997.9	4164.4

Ref: Choi and Okos, 1986

Table 4.2 Rheological properties of the fluids

Fluid	**Temperature [^{o}C]**	**μ, viscosity [Pa.s]**	
Freshwater[1]	25	0.8937e-3	
	50	0.5494e-3	
	75	0.3800e-3	
	100	0.2838e-3	
Saltwater[2]	25	0.8422e-3	
	50	0.5236e-3	
	75	0.3621e-3	
	100	0.2705e-3	
0.5 % CMC Solution[3]		K	n (Pa.s^n)
	25	0.91	0.60
	50	0.55	0.61
	75	0.47	0.62
	100	0.19	0.63

[1] Ref: Geankoplis et al., 1993; [2] Ref: Boufadel et al., 1999; [3]Ref: Vais et al., 2002

4.4 Results

4.4.1 Radial and Longitudinal Temperature Profiles

Time-temperature profiles at ten radial and eleven longitudinal locations were observed in saltwater, freshwater, and CMC solution heated in the continuous flow microwave system at three different flow rates. The temperatures were measured at the center and at three radial locations at a radius equal to ¼ R (referred as R1), ½ R (referred as R2), and ¾ R (referred as R3) at three angles (0^o, 120^o, 240^o) for each radius as shown in **Figure 4.2**. These radial points are hereafter mentioned as position 'angle_radial distance'; for example, if data was measured at angle 120^o and at radius R3, it will be referred to as 120_3. The longitudinal temperatures were measured at each 2.54 cm from the entrance of applicator tube in the cavity (y = 0 cm) to exit (y = 25.4 cm). The temperature data at each radial position versus longitudinal distance (**Figure 4.4**, **4.5**, and **4.6**) showed a low standard deviation between replicate which confirms reliability of the fiber optic system used for temperature measurement in this study.

Saltwater exhibited a more uniform temperature distribution throughout the cross section of the applicator tube at all longitudinal locations (**Figure 4.4**) as compared to other fluids. The average radial temperature differences were less than 13 ^oC, 11 ^oC, and 21 ^oC for saltwater at 1 lit/m, 1.6 lit/m, and 2 lit/m respectively. The relationship between temperature and distance from the entrance of cavity was defined by a sigmoid shaped curve (with some flattening as flow rate increased). The rate of temperature increase was low initially, followed by higher rate in the middle of the tube, and then again low rate at the exit. The increased temperature in the middle section of the applicator tube was due to higher energy density at this location as a result of incident microwave introduction from the waveguide into cavity. Flattening of the sigmoid shaped temperature increase curve with flow rate was a direct effect of less time spent by the fluid in the microwave field at higher flow rates.

The cross-sectional temperature in freshwater followed a sigmoid shape similar to that of saltwater, but the temperature distribution was less uniform than that of saltwater (**Figure 4.5**). Temperatures observed at the center and position 120_1 (away from the direction of microwave) were slightly different than the other locations and were treated as exceptions. Radial temperature differences for freshwater were 25 ^{o}C (at y = 10.16 and y = 12.7 cm), 20 ^{o}C (y = 12.7 cm) and 18 ^{o}C (y = 12.7 and y = 15.2 cm) at the flow rates of 1 lit/m, 1.6 lit/m, and 2 lit/m respectively, without including the two noted exceptions (center and 120_1). For center and position 120_1 the temperature increased initially and then it decreased towards the exit of the cavity (**Figure 4.5**). Temperature decrease at the exit was a result of low electric field intensity at the exit and heat conduction to surrounding fluid of lower temperatures.

Non-uniform cross-sectional temperature distribution was seen in CMC solution (**Figure 4.6**). At all three flow rates the highest temperatures were clearly seen at the center of the tube followed by the temperatures at ¼R distance from the center (**Figure 4.6**). Temperature differences in the fluid at ¼R radius from center at different angle were 25 ^{o}C (at y =17.78 and y = 20.32 cm) at 1 lit/m, 20 ^{o}C (at y =7.62 and y =10.16 cm) at 1.6 lit/m and to 20 ^{o}C (at y =10.16 and y = 12.7 cm) at 2 lit/m respectively. The lower temperatures were found at the edges (240_3 and 0_3) which showed very little temperature increase compared to other locations. In the hot regions, an increase in temperature with distance was initially observed followed by a slight decrease. At 1 lit/min at some locations (center and120_1) the temperatures reached 100 ^{o}C in the cavity and did not change further with longitudinal distance as microwave energy absorbed was used to change the phase from liquid to vapor. Temperature decrease towards the exit for these locations was mainly due to a heat transfer to the colder regions due to very large temperature gradients.

4.4.2 Cross-sectional Temperature Distribution for Freshwater, Saltwater, and CMC Solution

Temperature data was interpolated from ten radial positions (at R1, R2, and R3 at angles 0^o, 120^o, 240^o, and at the center) and plotted in MATLAB 2007a at five different longitudinal locations for all three fluids at a flow rate of 1 lit/m to compare the cross-sectional temperature distribution for these fluids (**Figure 4.7**). It was observed that the more uniform distribution was seen in saltwater followed by freshwater whereas CMC solution showed a very high temperature region near the center.

4.4.3 Influence of Dielectric Properties and Flow Rate on Temperature Increase

The average temperature increase (ΔT) for freshwater, saltwater and CMC solution plotted against the inverse of volumetric flow rate ($1/\dot{V}$) showed that the temperature gained (ΔT) by all fluids decreased as the flow rate increased from 1 lit/m to 2 lit/m because of the less residence time spent by the fluid in the cavity (**Figure 4.8**). The power absorbed by the fluids was calculated based on inlet and outlet average temperature and physical properties of the material using calorimetric equation (4.4).

$$P_{abs} = \dot{m} C_p \Delta T \tag{4.4}$$

where, $\dot{m} = \rho \dot{V}$, P_{abs} is power absorbed by fluid (Watt), $\dot{m}$ is the mass flow rate (kg/s), C_p is specific heat of the fluid (J/kg K), ρ is fluid density, and ΔT is the difference between the inlet and outlet temperature of the fluid. Saltwater with highest dielectric properties absorbed more power (3960 W) followed by CMC solutions (2800 W) and freshwater (2520 W), from an incident power of 4000 W.

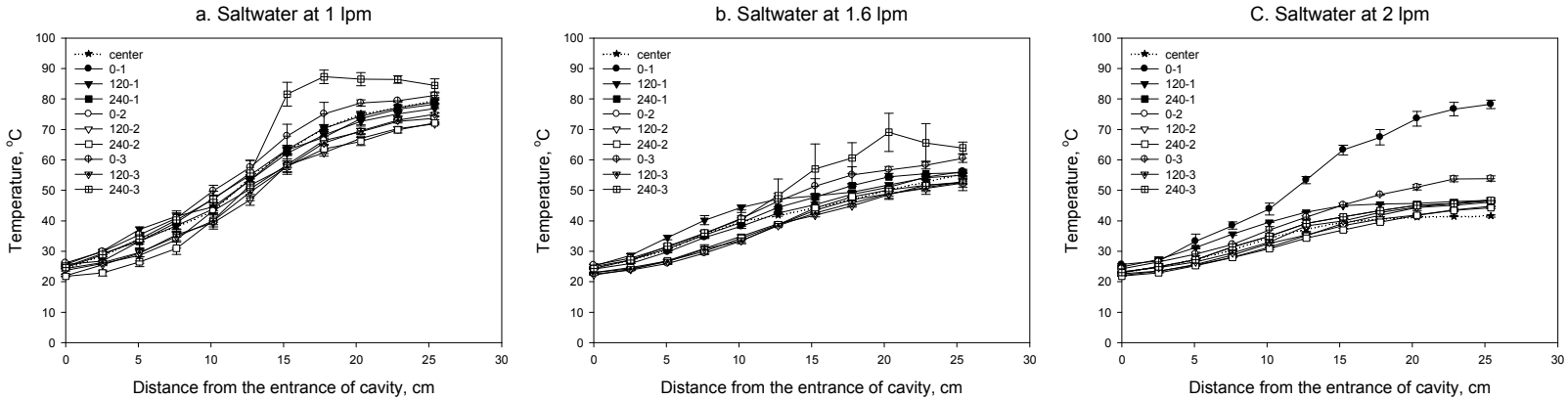

Figure 4.4 Temperature at ten radial and eleven longitudinal locations for saltwater at flow rates of **a.** 1 lit/m **b.** 1.6 lit/m and **c.** 2 lit/m

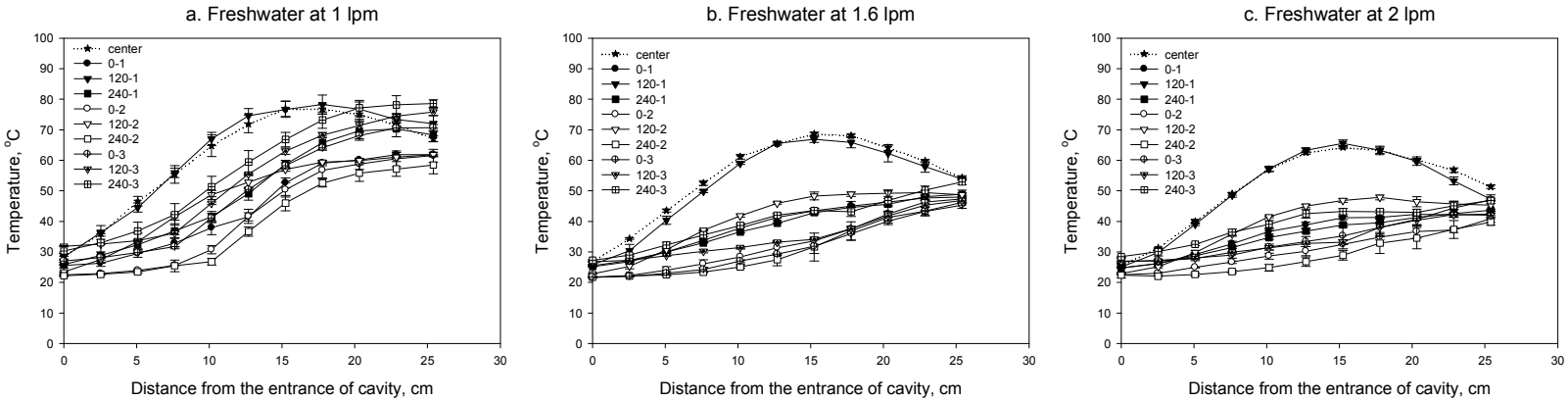

Figure 4.5 Temperature at ten radial and eleven longitudinal locations for freshwater at flow rates of **a.** 1 lit/m **b.** 1.6 lit/m and **c.** 2 lit/m

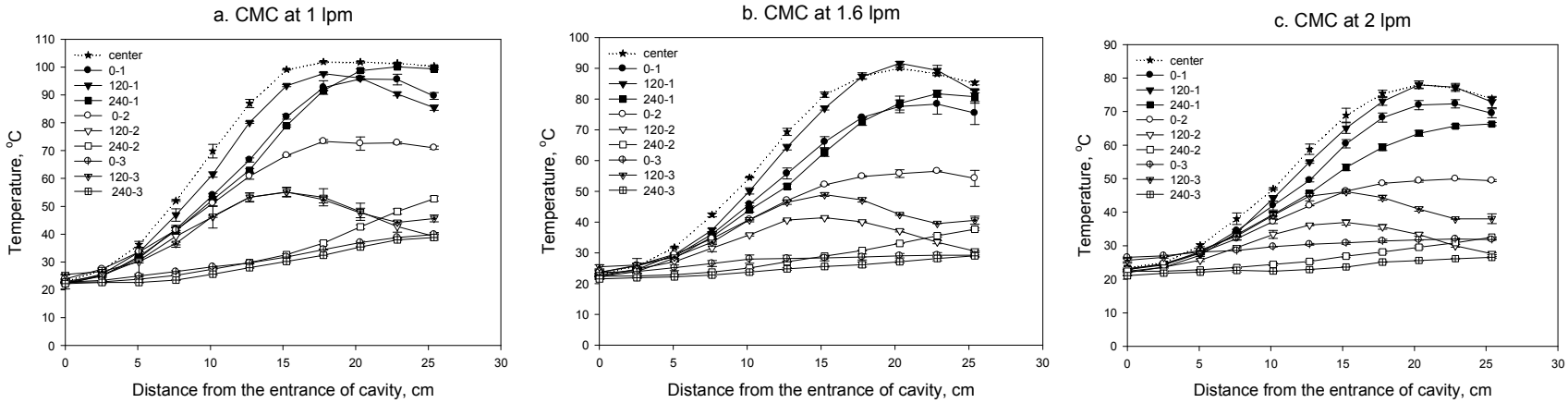

Figure 4.6 Temperature at ten radial and eleven longitudinal locations for 0.5 % CMC solution at flow rates of **a.** 1 lit/m **b.** 1.6 lit/m and **c.** 2 lit/m

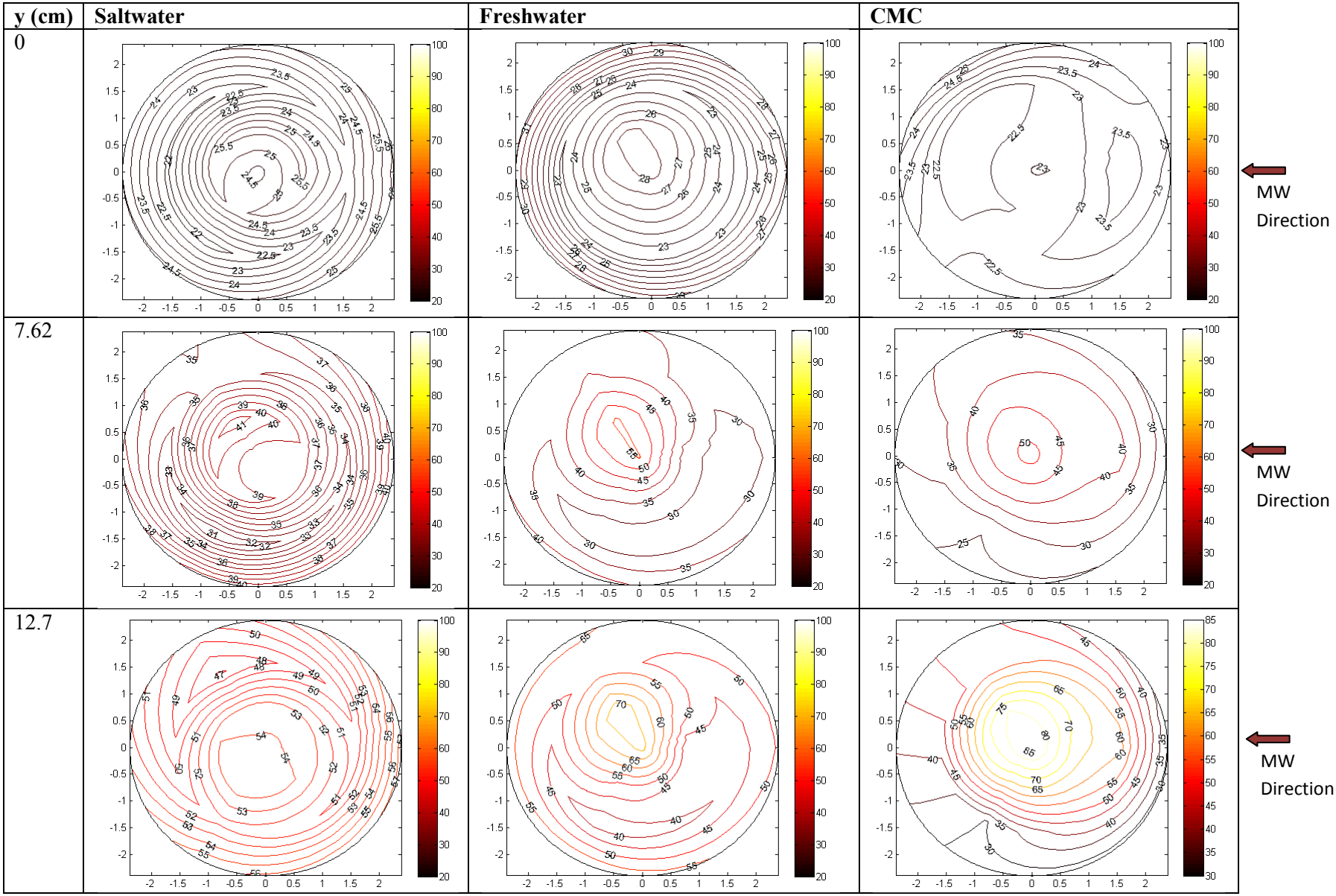

Figure 4.7 Temperature in x-z plane at different longitudinal distances (y) for freshwater, saltwater, and 0.5 % CMC solution at 1 lit/m (figure continued)

y (cm)	Saltwater	Freshwater	CMC	
17.78	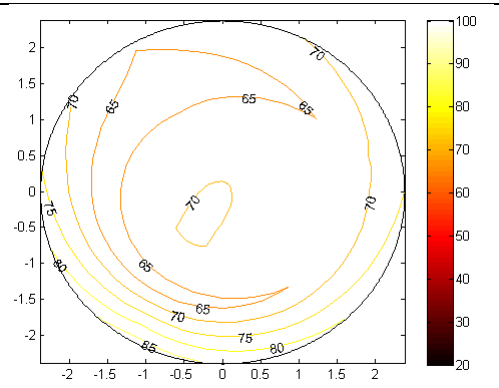	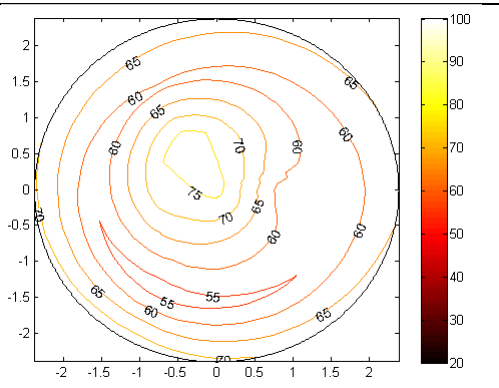	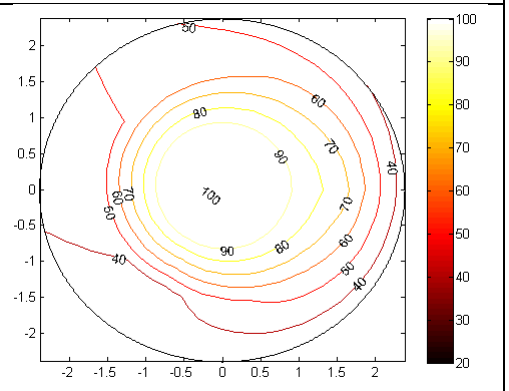	MW Direction
25.4	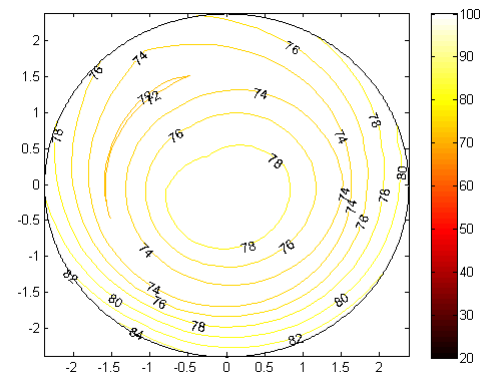	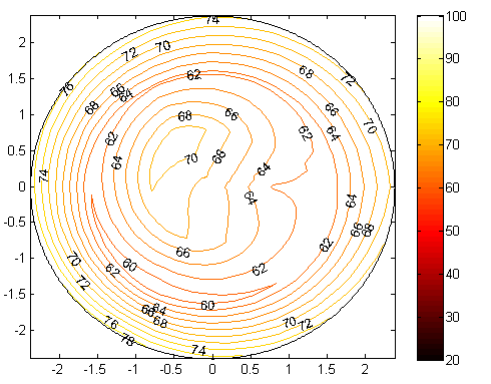	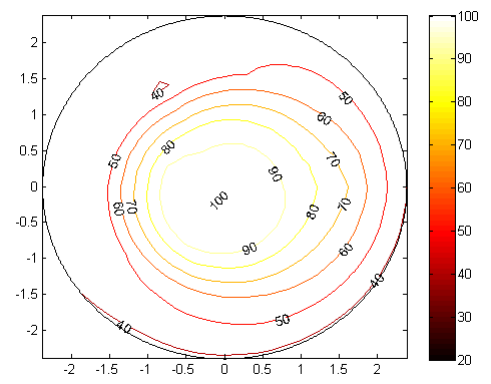	MW Direction

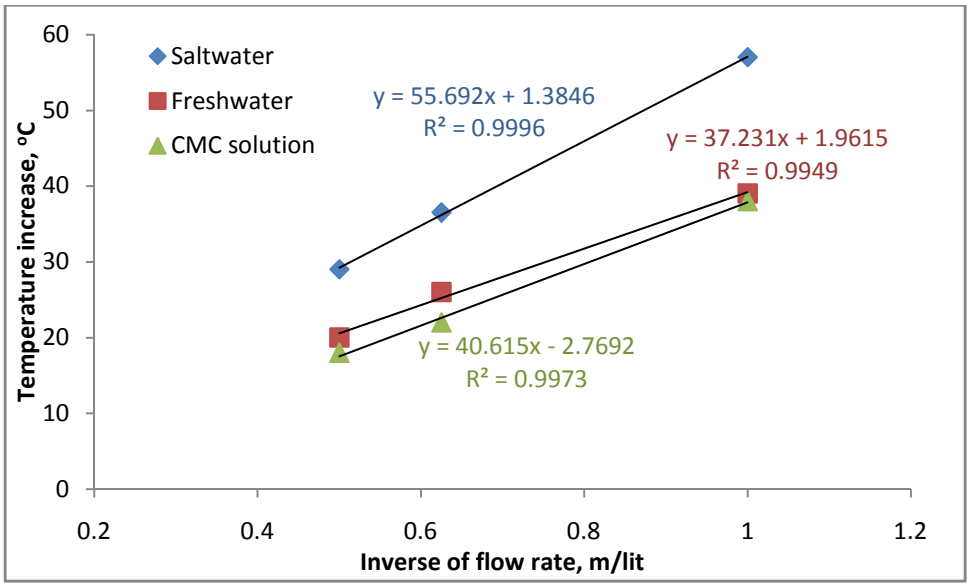

Figure 4.8 Average temperature increase for saltwater, freshwater, and CMC solutions at three flow rates

4.5 Discussion

Power absorbed by saltwater, of higher dielectric properties ($\varepsilon'' = 101.69$ at 25°C) was higher as compared to that absorbed by freshwater ($\varepsilon'' = 3.81$ at 25°C). Dielectrics loss for saltwater were 26 times higher as compared to freshwater and 11 times higher as compared to CMC at room temperature; hence better temperature gains were obtained in saltwater as compared to the other liquids. CMC solution ($\varepsilon'' = 8.94$ at 25°C) with dielectric properties values similar to those of freshwater showed similar but lower temperature gains. The lower temperature gains observed in CMC solution as compared with freshwater could be explained by the relative relaxation times of the two products. CMC (a derivative of cellulose) has long rigid molecular structure and highly viscous properties causing longer relaxation times than freshwater based on the equation (Metaxas and Meredith, 1983),

$$\tau = \frac{4\pi r^3 \eta}{k_b T} \tag{4.5}$$

where, τ is relaxation time (s), r is the radius of the molecule (m), η is viscosity of the solution (Pa.s), T is absolute temperature (K) and k_b is Boltzmann's constant (1.380 6504(24)×10^{-23} J/K). Longer relaxation times indicate less heat absorption due to slower responses of molecules to changing electric field.

All three liquids studied did not only show different temperature gains but also exhibited different cross-sectional temperature profiles. More uniform distribution was seen in saltwater followed by freshwater and non-uniform distribution in CMC solution (**Figure 4.4**, **4.5**, and **4.6**). Attenuation factors were used to understand temperature uniformity or lack thereof in the three studied fluids. The electric field intensity at a distance (z) from the surface of a large dielectric material is given by (Datta, 1990)

$$E = E_0 e^{-\alpha z} \tag{4.2}$$

where, E is electric field intensity (Vm^{-1}), E_0 is incident electric field (Vm^{-1}) and α is attenuation factor sited by (Tang, 2005)

$$\alpha = \frac{2\pi}{\lambda_0}\left[\frac{1}{2}\varepsilon'\left(\sqrt{1+\left(\frac{\varepsilon''}{\varepsilon'}\right)^2}-1\right)\right]^{\frac{1}{2}} \tag{4.3}$$

where, λ_0 is free space wavelength (m), ε' is dielectric constant, and ε'' is dielectric loss.

Attenuation factors for saltwater, freshwater, and CMC solutions calculated over a range of temperature (**Table 4.3**) showed that saltwater had the highest value of attenuation factor (α) followed by CMC and freshwater, respectively. A high attenuation factor for a material at a depth z indicates higher power absorption from the incident wave up to that particular depth. The value of α decreased with an increase in temperature for freshwater and increased with an

increase in temperature for CMC and saltwater (indicating higher power absorption at higher temperatures for CMC and saltwater and lower for freshwater).

Table 4.3 Attenuation factor and penetration depth

Temperature, ^{o}C	**Attenuation factor [m^{-1}]**		
	Saltwater	**Freshwater**	**CMC**
20	93.30	4.25	9.66
40	114.04	3.60	10.68
60	132.99	3.31	13.29
80	150.51	3.32	17.72
100	166.87	3.44	24.25

A simplified representation of radial electric field distribution calculated based on attenuation factors at room temperature and represented as percent incident electric field is shown in **Figure 4.9**. The electric field was assumed to be incident from four directions perpendicular to each other and was superimposed to calculate total electric field at each location as a function of radius. For freshwater and CMC solution, the electric field was mostly constant throughout the radius except at the tube center (r = 0 cm) where the electric field was higher (2 times the constant value), whereas for saltwater the electric field showed a decrease towards the center and slight increase at the center. The magnitude of electric field was lower for saltwater (average of 16 %) as compared to freshwater (average of 49 %) and CMC solution (average of 45 %), but the radial electric field distribution (**Figure 4.9**) was more uniform for saltwater as compared to freshwater and CMC solution.

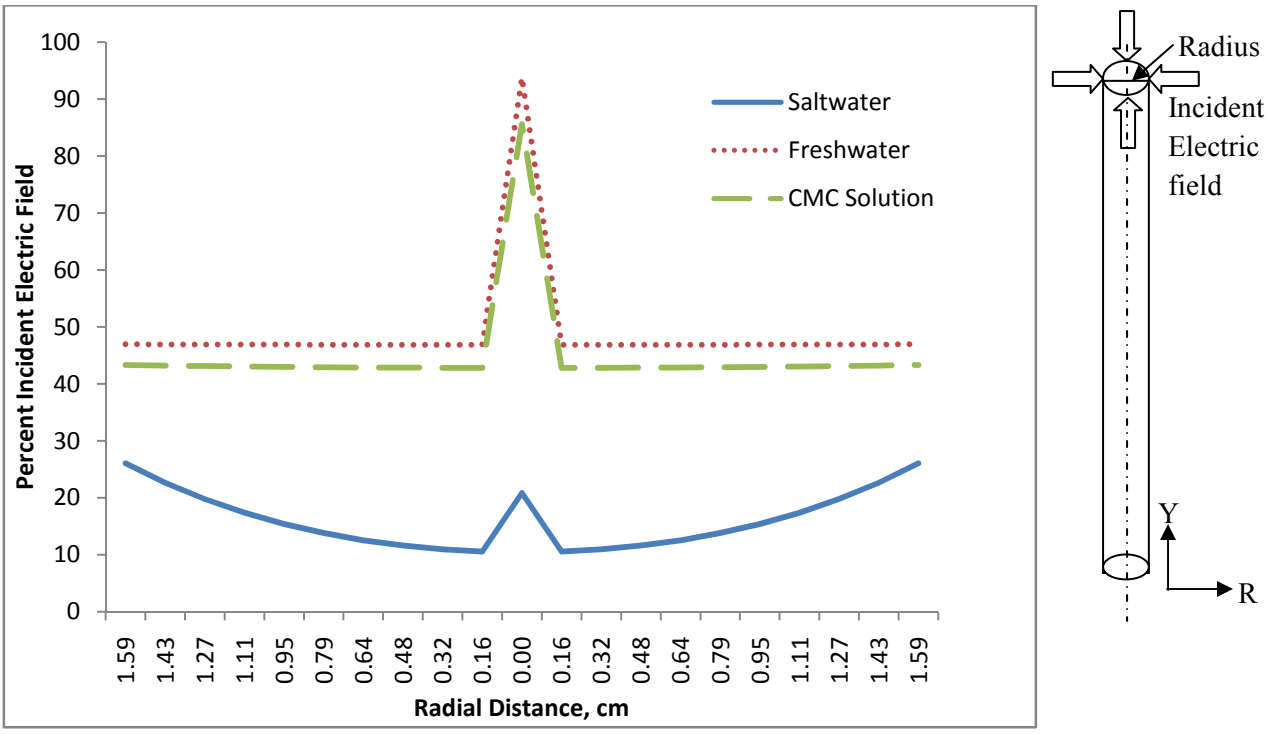

Figure 4.9 Electric field distribution in the radius of applicator tube

A more uniform radial electric field for saltwater (**Figure 4.9**) than for the other liquids suggested uniform heating and uniform cross-sectional temperature distribution in this product, which was confirmed experimentally as seen in **Figure 4.7**. The cross-sectional temperature distribution in freshwater was relatively uniform (**Figure 4.4**), but less uniform than the temperatures of saltwater (**Figure 4.5**) which can also be explained by the radial electric field distribution (**Figure 4.9**) and behavior of dielectric loss with temperature. For freshwater, the radial electric field distribution was higher at the center which resulted in formation of a hot spot near the center. The temperature in the hot spot increased from 28 to 70 ^{o}C, but the hot spot area did not increase; this was expected as the dielectric loss did not change much with temperature (from 3.81 at 25 ^{o}C to 2.75 at 100 ^{o}C) and hence heat absorption remained almost constant for freshwater as it travelled through the tube (**Figure 4.7**).

Very non-uniform temperature distribution was observed for CMC (**Figure 4.6**) because of several factors including temperature dependence of its dielectric properties and lack of mixing due to viscosity. As the CMC solution traveled in the cavity, the hot spot temperatures increased from 23 to 100 ^{o}C due to absorption of microwaves which resulted in a temperature increase in the fluid and a decrease in the relaxation time (**Figure 4.7**). This increase in temperature increased viscosity of the solution allowing more molecular rotation resulting into shorter relaxation time. Thus the initial increase in temperature caused decreased relaxation times which in turn resulted in further temperature increase (Metaxas and Meredith, 1983); the phenomenon known as thermal runaway effect was observed for CMC solution. Additionally, the lack of mixing due to viscosity also played an important role in obtaining un-uniform temperature distribution in the CMC solution. Since CMC solution is more viscous than freshwater and saltwater, it did not allow mixing and hence the central hot regions and surrounding cold regions did not mix while flowing in the tube resulting in the observed non-uniform temperature distribution.

The power distribution ($q_{gen} = 2\pi\varepsilon_o \varepsilon'' f \mid \vec{E} \mid^2$ where, ε_o = 8.854 x 10^{-12} F/m is free space permittivity, ε'' is relative dielectric loss, f is frequency in Hz, and $\vec{E}$ is electric field intensity in V/m) is a function of not only electric field intensity but also a function of dielectric loss. Hence higher temperature gains were obtained in saltwater as compared to freshwater and CMC solution of low dielectric properties (**Figure 4.8**). For CMC solution, the heated fluid became less viscous and moved faster though the cavity spending less time in the cavity at same flow rate than other fluids and thus gained low temperature.

4.6 Conclusion

The effect of different dielectric properties and flow rate on heating patterns of freshwater, saltwater and CMC in a continuous flow microwave system was studied by employing a single fiber optic probe. The most uniform temperature was obtained in saltwater at all three flow rates followed by freshwater and CMC. Power absorbed by saltwater (99% of the incident power) of high dielectric loss was higher as compared to freshwater (70% of the incident power), of lower dielectric loss. Non-Newtonian CMC solution (intermediate dielectric loss) gained lower power (63% of the incident power) than freshwater and saltwater mainly due longer relaxation times. Cross-sectional temperature distribution patterns of the fluid in the applicator tube showed that the hot spot for freshwater was near the center (away from the direction of the waves) and at the center for CMC. For saltwater the hot spot changed positions (as distance from the entrance increased) roughly about the center before settling in the very center, indicating mixing. The study was very useful in understanding the temperature distribution for fluids during continuous flow microwave heating. The temperature data obtained in the study can be used for rigorous validation of numerical modeling of continuous flow microwave heating and the method developed for temperature measurement can be used for a multitude of materials and microwave cavity geometries.

4.6 References

Boufadela, M.C., Suidana, M.T., Venosab, A.D. (1999). "Numerical modeling of water flow below dry salt lakes: effect of capillarity and viscosity". *Journal of Hydrology*, 221, 55–74.

Choi, Y. and M.R. Okos. (1986). "Effects of temperature and composition on the thermal properties of foods". In *Food Engineering and Process Applications, Vol. 1, Transport Phenomenon.* M. Le Maguer and P. Jelen (Ed), Elsevier Applied Science Publishers Ltd, London 93-101.

Clark, D.E. and W.H. Sutton (1996). "Microwave processing of materials". *Annual Reviews in Material Science*, 26, 299-331.

Coronel, P, Simunovic, J., Sandeep, K.P. (2003). "Temperature profiles within milk after heating in a continuous-flow tubular microwave system operating at 915 MHz". *Journal of Food Science*, 68(6), 1976-1981.

Coronel, P., Truong,V.D., Simunovic, J., Sandeep, K.P., Cartwright, G.D. (2005). "Aseptic processing of sweet potato purees using a continuous flow microwave system". *Journal of Food Science*, 70(9), 531–536.

Coronel, P, Simunovic, J., Sandeep, K.P., Cartwright, G.D., Kunar, P. (2008). "Sterilization solutions for aseptic processing using a continuous flow microwave system*". Journal of Food Engineering*, 85(4), 528-536.

Datta, A.K. 1990. "Heat and mass transfer in the microwave processing of food". *Chemical Engineering Progress*, 6, 47–53.

Geankoplis, C. J. (1993). *Transport Processes and Unit Operations*, McGraw-Hill Publications.

Gerbo, N.M., Boldor, D., and C.M. Sabliov (2008). "Design of a measurement system for temperature distribution in continuous-flow microwave heating of pumpable fluids using infrared imaging and fiber optic technology". *Journal of Microwave Power & Electromagnetic Energy*, 42(1), 55-65.

Goedeken, D.L., Tong, C.H., and R.R. Lentz (1991). "Design and calibration of a continuous temperature measurement system in a microwave cavity by infrared imaging". *Journal of Food Processing and Preservation,* 15(5), 331–337.

Hu, X. and K. Mallikarjunan (2002). "Mathematical modeling of heat transfer of microwave heated fish gel". *ASAE Annual International Meeting*, Chicago, USA.

Knoerzer, K., Regier, M. and H. Schubert (2005). "Measuring temperature distributions during microwave processing". In: *The Microwave Processing of Foods*, H. Schubert and M. Regier (Ed), CRC Press, 243-263.

Komarov, V.V. and J.M. Tang. (2004). "Dielectric permittivity and loss factor of tap water at 915 MHz", *Microwave and Optical Technology Letters*, 42 (5), 419-420.

Lau, M.H., Tang, J., Taub, I.A., Yang,T.C.S., Edwards, C.G., Mao R. (2003). "Kinetics of chemical marker formation in whey protein gels for studying microwave sterilization". *Journal of Food Engineering*, 60, 397–405.

Metaxas, A.C., Meredith, R.J. (1983). *Industrial Microwave Heating*. London, UK: Peter Peregrinus Publications Ltd.

Mullin, J., Bows, J. (1993). "Temperature measurement during microwave cooking". *Food additives and contaminants,* 10(6), 663-672.

Nott, K.P., Hall, L.D. (2005). "Validation and cross-comparison of MRI temperature mapping against fiber optic thermometry for microwave heating of foods". *International Journal of Food Science and Technology.* 40(7), 723-730.

Pandit R., Tang J., Liu F. and G. Mikhaylenko (2007). “A computer vision method to locate cold spot in foods during microwave sterilization processes”. *Pattern Recognition*, 40, 3667-3676.

Ramaswamy, H. S., Rauber, J. M., Raghavan ,G. S. V., Van De Voort, F. R. (1998). “Evaluation of shielded thermocouples for measuring temperature of foods in a microwave oven”. *Journal of food science and technology,* 35(4), 325-329.

Risman, P.O., Ohlsson, T. and Lingnert, H. (1993). “Model substances and their use in microwave heating studies”. *SIK report* No 588, 1-10.

Romano, V.R., F. Marra and U. Tammaro (2005). “Modeling of microwave heating of foodstuff: study on the influence of sample dimensions with a FEM approach”. *Journal of Food Engineering,* 71, 233–241.

Sabliov, C.M., K.P. Sandeep and J. Simunovic (2004). “High frequency electromagnetism coupled with conductive heat transfer – a method to predict temperature profiles in materials heated in a focused microwave system”, In: *The 4th World Congress on Microwave and Radio Frequency Applications*, R.L. Schulz and D.C. Folz (Ed.), 469-476.

Salvi, D.A., Boldor, D., Sabliov, C.M., and K.A. Rusch (2008). “Numerical and experimental analysis of continuous microwave heating of ballast water as preventive treatment for introduction of invasive species”. *Journal of Marine Environmental Engineering,* (In press).

Stephan, K.D., and J. A. Pearce (2005). “Microwave radiometry for continuous non-contact temperature measurements during microwave heating”. *Journal of Microwave Power Electromagnetic Energy*, 40(1), 49-61.

Steffe, J.F. (1996). *Rheological Methods in Food Process Engineering*. Freeman Press, East Lansing, MI, USA.

Swain, M.J., Spinassou, A., Swain, M.V.L. (2008). “A test procedure to characterize the heating performance of domestic microwave ovens”. *International Journal of Food Science & Technology*, 43(1), 15-23.

Tang J. (2005). “Dielectric properties of foods”. In: *The Microwave Processing of Foods*, H. Schubert and M. Regier (Ed), CRC Press, pp. 22-38.

Vais, A.E., Palazoglu, T.K., Sandeep, K.P., Daubert, C.R. (2002). “Rheological characterization of carboxymethylcellulose solution under aseptic processing conditions”. *Journal of Food Process Engineering,* 25(1), 41-61.

Yang, H.W. and S. Gunasekaran (2004). “Comparison of temperature distribution in model food cylinders based on Maxwell's equations and Lambert's law during pulsed microwave heating”. *Journal of Food Engineering*, 64 (4), 445-453.

Zhong, Q., Sandeep, K.P., Swartzel, K.R. (2003). “Continuous flow radio frequency heating of water and carboxymethylcellulose solutions”. *Journal of Food Science,* 68(1), 217-223.

Zhong, Q., Sandeep, K.P., Swartzel, K.R. (2004). “Continuous flow radio frequency heating of particulate foods”. *Journal of Innovative Food Science and Emerging Technologies*, 5(4), 475-483.

CHAPTER 5

NUMERICAL MODELING OF TEMPERATURE PROFILES DURING CONTINUOUS FLOW MICROWAVE HEATING FOR WATER, SALTWATER AND CMC SOLUTION AND EXPERIMENTAL VALIDATION

5.1 Introduction

In continuous flow microwave heating of liquids, volumetric heat generated as a function of electric field distribution and dielectric properties of the fluid is transferred in the flowing fluid by conduction and convection. Comprehensive 3-D numerical modeling of the process requires coupling of energy and momentum equations to Maxwell's equations. Numerous studies are available on coupling electromagnetism and conduction heating, particularly for solids (Lin et al., 1995; Mao et al., 2005; Romano et al., 2005; Zhang and Datta, 2006) as well as on coupling electromagnetism with free convection heating for liquids (Datta, et al., 1992; Ohlsson, 1993; Zhang et al., 2000). Coupling of electromagnetism with forced convection and conduction heat transfer is investigated by few researchers interested to numerical model the process of continuous flow microwave heating. Le Bail et al. (2000) simulated the temperature profiles in fluids under continuous heating assuming uniform volumetric power in the core of the flow. Ratanadecho et al. (2002) used a 2-D finite difference time domain (FDTD) formulation to solve Maxwell's equation and finite control volume method based on SIMPLE algorithm to solve heat transport and fluid flow equations in rectangular duct geometry; an iterative computational scheme was used to couple Maxwell's equations with momentum and heat transfer equations. Zhu et al. (2007a, 2007b, and 2007c) used a similar algorithm for numerical modeling of continuous flow microwave heating in cylindrical and rectangular ducts.

The above mentioned studies (Le Bail et al., 2000; Ratanadecho et al., 2002; Zhu et al., 2007a, 2007b, and 2007c) used complex alliances of FDTD algorithms and finite volume

methods using independent codes. In depth knowledge of programming and numerical analysis is required for development of such codes; in addition, authentication of independent codes with benchmark problems is necessary. Engineers not trained in associated programming languages have the alternative of using commercial multiphysics software packages to create a generic model. These software packages allow coupling of a variety of fundamental equations each describing a different physical phenomenon, provide multiple options for geometry and mesh generation, and various solvers and result visualization alternatives.

Multiphysics software packages such as ANSYS and COMSOL have been used for modeling of microwave heating. Coupling of electromagnetism and heat transfer with mass transfer was accomplished by Zhou et al. (1995) in ANSYS. Numerical modeling and validation of continuous flow microwave heating of liquids was also completed in ANSYS by Sabliov et al. (2007) and Salvi et al. (2008a). Researchers have also used COMSOL for modeling of microwave heating of solids (Komarov and Yakovlev, 2001; Hu and Mallikarjunan, 2002; Mirabito, et al., 2005; Curet et al., 2006; Hansson, 2006; Feldman et al., 2007), while others (Knoerzer et al., 2006) used COMSOL to couple electromagnetism with heat transfer from the available EM simulator Quickwave-3D via MATLAB interface. Simulated results were observed to be in agreement with measured values (Hu and Mallikarjunan, 2002; Knoerzer et al., 2006; Hansson, 2006; Curet et al., 2006) and with results from other EM simulators (Mirabito et al., 2005; Komarov and Yakovlev, 2001). However, no studies are available on relative comparison of coupled models in ANSYS and COMSOL based on electromagnetism, fluid flow, and heat transfer. This information could be critical in consolidating the understanding of the microwave heating process, and could be used as a tool in software selection.

Furthermore, rigorous experimental validation of continuous flow microwave heating is essential, which was limited in the past by the non-availability of extensive temperature data in the microwave cavity. Experimental measurement of the temperature in the continuous microwave is difficult due to the interference of the electromagnetic field by introduction of measuring devices and the continuous nature of the process. A comprehensive temperature measurement in the dielectric undergoing continuous flow microwave heating was accomplished using a new fiber optic probe system and was presented in a previous paper (Salvi et al., 2008b).

The goal of the present paper is to develop a complete 3-D model based on coupling of Maxwell's equation with heat and momentum transport equations in COMSOL Multiphysics (COMSOL, Inc**.,** MA, USA) and to compare the results with a similar, pre-developed model in ANSYS Multiphysics, and with experimental data. The objectives of the study are:

1. To numerically simulate the temperature in fluids with different dielectric and physical properties heated in a continuous flow microwave system by coupling electromagnetism, fluid flow and heat transport in COMSOL and ANSYS,
2. To verify the results from the developed COMSOL model by comparison with similar pre-developed ANSYS multiphysics model,
3. To improve the COMSOL model by including non-Newtonian flow and phase change,
4. To validate the developed numerical COMSOL model with rigorous experimental data.

5.2 Materials and Methods

The methodology was divided in two sections. Section one comprised of COMSOL Multiphysics model development and its verification with ANSYS Multiphysics. The second section included improvement of the COMSOL model and its validation with experimental results. Initially, simplified COMSOL model was developed and it was verified with pre-

developed ANSYS model for freshwater and 1.5 % saltwater flowing at 1 lit/min and 1.6 lit/min. For verification, the modeling parameters were ensured to be consistent in both software packages including microwave cavity geometry, applicator tube (3.81 cm diameter), incident power (4.5 kW), frequency (915 MHz), and material properties. The COMSOL model was further enhanced by incorporating non-Newtonian flow and phase change and the results were validated against experimental data for three liquids (freshwater, 3 % saltwater, and CMC solution) at 2 lit/min flow rate, applicator tube diameter 3.18 cm, and incident power of 4 kW.

Numerical modeling of continuous flow microwave heating in ANSYS and COMSOL includes coupling of three physics phenomena, viz. electromagnetism, fluid flow and heat transfer defined by the following governing equations.

5.2.1 Governing Equations

Electric field distribution is governed by Maxwell's equations. The wave equation obtained from Maxwell's equations is solved to determine electric field distribution in a TE_{10} rectangular waveguide as follows,

$$\nabla \times \left(\frac{1}{\mu'} \nabla \times \vec{E} \right) - \frac{\omega^2}{c} \left(\varepsilon' - i\varepsilon'' \right) \vec{E} = 0 \tag{5.1}$$

where, $\vec{E}$ is electric field intensity (V/m), ε' is relative permittivity or dielectric constant of a material, ε'' is relative dielectric loss of a material, ω is angular wave frequency ($2\pi f$, Hz), μ' is relative permeability of the material and c is speed of light in free space (3×10^8, m/s). The electric field intensity obtained from above equation and material properties are required to calculate the volumetric power generation due to microwave by using following equation,

$$Q = \sigma \mid \vec{E} \mid^2 = 2\pi \varepsilon_o \varepsilon'' f \mid \vec{E} \mid^2 \tag{5.2}$$

where, σ is electrical conductivity of the material (S/m), ε_o is free space permittivity (8.854×10^{-12}, F/m) and f is frequency (Hz)

This volumetric power generation term calculated by solving Maxwell's equations is used as the energy source term in solving Fourier's energy balance equation (equation 5.3) to calculate the temperature distribution due to conduction and convection,

$$\frac{\partial T}{\partial t} + \vec{v}\nabla T = \frac{k}{\rho C_P}\nabla^2 T + \frac{Q}{\rho C_P} \tag{5.3}$$

where, ρ is material density (kg/m^3), C_p is specific heat (J/kg K), k is thermal conductivity (W/mK), T is temperature, (K), $\vec{v}$ is velocity vector (m/s) and Q is the volumetric heat generation due to microwaves (W/m^3).

Velocity profiles are obtained by solving the Navier-Stokes equation (describing the momentum balance and continuity) below,

$$\rho\frac{\partial \vec{v}}{\partial t} = -\nabla P + \mu\nabla^2\vec{v} + \rho g \tag{5.4}$$

$$\nabla \cdot \vec{v} = 0 \tag{5.5}$$

where, ∇P is the pressure force on element per unit volume (N/m^2), g is the acceleration due to gravity (m/s^2), and μ is viscosity (Pa.s) for Newtonian fluids.

5.2.2 Algorithm Development

The algorithm for coupling electromagnetism with fluid flow and heat transfer was developed in ANSYS as well as COMSOL (**Figure 5.1**). First, the wave equation (equation 5.1) was solved to calculate the electric field distribution and heat generation (equation 5.2) taking

dielectric properties of the liquids into account. The heat generation term was used as source term in solving energy and balance equation (equations 5.4-5.5) based on the physical and thermal properties of the liquids. The energy, momentum and continuity equations were solved simultaneously to obtain velocity and temperature profiles. While developing the algorithm, fluid flow was assumed to be incompressible and the PTFE tube was considered completely transparent to microwaves. Specifics on model development in ANSYS and COMSOL are described below.

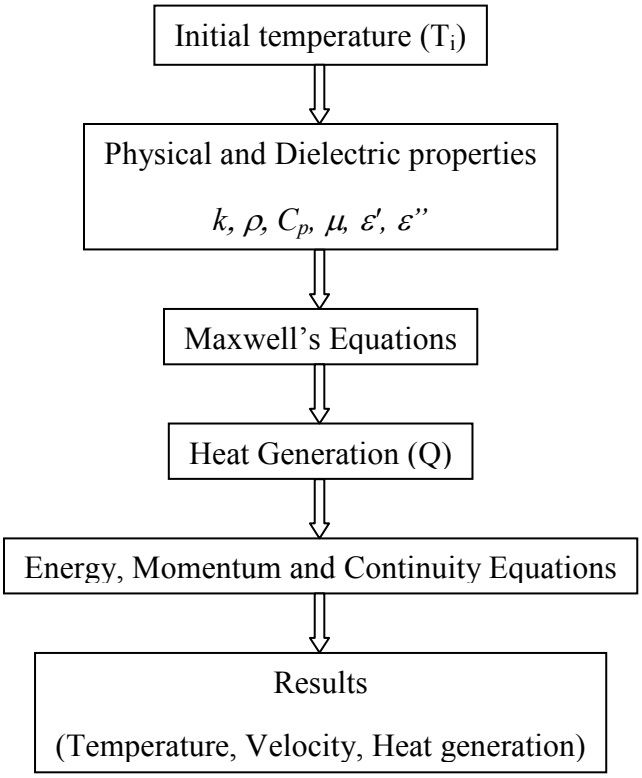

Figure 5.1 Algorithm for coupling of electromagnetism and heat and mass transfer

5.2.3 Model Development in ANSYS

The ANSYS model was developed by one way coupling considering temperature independent physical and dielectric properties of the liquids heated in the continuous microwave system (**Figure 5.2**). Tetrahedral elements HF119 (size 0.03m for waveguide and cavity and 0.005 for applicator tube) were used in the electromagnetic module (for solving Maxwell's

equations) and tetrahedral elements FLUID142 (size 0.005) were applied in the FLOTRAN module (for solving fluid flow and heat transfer). Material properties for freshwater and 1.5 % saltwater were obtained from literature (**Table 5.1** and **5.2**). Applicator tube (diameter 3.81 cm) was considered transparent to microwaves. Boundary conditions for electromagnetism included the TE_{10} mode specific to rectangular waveguide port, perfect electric conductor walls of waveguide and cavity, 915 MHz frequency, and 4.5 kW input power. Sparse direct solver was used to solve Maxwell's equation and the heat generation term was transferred using ANSYS Multifield Solver between dissimilar meshes. The heat generation was used as source term in solving energy, momentum, and continuity equations. Boundary conditions in FLOTRAN included inlet velocities (0.021 m/s at 1 lpm and 0.034 m/s at 1.6 lpm), inlet temperature (25°C), outlet pressure (1 atm), and adiabatic conditions at the applicator wall. In this simplified model, phase change not was considered and the model was developed for Newtonian flow. The model was validated for ballast water applications in the past (Salvi et al., 2008), and compared against COMSOL results in the present paper.

Table 5.1 Physical properties of fluids

Fluid	Thermal conductivity (k), W/m K	Material density (ρ), kg/m3	Specific heat (Cp), J/kg K	Viscosity (μ), Pa.s	
Freshwater	0.6110[1]	994.9[1]	4177.3[1]	0.8937e-3[2]	
1.5 % Saltwater	0.6035[1]	1037.6[1]	4086.2[1]	0.8629e-3[2]	
3 % Saltwater	0.6035[1]	1037.6[1]	4086.2[1]	0.8422e-3[3]	
CMC	0.6091[1]	997.9[1]	4164.4[1]	K	n (Pa.s^n)
				0.916[4]	0.60[4]

Ref: [1] Choi and Okos, 1986; [2] Geankoplis et al., 1993; [3] Boufadel et al., 1999; [4]Vais et al., 2002

Table 5.2 Dielectric properties of the fluids

Fluid	Dielectric loss (ε′)	Dielectric Constant (ε″)
Freshwater[1]	84.89	4.08
1.5 % Saltwater[2]	76.5	52.08
3 % Saltwater[3]	73.29	95.89
CMC Solution[3]	77.79	8.90

Ref.: [1]Komarov and Tang, 2004; [2]Ikediala *et al.*, 2002; [3]Coronel et al., 2008

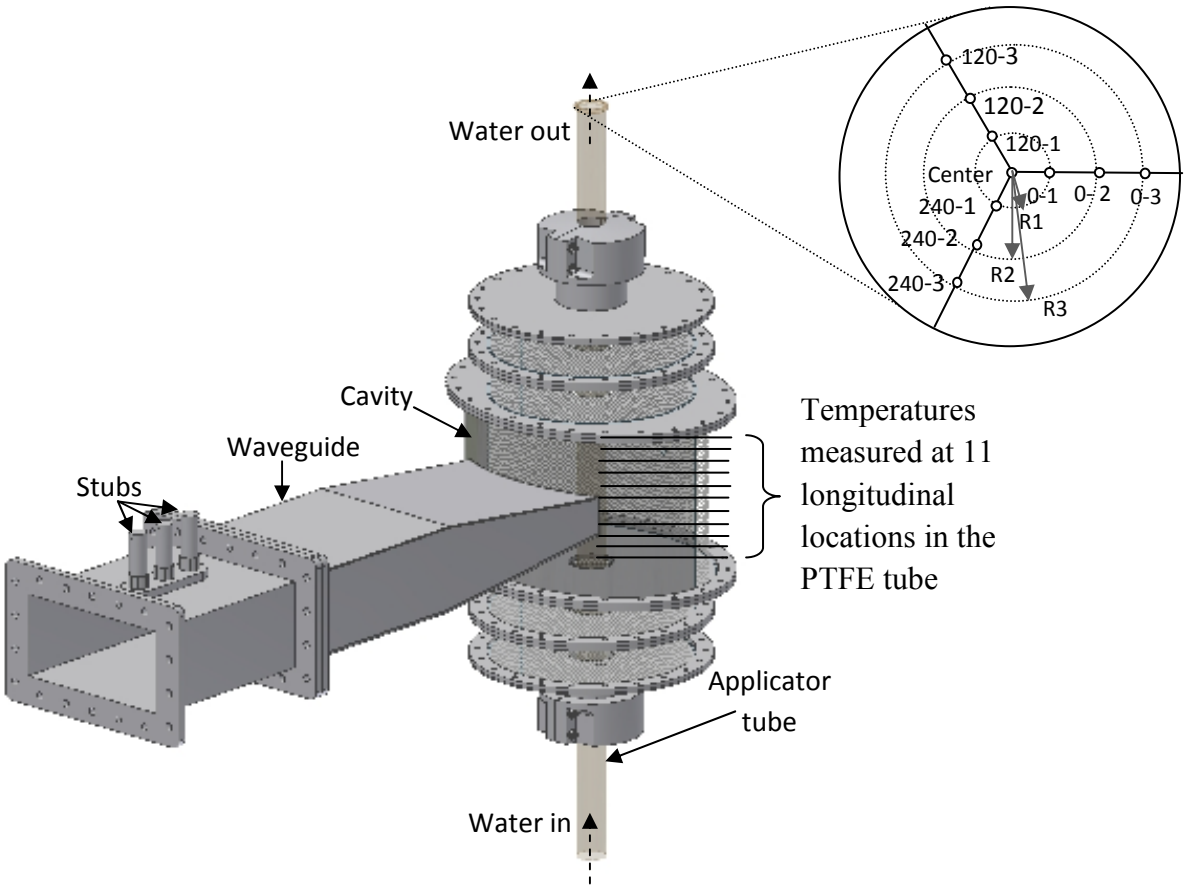

Figure 5.2 Continuous flow microwave system (IMS) with temperature measurement locations

5.2.4 Model Development in COMSOL

Analysis of electromagnetic waves in COMSOL 3.4 (formerly known as FEMLAB) was accomplished in the RF and microwave application module. The software does not have a predefined module to couple electromagnetism with heat transfer and fluid flow. Hence, the RF

module (used for microwave and radio frequency heating) was coupled next with the Fluid Dynamics module (used to solve momentum and continuity equations) and the Heat Transfer module (used to solve energy balance equations) to solve the temperature profile in the liquid heated in a continuous microwave system.

In contrast to ANSYS, the same mesh can be used for RF module (for solving electromagnetism) as well as Fluid Dynamics and Heat Transfer module in COMSOL and as such the transfer of the generated heat is simplified. For fair comparison, a COMSOL model was developed based on similar boundary conditions and mesh sizes as in ANSYS as follows.

The geometry representing the experimental setup (**Figure 5.2**) was created that included the waveguide, elliptical cavity and applicator tube. The computational domain was meshed using a tetrahedral grid. For electromagnetic problems, the element size S_{max} requirement was decided based on the Nyquist criterion (Mirabito et al., 2005)

$$S_{\max} < \frac{\lambda}{2} = \frac{c}{2f\sqrt{\varepsilon'\mu'}} \tag{5.6}$$

where, λ is the wavelength (m), f is the frequency of the wave (Hz), c is the speed of light in a vacuum (m/s), ε′ is the dielectric constant, and μ′ is the relative permeability. Some studies suggest that an acceptable criterion for finite element solution of Maxwell's equations is to use six grids per wavelength (Zhang et al., 2001), which is more stringent than Nyquist criterion. Based on material properties and these criteria the mesh size used in this model was 0.03 m in the waveguide and cavity, and 0.005 m in the applicator tube.

The boundary conditions for RF module included, perfect electric conductors walls of the waveguide implying that $\hat{n} \times \vec{E} = 0$. At the port, 4.5 kW of electromagnetic energy was supplied

through a rectangular TE_{10} mode at an operating frequency of 915 MHz. The PTFE applicator tube was assumed negligible in thickness and transparent to microwaves. Continuity boundary was used between two dielectrics implying $\hat{n} \times \left(\vec{E}_1 - \vec{E}_2\right) = 0$. For energy and momentum balance equation average initial velocities (0.021 m/s at 1 lpm and 0.034 m/s at 1.6 lpm) were used. Zero velocity condition was applied at the interior wall of the applicator tube. The inlet temperature was set according to measured initial temperature value of 25^{o}C, and the outlet pressure was set to atmospheric pressure. Adiabatic conditions were applied at the applicator wall (no heat was assumed exchanged between the dielectric and the air in the elliptical cavity). The heat generation from electromagnetic module was used as a source term in the heat transfer equation. The material properties were same as used in ANSYS model (**Table 5.1** and **5.2**).

The wave equation (equation 5.1) was solved in RF module using generalized minimum residual solver (GMRES) to calculate the heat generation (equation 5.2). The energy and momentum equations (equation 5.4-5.5) were solved in Fluid Dynamics and Heat Transfer module using parallel direct linear solver (PARDISO) by using the heat generation from the RF module to get the velocity and temperature profiles.

Further, this COMSOL model was extended to accommodate phase change and non-Newtonian flow and the numerical results were validated using experimental data. The development of improved COMSOL model and experimental procedure are described in the following sections.

5.2.5 Development of Improved COMSOL Model

The above simplified model was developed for Newtonian fluids. Most liquid food products are non-Newtonian and hence it was necessary to improve the model by incorporating

non-Newtonian flow. The viscosity used (μ) in the previous model was replaced by apparent viscosity (μ-Pa.s) for non-Newtonian fluids following power law (Steffe, 1992)

$$\mu = K(\dot{\gamma})^{n-1} \tag{5.7}$$

where, K is flow behavior index and n is consistency coefficient (Pa.s^n) for the fluid and $\dot{\gamma}$ (s^{-1}) is shear rate.

The boundary conditions applied were modified in the improved COMSOL model to represent the actual experimental conditions. These modified boundary conditions were- incident power (4 kW), average initial velocity (0.0419 m/s), inlet temperature 25^{o}C for 3 % saltwater and 22^{o}C for freshwater and CMC. The dimensions of the applicator tube were also changed to those specific to the tube (3.84 cm diameter and 25.4 cm length) available experimentally. Thermal conductivity, specific heat and density for the fluids were obtained from literature (Choi and Okos, 1986; Geankoplis et al., 1993; Boufadel et al., 1999; Vais et al., 2002). The dielectric properties for saltwater and CMC solution were calculated as a function of concentration (g/l) and temperature (^{o}C) (Coronel et al., 2008). For freshwater, the dielectric properties were calculated using a correlation given by Komarov and Tang (2004) (**Table 5.2)**.

Phase change, another phenomenon that plays a vital role in microwave heating models was included in the improved model. Microwaves generate high volumetric heat density instantaneously in small volume of dielectric materials leading to boiling temperatures in the liquid. The heat is then transferred by convection and conduction in the liquid. The specific heat accounts for the amount of heat used to increase the temperature of the liquid up to boiling point. At boiling point, phase change from liquid to vapor occurs without an increase in the temperature, accounted for by latent heat. High volumetric heat densities during microwave

heating can sometime result in vaporization of the liquid. Since the Convection Conduction Heat Transfer module in COMSOL does not take this latent heat into account, apparent specific heat method is used to incorporate phase change phenomenon following a method described in the literature (Vallejos and Duston, 2005; Curet et al. 2006; Pryor, 2007; COMSOL, 2008). The specific heat in Fourier's energy equation is replaced by apparent specific heat ($Cp + \delta\Delta H$), where ΔH is latent heat and δ is Gaussian function (equation 5.8) used to increase the specific heat smoothly in small phase change region.

$$\delta = \frac{\exp(-(T - T_b)^2 / (\Delta T)^2}{\Delta T \sqrt{\pi}} \tag{5.8}$$

where, T_b is boiling temperature (^oC) and ΔT (^oC) half width of the phase change temperature zone. As the phase change takes place in very narrow temperature zone, the problem was solved in three steps to obtain the solution. The parametric solver was used to allow for a gradual change in ΔT from 50 to 10 ^oC during first step. In the second step, adaptive meshing was performed to refine the mesh in phase changing region assuming the value of ΔT as 10 ^oC. Parametric solver was used again to change ΔT from 10 to 3 ^oC in the final step.

5.2.6 Experimental Measurement of Temperature

The experimental setup included a 915 MHz continuous-flow microwave system (provided by Industrial Microwave Systems (IMS, NC, USA) (**Figure 5.2**). The system consisted of a 5 kW microwave generator, circulator, water load, power coupler, tuning coupler, connecting waveguide, elliptical focusing cavity and an PTFE (polytetraflouroethylene) applicator tube (3.81 cm diameter and 25.4 cm height). Freshwater water, CMC solution (0.5 %) and saltwater (3%) were heated through the continuous-flow microwave system at 4kW of power and flow rate of 2 lit/m. Saltwater was prepared by adding 3 % sea salt (Crystal Sea

Marinemix™ salt, Marine Enterprises International, MD, USA) to tap water and CMC solution was prepared by adding 0.5 % Pre-Hydrated CMC 6000 Powder (TIC Gums Inc., MD, USA) to tap water; both solutions were prepared 24 hours in advance to achieve chemical equilibrium. The temperature was measured at 110 different radial and longitudinal locations using fiber optic temperature probes (Neoptix T1, Neoptix Inc., Québec City, Canada). Specially designed fiber optic temperature measurement device (as described in Salvi et al., 2008a) was used to measure temperature at as many as ten radial points in a cross section of liquid in cylindrical tube; tube was divided in such 11 cross sections at different longitudinal distances (**Figure 5.2**).

5.3 Results

5.3.1 Validation of the COMSOL Model by Comparison of the Simulated Results with ANSYS Model

The COMSOL and ANSYS models were compared at two different salinities (0 and 1.5 %) and two different flow rates (1 lit/m and 1.6 lit/m) in terms of electromagnetic power density and temperature profiles.

5.3.1.1 Electromagnetic Power Generation Density

Total volumetric power generation (equation 5.2) was calculated based on material properties and electric field distribution obtained by solving Maxwell's equations. The total electromagnetic power generation for freshwater was 826 W as predicted by the model developed in COMSOL, as compared to 729 W as predicted by ANSYS whereas for 1.5 % saltwater these values were 2883 W by COMSOL and 2511 W by ANSYS. In general, prediction of power loss by both models was in close agreement (5-13% variation). Cross axial and cross sectional electromagnetic power density profiles are shown in **Figure 5.3** and **5.4** respectively. Cross axial power density profiles (**Figure 5.3)** for both models exhibited Mathieu function distribution with highest electromagnetic power density at the center of the tube and

lower around the walls. The discrepancy in the power densities values in the center between ANSYS and COMSOL model was 6 % for freshwater and 12 % for saltwater. The high power density region in the central part of the applicator tube due to incident electromagnetic waves was evident in both models (**Figure 5.3)**.

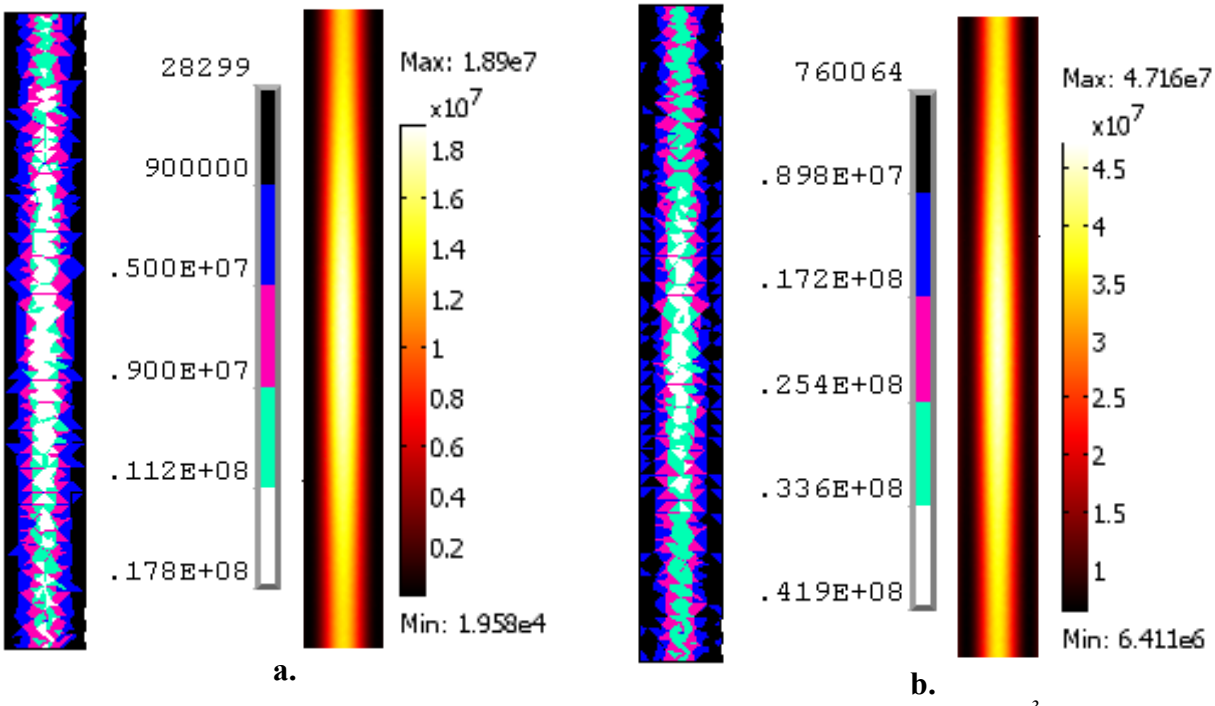

Figure 5.3 Cross-axial (x-y) plane view of e*lectromagnetic power density (W/m^3)* by ANSYS and COMSOL for **a.** freshwater and **b.** saltwater (1.5 %)

The cross sectional profiles revealed the high power density regions located slightly off center and lower density regions at the edges for freshwater (**Figure 5.4a** and **b**), and higher densities slightly off center and at the edges away from the direction of microwaves for 1.5 % saltwater (**Figure 5.4c** and **d**). The electromagnetic power density in COMSOL was observed to be in the range of 168.76-2.058x10^7 W/m^3 for freshwater and 2.36 x10^6-4.58 x10^7 W/m^3 for 1.5 % saltwater. The upper bound of the range was 15 % higher in COMSOL than that of ANSYS.

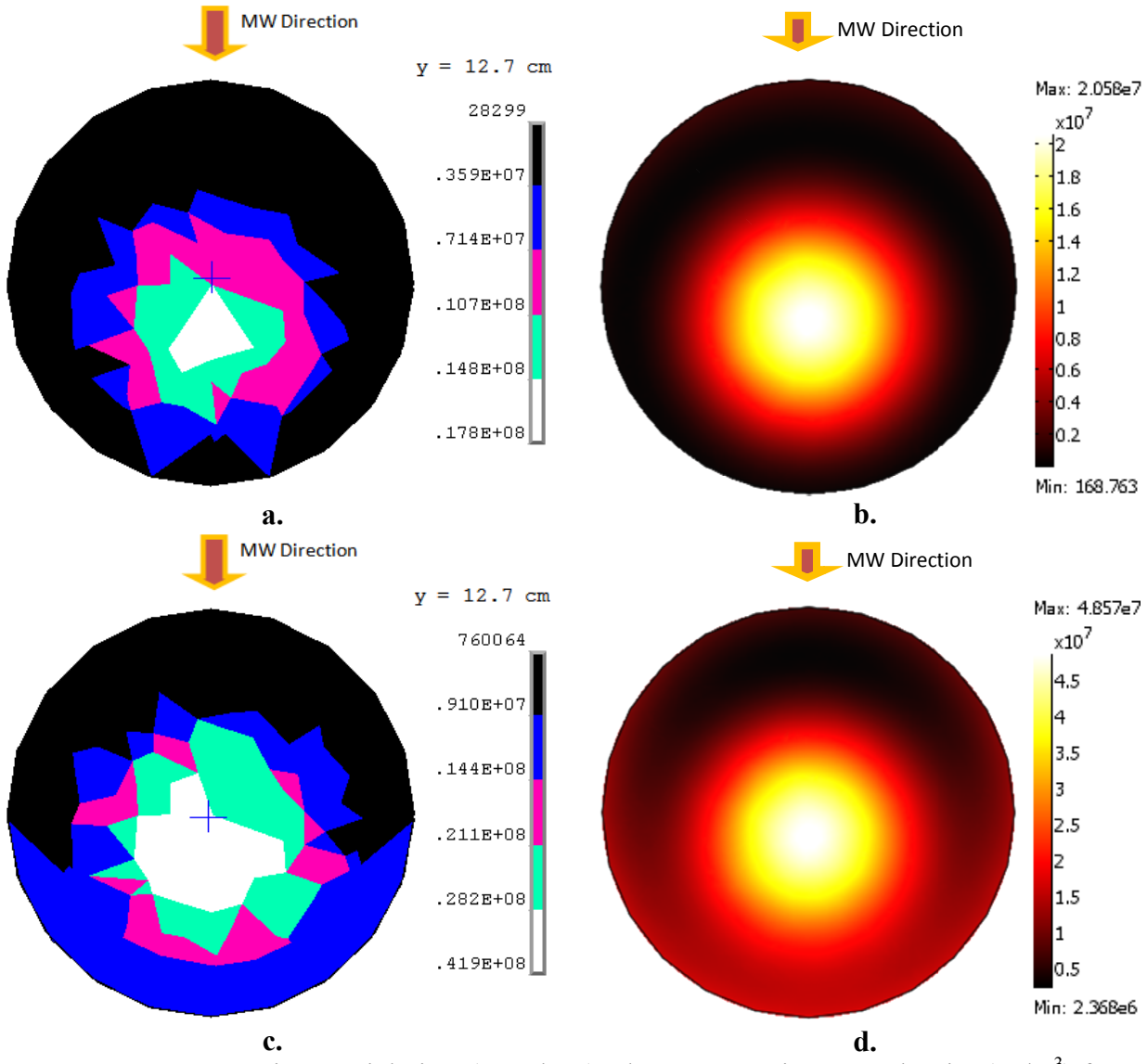

Figure 5.4 Cross-section spatial view (x-z plane) electromagnetic power density (W/m^3) for freshwater in **a.** by ANSYS and **b.** by COMSOL and for saltwater (1.5%) **c.** by ANSYS and **d.** by COMSOL at the center of the tube

5.3.1.2 Cross-section Spatial Temperature Distribution (x-z plane)

Cross sectional temperature profiles obtained from the models developed in ANSYS and COMSOL for both flow rates (1 and 1.6 lit/min) for 1.5 % saltwater and freshwater are presented in **Figures 5.5**. For freshwater, the temperature values ranged from 26-42^{o}C for ANSYS (**Figures 5.5a**) and 25-47^{o}C for COMSOL (**Figures 5.5b**) at 1 lit/min and 25-37^{o}C for ANSYS (**Figures 5.5c**) and 24-39^{o}C for COMSOL (**Figures 5.5d**) at 1.6 lit/min. The spatial temperature distribution profiles from both models were clearly identical with the hot spot slightly off-center

opposite to the direction of incident microwave for both models in freshwater. Similarly, for 1.5 % saltwater (**Figure 5.6**) the temperature profiles matched well with highest temperature at the edges (away from the direction of microwave) and lowest temperatures near waveguide (MW direction) at both flow rates. The temperature values ranged from 29-115^{o}C for ANSYS (**Figure 5.6a**) and 27-85 ^{o}C for COMSOL (**Figure 5.6b**) at 1 lit/min and 27-91^{o}C for ANSYS (**Figure 5.6c**) and 26-66^{o}C for COMSOL (**Figure 5.6d**) at 1.6 lit/min. The cross sectional temperature values for saltwater (1.5 %) (**Figure 5.6**) from COMSOL model at the center of the tube were similar with results from ANSYS model, but at the edges a higher discrepancy was observed (≈ 1.35 times higher for both flow rates). This discrepancy was attributed to the result of load transfer between same versus dis-similar meshes, differences in the meshing algorithms, and the numerical solvers used.

In general, both ANSYS and COMSOL provided an interface for multiphysics coupling electromagnetism with fluid flow and heat transfer. ANSYS used different mesh elements for different physical phenomenon and the coupling was achieved by transfer of results from one physics to another between dissimilar meshes. However, for such coupling a compatible element was essential in information transfer between the modules. Future versions of ANSYS will facilitate such linking and embedded coupling of modules such as those inherent in this study should be available. COMSOL, on the other hand, offered common elements that can be used to couple all physics providing a flexible model setup.

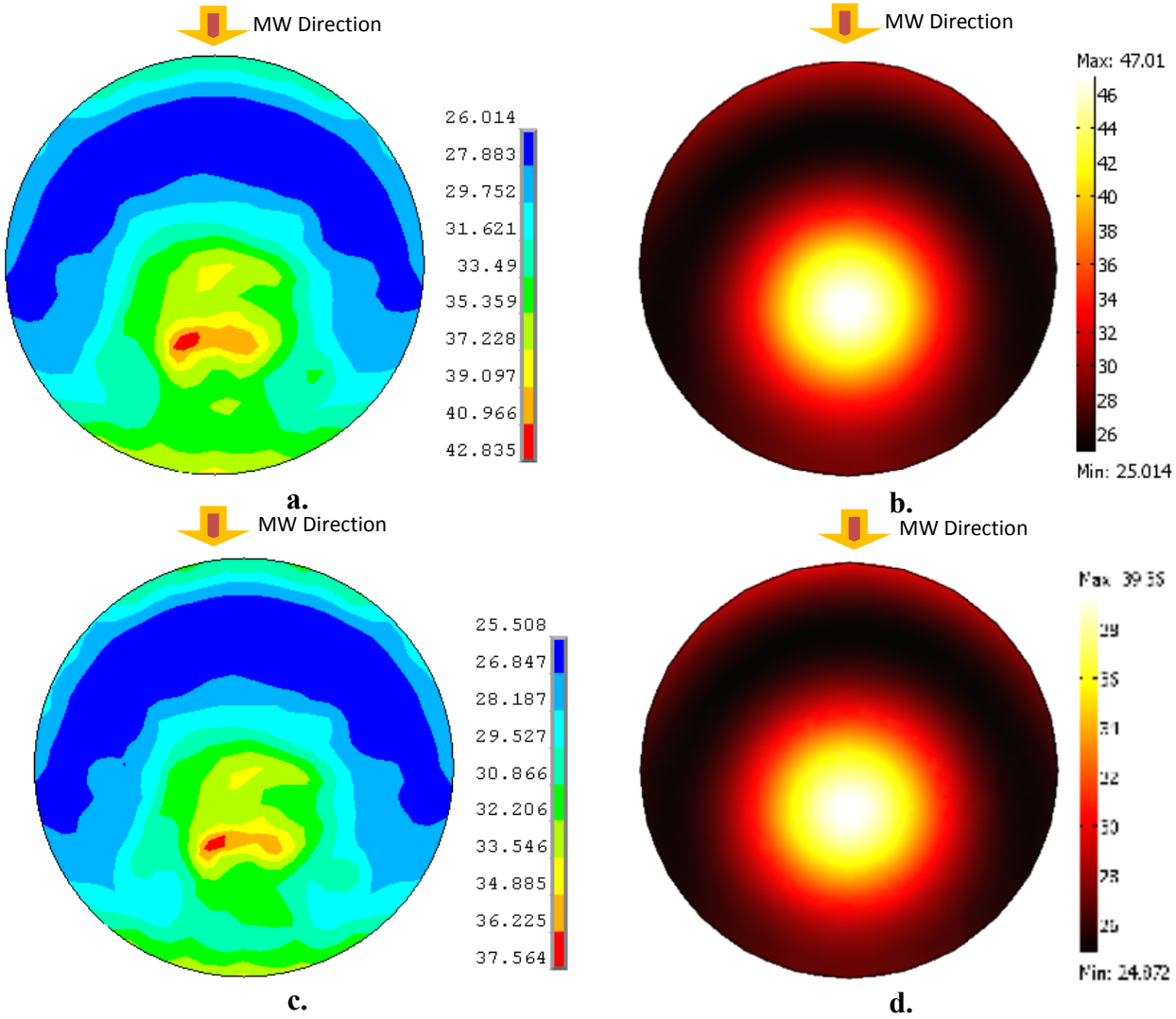

Figure 5.5 Cross-section spatial temperature distribution (x-z plane) for freshwater heated at 1 lit/min **a.** by ANSYS and **b.** by COMSOL and at 1.6 lit/min **c.** by ANSYS and **d.** by COMSOL at the center of the tube

Some limitation of COMSOL faced in this study in terms of memory requirement for solving models with large number of grid elements is mentioned in the literature (Achkar et al., 2008). On the other hand, embedded parametric solver available in COMSOL was particularly appropriate for easily incorporating phase change phenomenon. Overall, the electromagnetic power density and temperature distribution from COMSOL model matched well with pre-validated ANSYS model. This verification ensured accuracy of COMSOL model.

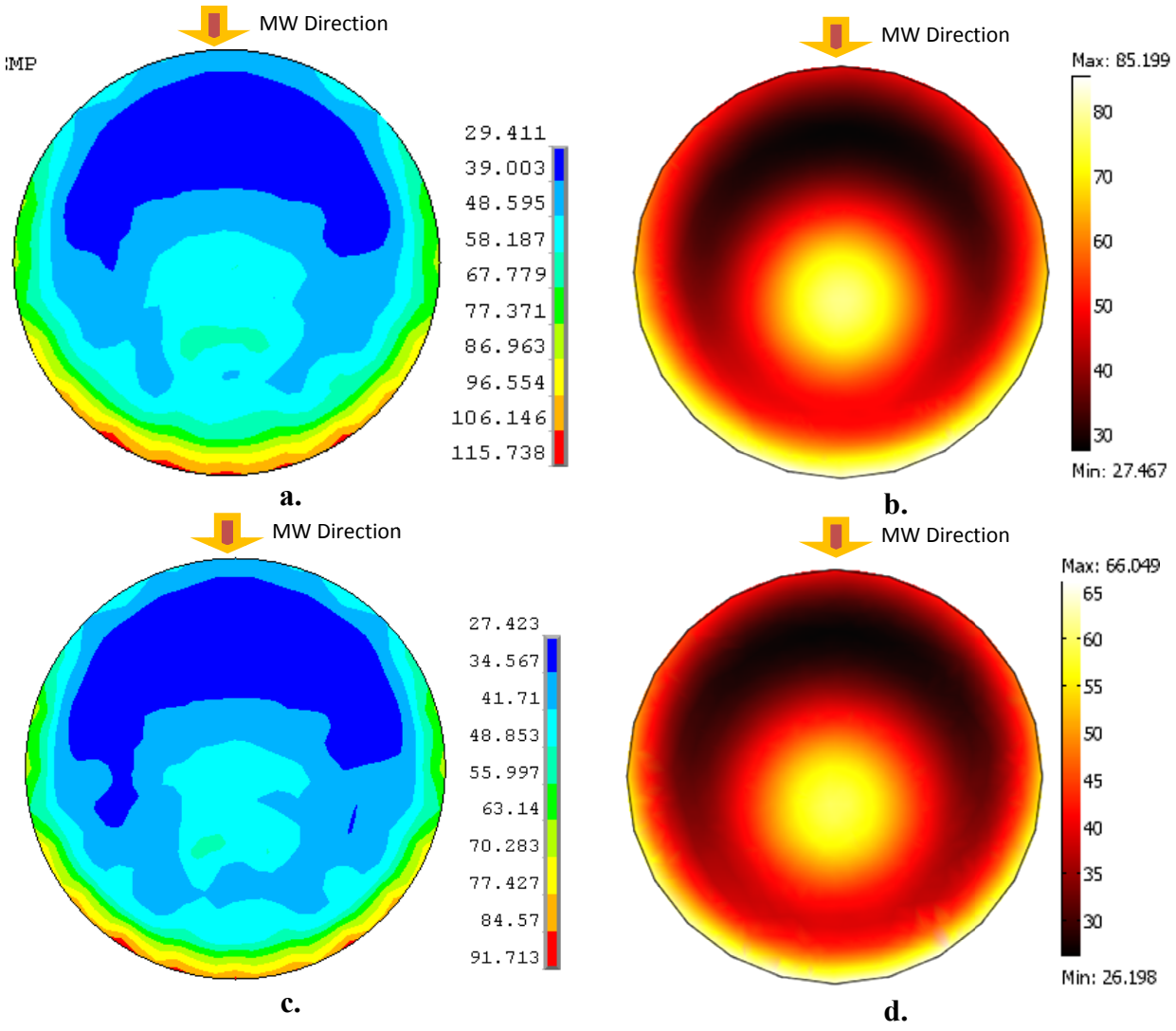

Figure 5.6 Cross-section spatial temperature distribution (x-z plane) for saltwater (1.5%) heated at 1 lit/min **a.** by ANSYS and **b.** by COMSOL and at 1.6 lit/min **c.** by ANSYS and **d.** by COMSOL at the center of the tube

5.3.2 Validation of the COMSOL Model against Experimental Data

The verified COMSOL model was further enhanced to accommodate non-Newtonial flow and phase change and the results were compared with experimental data for CMC solution, saltwater (3 %) and freshwater at 2 lit/min flow rate. The total electromagnetic power generation from the model was 1953 W for CMC solution, 3568 W for 3 % saltwater, and 742 W for freshwater as compared to experimental values of 2520 W, 3960W, and 2800 W, respectively.

The power generation values were predicted well for saltwater (90 % accuracy) followed by CMC (78 % accuracy). The predicted power generation value was very low (27%) for freshwater as compared to experimental data. The temperature profiles in freshwater cannot be verified as the simulated power generation was much different than that measured experimentally, most likely due to the dissimilar dielectric properties of the tap water used in the experiments, as compared to the values found in the literature.

A comparison between average experimental and average simulated temperature at each cross section at 11 longitudinal locations is shown for CMC solution, 3 % saltwater and freshwater (**Figure 5.7**). A fairly good agreement was observed between the average experimental and simulated values for 3 % saltwater (R-Square value 0.94), followed by CMC (R-Square value 0.86), and freshwater (R-Square value 0.59). A direct effect of low power generation in the model reflected in low R-square values for freshwater.

To understand temperature profiles at particular radial locations (center and half radius at angle 0 120 and 240), experimental and simulated temperatures were plotted against longitudinal distance from the entrance of the cavity for all three fluids at 2 lit/min (**Figure 5.8**, **5.9,** and **5.10**). For CMC (**Figure 5.8)**, the model under-predicted the temperature at center (difference as high as 29^{o}C) and at angle 0 (difference as high as 20^{o}C), and matched better at angle 120 and 240. Non-mixing in viscous CMC solution was considered by inclusion of non-Newtonian flow in the model, but the dielectric loss increase with temperature for CMC was not considered in the model and hence under-prediction was seen in the central high temperature region.

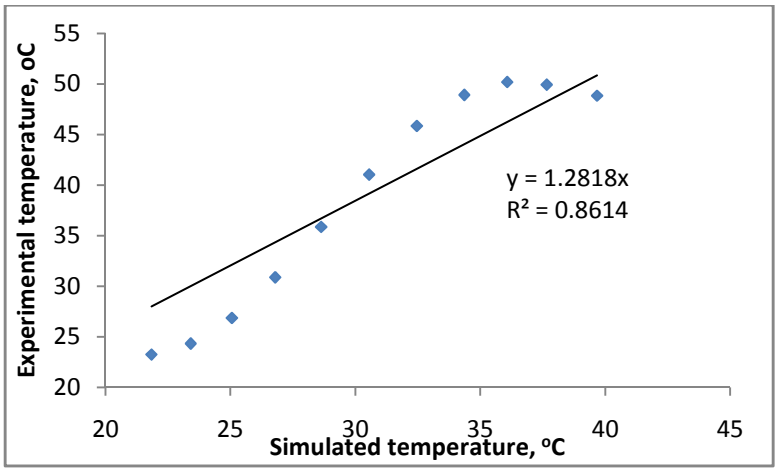

a.

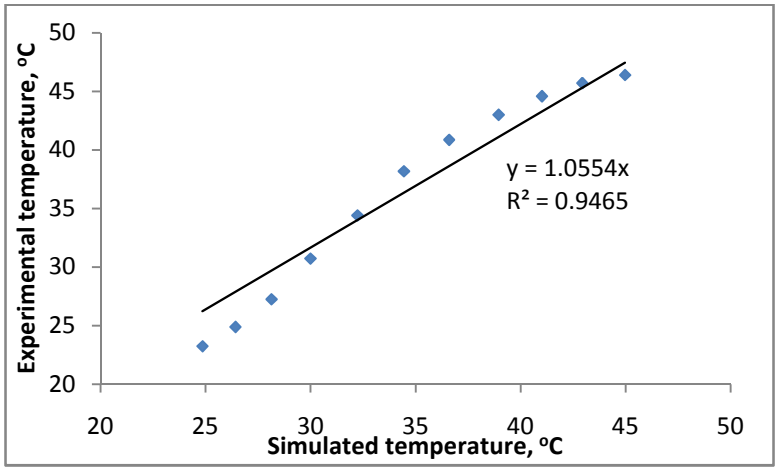

b.

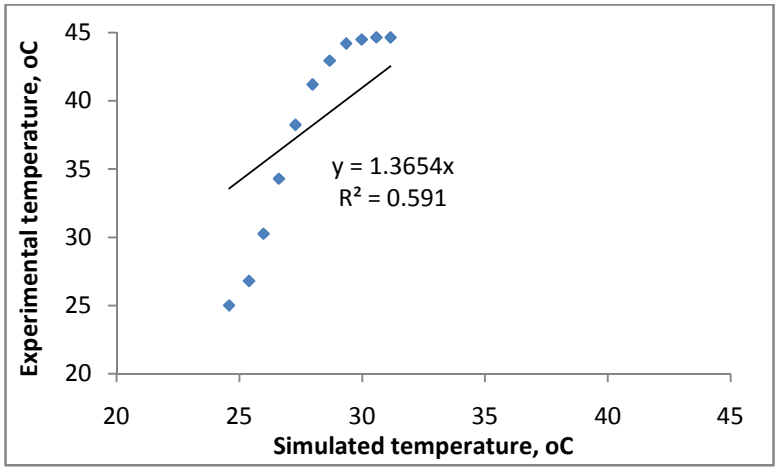

c.

Figure 5.7 The comparison between average experimental and average simulated temperature for **a.** CMC solution **b.** 3 % saltwater and **c.** freshwater

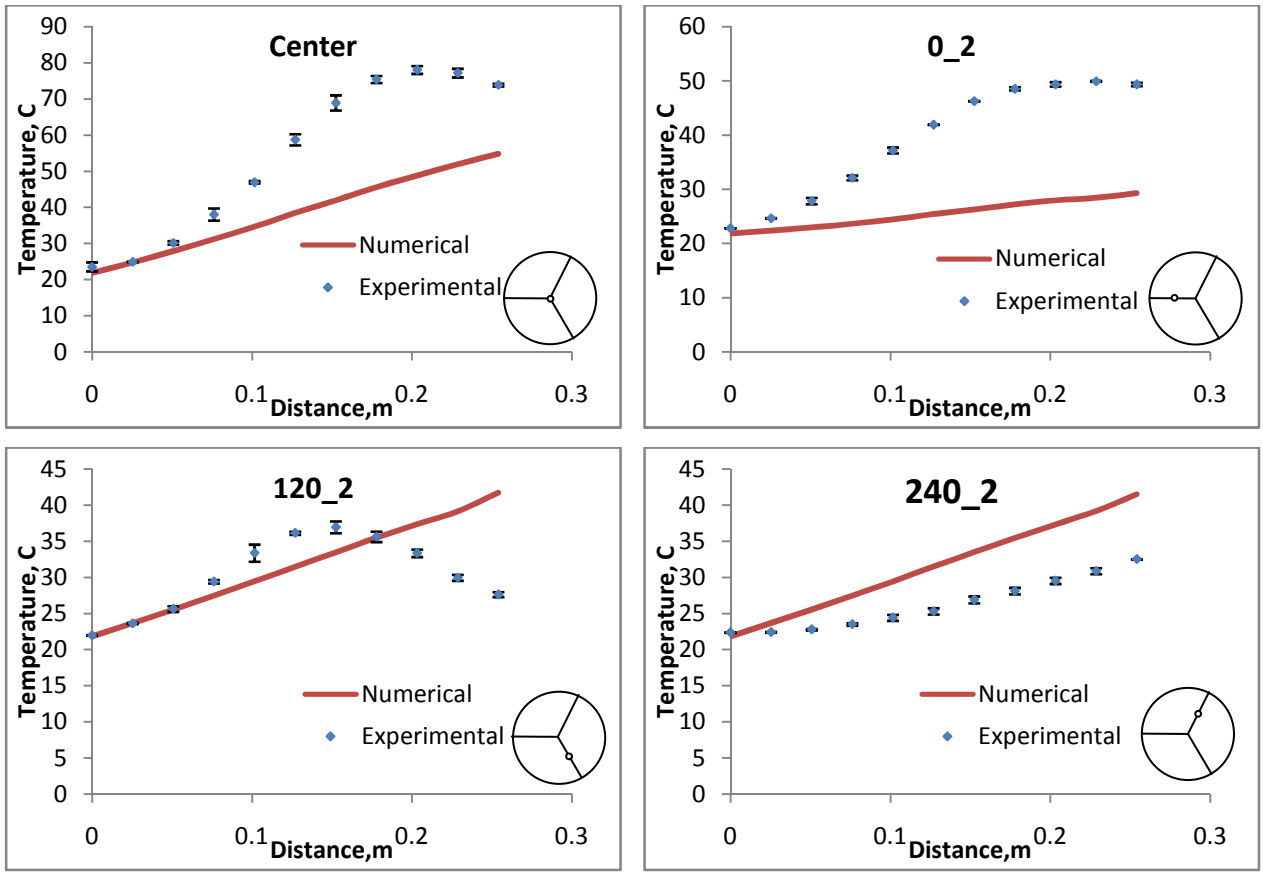

Figure 5.8 Simulated temperatures at selected radial locations against distance from the entrance of the cavity for CMC solution

For 3 % saltwater, the simulated temperature matched well with the experimental data except at angle 0 (direction of the incident microwaves) (**Figure 5.9)**. At angle 0, the difference between experimental and numerical was as high a 14^{o}C. On contrary to CMC, saltwater (3 %) showed uniform temperature distribution in cross section both numerically as well as experimentally. For example, in the cross section at the end of the cavity (0.254 m), temperature values range from 30-42 ^{o}C numerically, as compared to the 40-45 ^{o}C range experimentally. For freshwater, temperature differences as high as 30^{o}C were observed **(Figure 5.10)**, this was expected due to the lower heat generation values calculated in RF module.

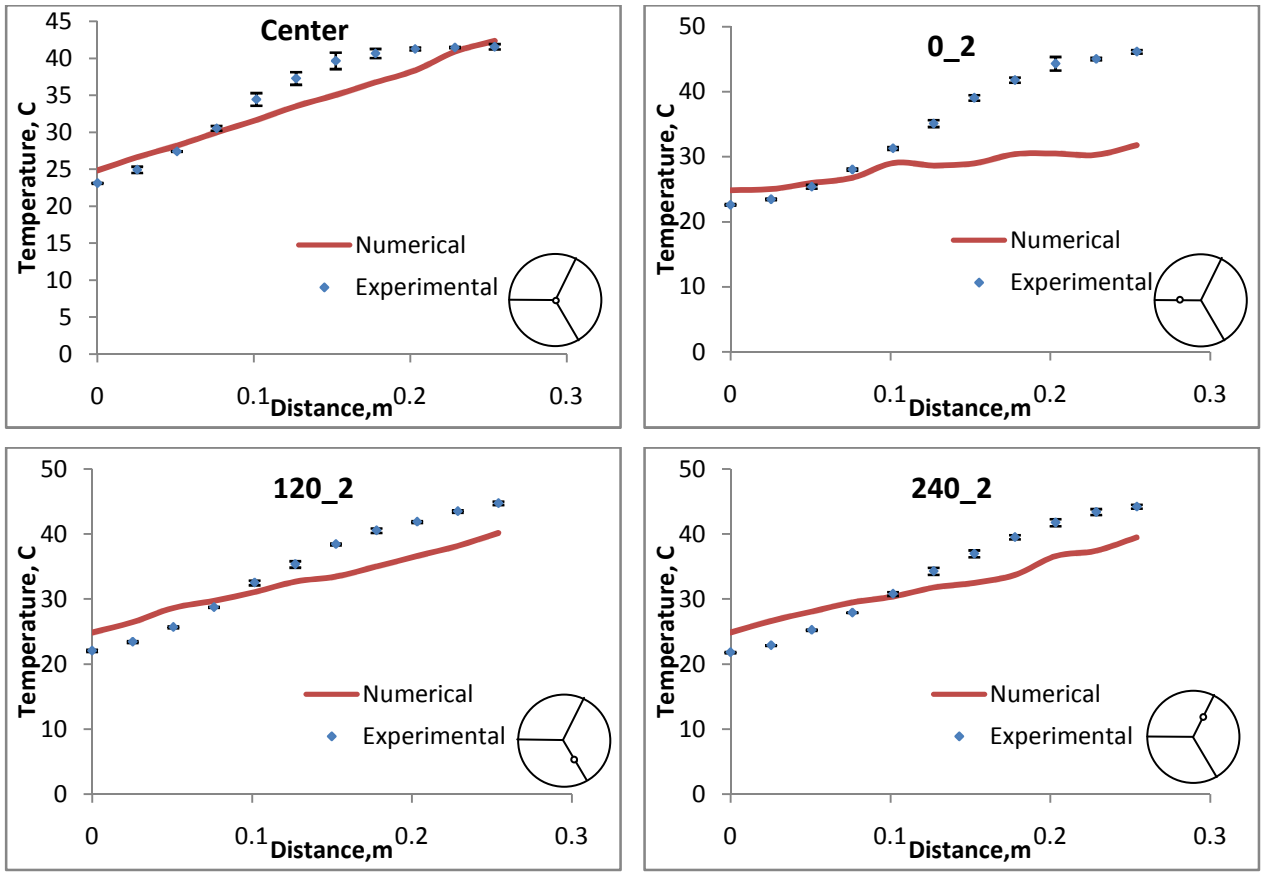

Figure 5.9 Simulated temperatures at selected radial locations against distance from the entrance of the cavity for saltwater (3%)

5.3.3 Cross-section Spatial Temperature and Electromagnetic Power Density Profiles

The results obtained from the model were used to understand the microwave heating in all three liquids in a continuous flow microwave system. The cross section spatial electromagnetic power density and temperature distributions were studied in the middle of the tube (**Figure 5.11, 5.12,** and **5.13**). The heat generation was observed concentrated in the center of the tube for both CMC solution (4.6×10^7 W/m^3) and freshwater (1.86×10^7 W/m^3) (**Figure 5.11a,** and **5.13a**). Electromagnetic power generation is a function electric field intensity and dielectric loss. Since dielectric loss for CMC solution ($\varepsilon'' = 8.9$) and freshwater ($\varepsilon'' = 4.08$) were comparable in order of magnitude, similar power generation profiles were seen and lower values for freshwater were observed in comparison to CMC and saltwater (3 %). As a result of higher

dielectric loss (ε"= 95.89), the electromagnetic power density was higher for saltwater (3 %). As the microwave system was designed using dielectric properties of saltwater, a more uniform electromagnetic power density was observed ($0.8x10^7$-$3.8x10^7$ W/m^3) for this product (**Figure 5.12a)**. The temperature distribution in cross section spatial view for saltwater (3 %) was also more uniform; a direct influence of electromagnetic power density uniformity was observed. The higher temperature at the outer edges was as a result of zero velocity fluid at the edges due to laminar flow conditions.

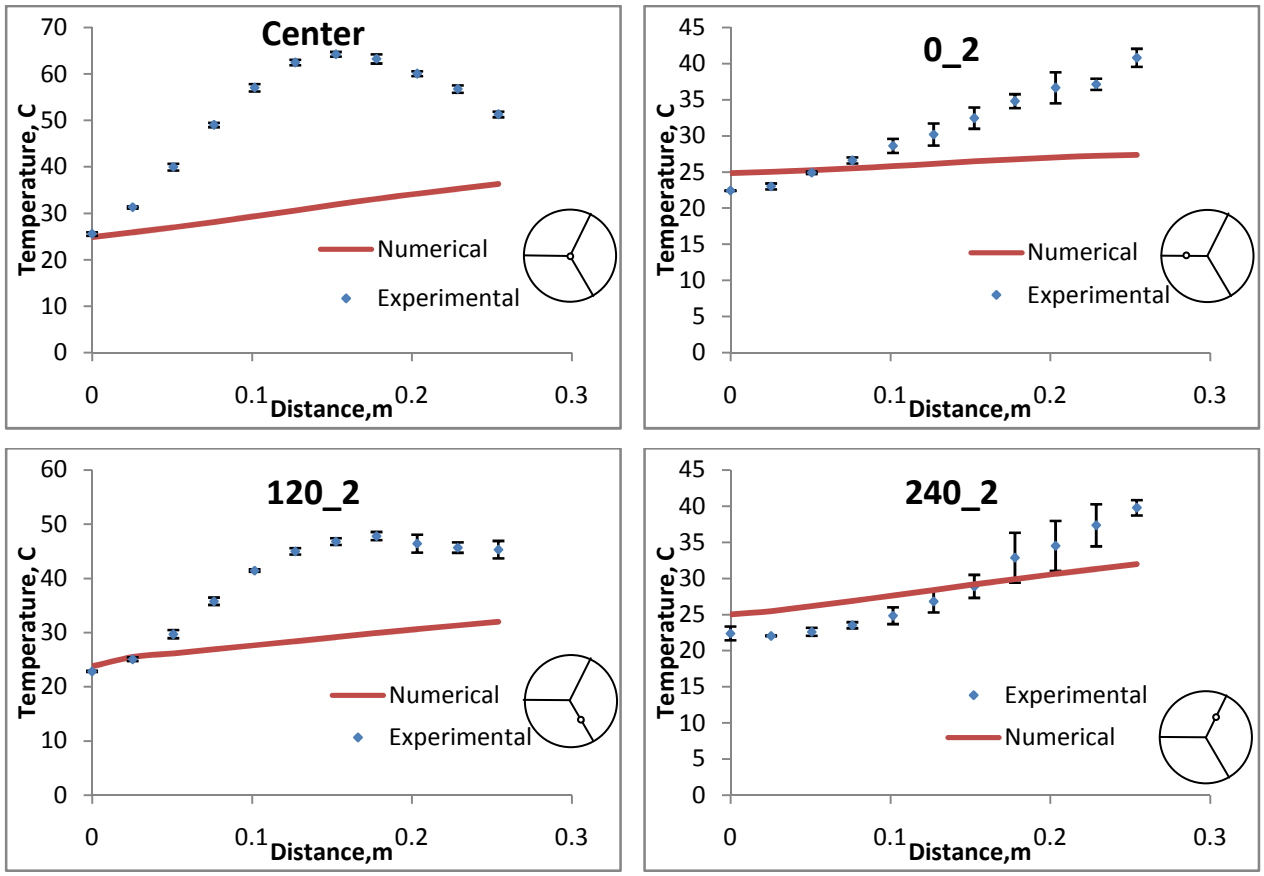

Figure 5.10 Simulated temperatures at selected radial locations against distance from the entrance of the cavity for freshwater

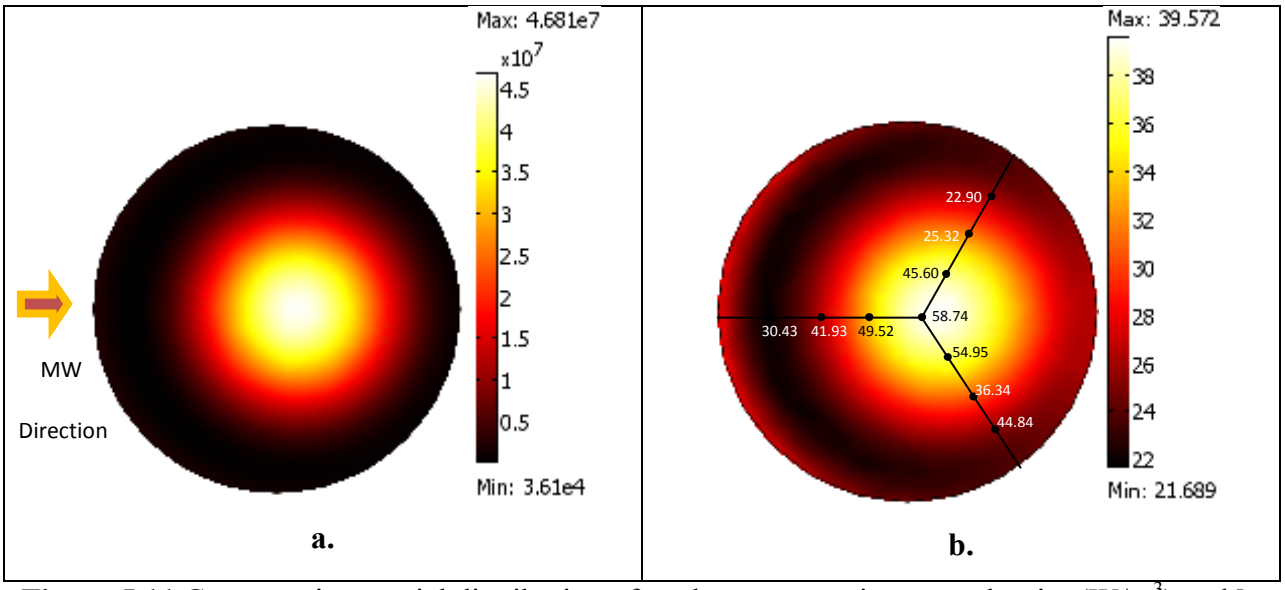

Figure 5.11 Cross section spatial distribution of **a.** electromagnetic power density (W/m^3) and **b.** temperature for CMC solution

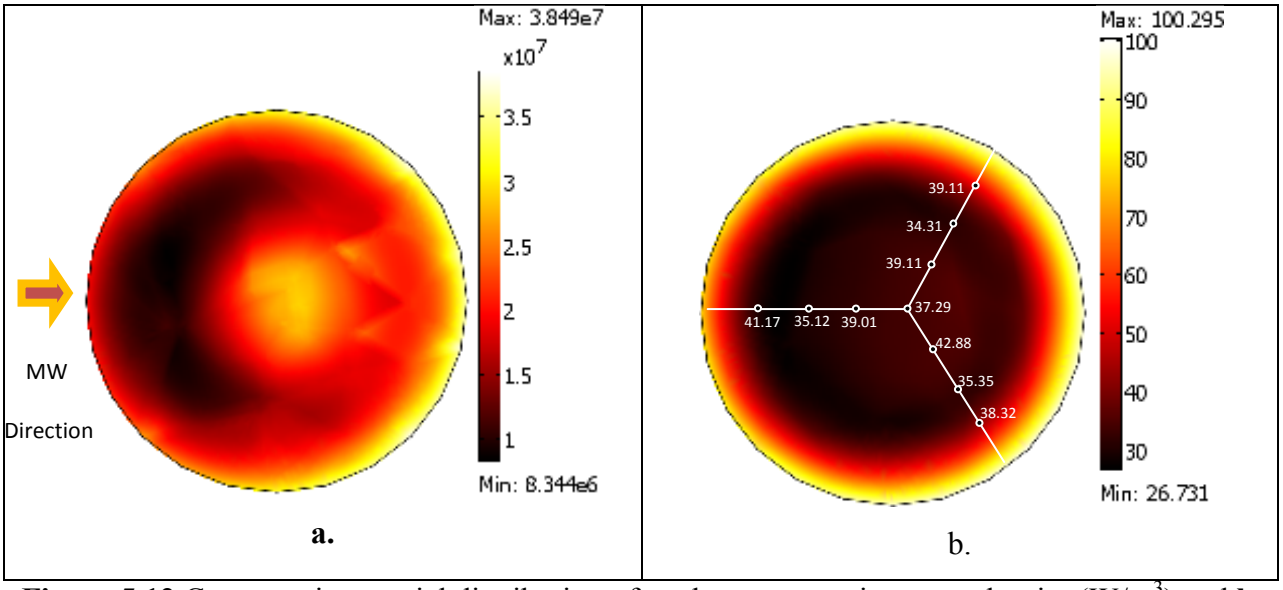

Figure 5.12 Cross section spatial distribution of **a.** electromagnetic power density (W/m^3) and **b.** temperature for 3 % saltwater

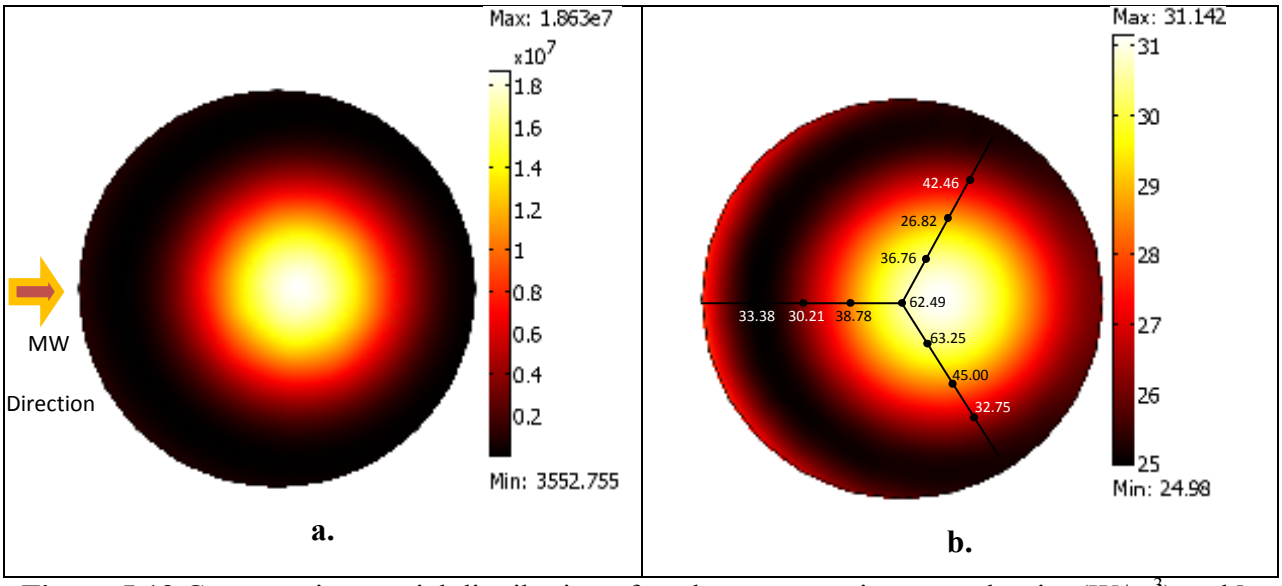

Figure 5.13 Cross section spatial distribution of **a.** electromagnetic power density (W/m^3) and **b.** temperature for freshwater

The temperature distribution for CMC showed higher temperature near the center (opposite to incident wave direction) followed by lower temperature at the edges (**Figure 5.11b**); a similar trend was observed in the experimental data. The simulated values were under-predicted for CMC solution in general due to the temperature independent properties assumption in the model. The simulated values (35-50 ^{o}C) matched closely for 3 % saltwater with the experimental values (35-43 ^{o}C) (**Figure 5.12b**). For freshwater, the numerical model under-predicted the temperature values due to low heat generation values (**Figure 5.13b**). Overall, the model predictions of heat generation and temperature were fairly good for CMC solution and 3 % saltwater.

5.4 Conclusions

A numerical model was developed in COMSOL to simulate continuous flow microwave heating of liquids. The COMSOL model was compared with a pre-validated ANSYS model and was found in close agreement. Although ANSYS and COMSOL offered an interface for coupling of electromagnetism, with fluid flow and heat transfer, COMSOL provided a flexible

model setup as compared to ANSYS. Multiphysics modeling in ANSYS was subject to availability of coupled elements as compared to COMSOL where same elements were used to couple a variety of physics phenomenon.

Verified COMSOL model was further extended to incorporate the phase change and non-Newtonian flow. The phase change phenomenon was included in the model via apparent specific heat method. The model confirmed that the power generation was very much dependent on the dielectric properties of the liquid. For CMC and 3 % saltwater the difference between numerical and experimental heat generation was 22% and 10% respectively. The prediction of temperature values were fairly good for 3 % saltwater, and CMC; and for freshwater the results did not match well due to difference in dielectric properties. This study concludes that results from COMSOL and ANSYS models were comparable. However, to avail the flexibility in multiphysics coupling, COMSOL model was extended and its validation was confirmed by experimental data. The numerical model helped in greater understanding of the process of continuous flow microwave heating and can be used in the future for optimizing the microwave heating process.

5.5 References

Achkar, H., Pennec, F., Peyrou, D., Sartor, M., Plana, R., Pons, P., (2008). "Use the reverse engineering technique to link COMSOL and ANSYS softwares". 9th. International Conference on Thermal, Mechanical and Multiphysics Simulation and Experiments in Micro-Electronics and Micro-Systems, EuroSimE.

Boufadela, M.C., Suidana, M.T., Venosab, A.D. (1999). "Numerical modeling of water flow below dry salt lakes: effect of capillarity and viscosity". *Journal of Hydrology*, 221, 55–74.

COMSOL Multiphysics (2008). "Documentation for COMSOL Release 3.4". COMSOL, Inc., MA, USA, http://www.comsol.com.

Choi, Y. and M.R. Okos. (1986). "Effects of temperature and composition on the thermal properties of foods". In *Food Engineering and Process Applications, Vol. 1, Transport Phenomenon.* M. Le Maguer and P. Jelen (Ed), Elsevier Applied Science Publishers Ltd, London 93-101.

Coronel, P, Simunovic, J., Sandeep, K.P., Cartwright, G.D., Kunar, P. (2008). "Sterilization solutions for aseptic processing of foods in continuous flow microwave systems operating at 915 MHz". *Journal of Food Engineering*, 85(4), 528-536.

Curet, S., Rouaud, O. and L. Boillereaux (2006). "Heat transfer models for microwave thawing applications". *Excerpt from the Proceedings of the COMSOL Users Conference*, Paris, France.

Datta, A., H. Prosetya and W. Hu (1992). "Mathematical modeling of batch heating of liquids in a microwave cavity". *Journal of Microwave Power and Electromagnetic Energy*, 27(1), 38–48.

Feldman, D., Kiley, E., Weekes, S. and V. V. Yakovlev (2007). "1D and 2D coupled electromagnetic-thermal models for combined convective-microwave heating in a pulsing regime". 9th Seminar *Computer Modeling & Microwave Power Engineering*, Valencia, Spain.

Geankoplis, C. J. (1993). *Transport Processes and Unit Operations,* McGraw-Hill Publications.

Hansson, L., Lundgren, N., A.A.O. Hagman (2006). "Finite element modeling (FEM) simulation of interactions between wood and microwaves". *Journal Wood Science*, 52, 406–410.

Hu, X. and K. Mallikarjunan (2002) "Mathematical modeling of heat transfer of microwave heated fish gel". *ASAE Annual International Meeting*, Chicago, USA.

Ikediala, J.N., Hansen, J.D., Tang, J., Drake, S.R., Wang, S. (2002). "Development of a saline water immersion technique with RF energy as a postharvest treatment against codling moth in cherries". *Postharvest Biology and Technology*, 24, 209–221.

Knoerzer, K., Regier M. and H. Schubert (2006). "Microwave heating: a new approach of simulation and validation". *Chemical Engineering & Technology*, 29 (7), 796 – 801.

Komarov, V., Tang, J. 2004. "Dielectric permittivity and loss factor of tap water at 915 MHz". *Microwawe and Optical Technological. Letter.*, 42(5), 419-420.

Komarov, V.V. and V.V. Yakovlev (2001). "Simulations of components of microwave heating applicators by FEMLAB, MicroWaveLab and QuickWave-3D", *Proceedings on 36th Microwave Power Symposium (San Francisco, CA, April 2001)*, 1-4.

Le Bail, A., T. Koutchma and H.S. Ramaswamy (2000). "Modeling of temperature profiles under continuous tube-flow microwave and steam heating conditions". *Journal of Food Process Engineering,* 23, 1-24.

Lin, Y. E., Anantheswaran, R. C. & V. M. Puri (1995). "Finite element analysis of microwave heating of solid foods". *Journal of food Engineering*, 25, 85-112.

Mao, W., Watanabe, M., Sakai, N. (2005). "Analysis of temperature distributions in Kamaboko during microwave heating". *Journal of Food Engineering,* 71, 187–192.

Mirabito, C., Narayanan, A., Perez, D., Stone, B. (2005). "FEMLAB model of a coupled electromagnetic-thermal boundary value problem". Research Experience: Worcester Polytechnic Institute, MA.

Ohlsson, T. (1993). "In-flow microwave heating of pumpable foods". *Developments in Food Engineering: Proceedings of the 6th International Congress on Engineering and Food*, 322-324.

Pryor R.W. (2007). "Modeling materials through a phase transition: using COMSOL Multiphysics and applying physics first principles techniques". *The Proceedings of the COMSOL Conference 2007*, Boston

Ratanadecho, P., K. Auki and M. Akahori (2002). "A numerical and experimental investigation of the modeling of microwave heating for liquid layers using a rectangular wave guide (effects of natural convection and dielectric properties)", *Applied Mathematical Modeling*, 26, 449–472.

Romano, V.R., Marra , F. and U. Tammaro (2005). "Modelling of microwave heating of foodstuff: study on the influenceof sample dimensions with a FEM approach". *Journal of Food Engineering*, 71, 233–241.

Sabliov, C.M., Salvi D.A. and D. Boldor (2007). "High frequency electromagnetism, heat transfer and fluid flow coupling in ANSYS Multiphysics". *Journal of Microwave Power & Electromagnetic Energy*, 41(4).

Salvi, D.A., D. Boldor, C.M. Sabliov and K.A. Rusch (2008a). "Numerical and experimental analysis of continuous microwave heating of ballast water as preventive treatment for introduction of invasive species". *Journal of Marine Environmental Engineering* (In press).

Salvi, D., Boldor, D., Sabliov C. M., Ortego, J., Arauz, C. (2008b). "Experimental study of temperature profile in liquids heated in a continuous flow microwave system - effect of flow rate, physical and dielectric properties on temperature distribution". *Institute of Food Technologist Annual Meeting and Food Expo*, Paper no. 207-05, New Orleans

Steffe, J.F. (1912). *Rheological Methods in Food Process Engineering*, Freeman Press, MI, USA.

Vallejos, P.A.E. and C. Duston (2005). Carbon foam filled with phase change materials for passive temperature management". *The Proceedings of the COMSOL Conference 2005*, Boston

Vais, A.E., Palazoglu, T.K., Sandeep, K.P., Daubert, C.R. (2002). "Rheological characterization of carboxymethylcellulose solution under aseptic processing conditions". *Journal of Food Process Engineering,* 25(1), 41-61.

Zhang, H., Datta, A.K., Taub, I. A., Doona, C. (2001). "Electromagnetics, heat transfer, and thermokinetics in microwave sterilization". AIChE Journal, 47(9), 1957- 1968.

Zhang, J. and A.K. Datta (2006). "Mathematical modeling of bread baking process". *Journal of Food Engineering*, 75, 78–89.

Zhang, Q., Jackson, T.H., Ungan, A. (2000). "Numerical modeling of microwave induced natural convection"., *International Journal of Heat and Mass Transfer,* 43, 2141-2154.

Zhou, L., Puri, V. M., Anantheswaran, R. C. and G. Yeh (1995). “Finite element modeling of heat and mass transfer in food materials during microwave heating – model development and validation”. *Journal of Food Engineering,* 25, 509-529.

Zhu J., A.V. Kuznetsov and K.P. Sandeep (2007a). “Numerical simulation of forced convection in a duct subjected to microwave heating”, *Heat Mass Transfer*, 43(3), 255-264.

Zhu J., A.V. Kuznetsov and K.P. Sandeep (2007b). “Mathematical modeling of continuous flow microwave heating of liquids (effects of dielectric properties and design parameters)”. *International Journal of Thermal Sciences*, 46 (4), 328-341.

Zhu J., A.V. Kuznetsov and K.P. Sandeep (2007c). “Numerical modeling of a moving particle in a continuous flow subjected to microwave heating”. *Numerical Heat Transfer, Part A*, 52, 417 – 439.

CHAPTER 6

CONCLUSIONS AND FUTURE WORK

6.1 Conclusions

The study presents numerical and experimental investigation of continuous flow microwave heating. Numerical model developed in this study by coupling electromagnetism with convection heat transfer and fluid flow was a unique model to simulate continuous flow microwave heating in ANSYS Multiphysics. The model was used to understand the effect of flow rates on the temperature profiles of water heated in a continuous-flow focused microwave system. It was observed that the fluid volumes at the center of the tube received more heat following Mathieu-type electric field distribution. The total energy absorbed by water was 1.2 kW (of incident 5 kW) with the temperature increase from 25°C to 42°C and to 34°C for 1.0 l/min and 2.0 l/min respectively. A slightly higher temperature of water near the tube's wall was caused by the mismatch between the parabolic velocity profile and the Mathieu-type electric field distribution.

The developed numerical model was partially validated using synthetic ballast water at different salinities (0 and 1.5%) flowing at 1.6 l/min flow rate. The predicted temperature values were in good agreement with the experimental results for temperatures below boiling (with average absolute errors of 3°C and 3.9°C at 0 and 1.5% salt concentration). Results from the validated model suggested that the microwave power generation and temperature distribution was influenced mostly by fluids' dielectric properties and residence time in the cavity for a specific microwave geometry. Small differences in the numerical and experimental temperatures were attributed to simplifying assumptions made in developing the model, and to experimental errors. Upgrade of the model to incorporate more complex boundary conditions, phase change,

and non-Newtonian flow was required. It was also concluded that numerous experimental temperature data is required for extensive validation of the model.

Rigorous experimental analysis was performed employing a new custom made system using fiber optic probe to measure the temperatures at 110 locations in applicator tube in three different fluids at three different flow rates during continuous flow microwave heating. Out of three different fluids used in the experiments saltwater, of high dielectric properties absorbed more power (3960 W) followed by CMC solutions (2800 W) and freshwater (2520 W) from an incident power of 4000 W. Considering that the microwave system used in the study was designed for saltwater dielectric properties, this product had most uniform temperature distribution followed by freshwater. Due to its non-Newtonian nature and thermal runaway effect, CMC exhibited non uniform temperature distribution. The data obtained from the study was found useful for rigorous numerical validation of an improved COMSOL model developed to predict temperature profiles in a liquid undergoing microwave heating.

The new improved continuous flow microwave heating model was developed in COMSOL Multiphysics incorporating non-Newtonian flow and phase change. The phase change was taken into account using apparent specific heat method. The accuracy of the model was verified by comparison with pre-developed ANSYS model. A comparative study for two software packages implied that COMSOL provided a flexible model setup as compared to ANSYS where multiphysics modeling was subject to availability of coupled elements. Comparison of the model with experimental data suggested that the model predictions were in fairly good agreement for saltwater and CMC solution.

It was concluded that the process of continuous flow microwave heating was successfully simulated using different multiphysics software packages by coupling of high frequency

electromagnetism, fluid flow and heat transfer. Extensive validation of the model was performed using experimental data obtained by employing a new fiber optic probe design. The developed model will greatly aid in understanding of the microwave heating process and it can be a critical tool for researchers and engineers in the academic and industrial settings interested in continuous flow microwave heating.

6.2 Future Work

Continuous flow microwave heating model in COMSOL was used to understand the effect of properties and flow rates on the temperature distribution in the liquids heated in a continuous flow microwave system of known geometric dimensions. The numerical model developed can be coupled iteratively to incorporate temperature dependence of the dielectric and physical properties. The model can be applied to understand the effect of cavity geometry, applicator diameter and input power on continuous flow microwave heating of actual pumpable food products. The model can also be used as a base for future developments by addition of other physical phenomena. For example, processes such as microwave assisted extraction can be simulated by addition of mass transfer and multiphase flow in the current model. Further, the temperature data obtained from the current model can be used to determine microbial inactivation kinetics in the food products treated by continuous flow microwave heating to model the processes such as sterilization.

A more in-depth, comparative analysis of COMSOL and ANSYS is needed. Different combinations of mesh size and mesh types could be studied to ascertain model precision in prediction of temperature. The study also needs to consider the effect of solver selection on memory requirement, accuracy, and solving time. Such study could be useful in optimizing the model parameter and in software selection process.

The experimental method developed to measure three dimensional temperature distribution in liquid food product heated in a continuous flow microwave system can be extended to measure temperature in particles suspended in liquids or applied to an actual food product. Current experimental method requires multiple runs to obtain the three dimensional temperature data; the method can be improved to obtain the data in a single run.

APPENDIX: LETTERS OF PERMISSION

Letter of Permission from Journal of Microwave Power and Electromagnetic Energy

From: editor@jmpee.org [mailto:editor@jmpee.org]
Sent: Tuesday, June 24, 2008 11:04 AM
To: Sabliov, Cristina M.
Cc: execdir@impi.org; admin@jmpee.org; vadim@WPI.EDU
Subject: RE: FW: JMPEE Special Issue 41(4)

Dear Prof. Sabliov,

Your co-author and student, Ms. Deepti Salvi, is permitted to include your paper 'High frequency electromagnetism, heat transfer and fluid flow coupling in ANSYS Multiphysics' (by Sabliov et al. JMPEE 41(4): 2008) in her dissertation for academic (non-profit) purposes.

A further publication of this dissertation as a monograph or a book requires the permission of the IMPI's Executive Director (cc'd)).

On behalf of JMPEE, we wish Ms. Salvi a great success in her Doctorate examination and her future career.

Best wishes,

Eli

Eli Jerby, Ph.D.
Editor-in-Chief
Journal of Microwave Power and Electromagnetic Energy (JMPEE)
E-mail: editor@jmpee.org
Website: www.jmpee.org
Telefax +972-3-640-8048

-------- Original Message --------
Subject: FW: JMPEE Special Issue 41(4)
From: "Sabliov, Cristina M." <CSabliov@agcenter.lsu.edu>
Date: Mon, June 23, 2008 5:26 pm
To: "editor@jmpee.org" <editor@jmpee.org>

Dear Dr. Eli Jerby,

I would like to request your permission to include the paper entitled 'High frequency electromagnetism, heat transfer and fluid flow coupling in ANSYS Multiphysics' (by Sabliov et al. originally published in the JMPEE Special Issue 41(4): 2008) in the dissertation of the co-author Deepti Salvi, PhD student in my lab. This permission is required internally by our graduate school. We thank you in advance for your consideration.

Sincerely, Cristina Sabliov.

PS. The paper is attached to this message. Thank you! Cristina.

Letter of Permission from Journal of Marine Environmental Engineering

From: Guy Griffiths [mailto:Journals@oldcitypublishing.com]
Sent: Wednesday, June 18, 2008 10:29 AM
To: Boldor,Dorin
Subject: Re: JMEE / Paper Number: JMEE MB-30 (Salvi)

Permission is granted.

_____

Guy Griffiths
Old City Publishing
628 North 2nd Street
Philadelphia, PA 19123, USA
Tel: 215 925 4390
Fax: 215 925 4371
E-mail: guy@oldcitypublishing.com
Web: oldcitypublishing.com

-------- Original Message --------
From: Dorin Boldor <DBoldor@agcenter.lsu.edu>
Date: Mon, 16 Jun 2008 16:40:18 -0500
To: Guy Griffiths <Journals@oldcitypublishing.com>
Subject: Re: JMEE / Paper Number: JMEE MB-30 (Salvi)

Dear Mr. Griffiths,
We would like to request your permission to use the publication accepted by JMEE as a stand alone chapter in the PhD dissertation of Ms. Deepti Salvi (the first author on this paper). Our university is asking to have this permission for all work that has been accepted for publication prior to submitting the dissertation.

Thank you,
Dorin

VITA

Ms. Deepti Salvi was born and brought up in a small beautiful town of Dapoli, Maharashtra, India. She completed her undergraduate studies from Dr. B.S. Konkan Agricultural University, Dapoli in June 2003. Later, she joined to Asian Institute of Technology, Thailand, and completed her Master of Engineering in August 2005. During her stay in Bangkok she got married to Mr. Abhijit Patil in December 2003. In August 2005, she joined Louisiana State University, Baton Rouge, USA, to pursue doctoral studies. She expects to receive the degree of Doctor of Philosophy at the August 2008 commencement.